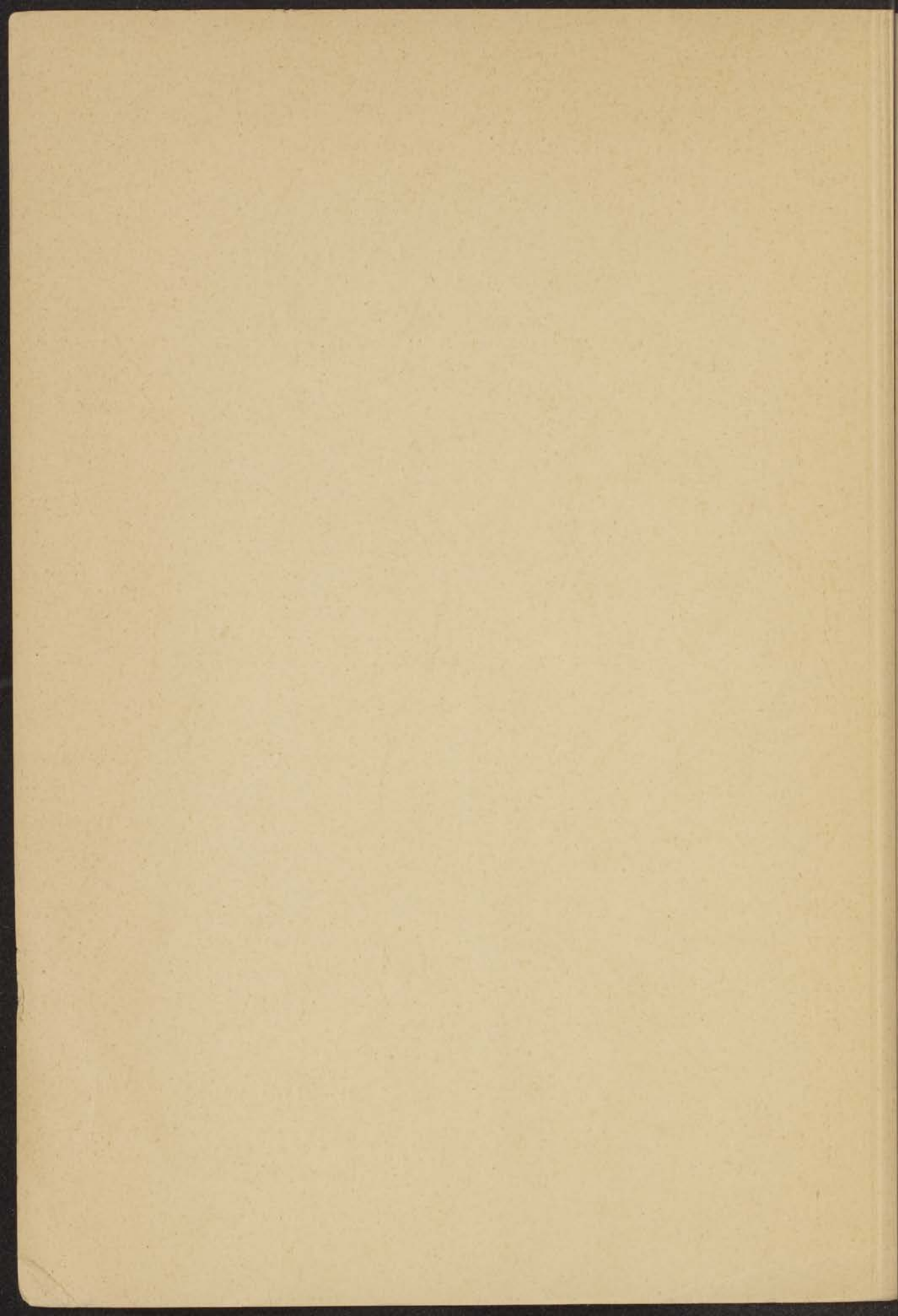


ON THE POWER TRANSFER  
BETWEEN PARAMAGNETIC SPINS  
AND CRYSTAL LATTICE



B. BÖLGER



- 3 NOV. 1959

ON THE POWER TRANSFER BETWEEN  
PARAMAGNETIC SPINS AND CRYSTAL LATTICE



kast dissertaties

THE UNIVERSITY OF CHICAGO  
LIBRARY



## STELLINGEN

### I

De interpretatie, die ESCHENFELDER en WEIDNER aan hun metingen van de verzadiging der paramagnetische resonantie gaven is onjuist.

Zie [4.1] van dit proefschrift.

### II

De interpretatie, die YOKOTA geeft van de paramagnetische spin-roosterrelaxatie is aanvechtbaar.

M. YOKOTA, *J. Phys. Soc. Jap.* **10**, 762 (1955).

### III

De hysterese verschijnselen, waargenomen met antiferromagnetische resonantie in  $\text{CuCl}_2 \cdot 2\text{H}_2\text{O}$  bij 4000 MHz door UBBINK, kunnen aan een opwarming van het spinsysteem worden toegeschreven.

J. UBBINK, Proefschrift, Leiden (1953).

### IV

De afleiding, die VAN VLECK geeft van de z.g. Brons-Van Vleck formule is niet geheel juist. De invloed van plaatsruil-interacties op de constante  $p$ , voorkomende in deze formule, alsmede de anisotropie hiervan, kunnen waardevolle inlichtingen geven omtrent het mechanisme der spin-roosterrelaxatie.

Zie [1.5]; [1.7] en [4.5] van dit proefschrift.

### V

Met behulp van electronen-kernspin-dubbelresonantie kan het mechanisme der electronen-spindiffusie nader bestudeerd worden.

Zie [4.7] van dit proefschrift.

### VI

Door een geringe wijziging van de opstelling, door DUYSSENS gebruikt voor de meting van fluorescentie intensiteiten, zouden de fluctuaties van het opvallend licht geëlimineerd kunnen worden.

L. N. M. DUYSSENS, Proefschrift, Utrecht (1952).

### VII

Voor de ontwikkeling van optische masers is het van belang de spectroscopische metingen van BECQUEREL, zoals die aan robijn, uit te breiden.

J. BECQUEREL, Notice sur les travaux scientifiques Hermann & Cie. Paris (1934).

### VIII

Met behulp van de electronenspin-resonantie van 1,1-diphenyl-2-picrylhydrazyl is het mogelijk nadere gegevens te verkrijgen omtrent stoffen met een zwak zuur karakter, zoals amfotere oxyden.

J. H. LUPINSKI, Proefschrift, Leiden (1959) Hfdst. I.

## IX

Van de tot nu toe geconstrueerde versterkers voor microgolven blijkt een niet-reciproke lopende golf-maser de gunstigste eigenschappen te hebben. Het gebruik van zulk een versterker zou de radioastronomie een grote stap vooruit brengen.

## X

Bij de constructie van een maser kan men bij hogere temperaturen magnetisch meer geconcentreerde preparaten gebruiken dan bij lagere temperaturen.

Zie [4.1] van dit proefschrift.

## XI

De verklaring, die ALERS geeft van de door hem gevonden afwijkingen van de regel van WIEDEMANN en FRANZ voor Zn in magneetvelden is onjuist.

P. B. ALERS, Phys. Rev. 101, 41 (1956).

## XII

Voor het bereiken van lage temperaturen door middel van adiabatische demagnetisatie is het gunstiger kristallen met een grote roosterconstante te gebruiken dan magnetisch verdunde kristallen.

## XIII

Het verdient aanbeveling het contact tussen het spin en het roosterstelsel te beschrijven met de in dit proefschrift ingevoerde vermogensoverdrachtcoëfficiënt  $\eta$  en niet met de relaxatietijd  $\tau_1$  of  $\rho$ .

Zie [1.7] van dit proefschrift.

## XIV

Vergelijking van de uitkomsten der bepaling van de samenstelling van verdunde legeringen op de door GERRITSEN e.a. aanbevolen methode met die der röntgenfluorescentie methode, kan informatie geven omtrent clustervorming.

A. N. GERRITSEN, MISS. G. J. LOSS EN J. M. L. C. VAN DER AA, Appl. Sci. Res. A6, 385 (1956)

## XV

Vergelijking van de heliumtemperatuurschaal van 1958 met de verdampingswarmten gemeten door BERMAN en MATE door middel van de relatie van CLAPEYRON, toont een verschil aan groter dan de opgegeven meetnauwkeurigheid. Dit verdient nader onderzoek.

R. BERMAN en C. F. MATE, Phil. Mag. 29, 461 (1958).

## XVI

De toepassing van een uitlaatgas-turbocompressor in snellopende dieselmotoren verhoogt niet alleen het motorvermogen en rendement, doch zou ook een belangrijke verhoging van de nuttige last toelaten voor wegtransportmiddelen. Aan het gebruik van dergelijke installaties en van z.g. interkoeling is tot nu toe te weinig aandacht besteed.

# ON THE POWER TRANSFER BETWEEN PARAMAGNETIC SPINS AND CRYSTAL LATTICE

PROEFSCHRIFT

TER VERKRIJGING VAN DE GRAAD VAN  
DOCTOR IN DE WIS- EN NATUURKUNDE  
AAN DE RIJKSUNIVERSITEIT TE LEIDEN,  
OP GEZAG VAN DE RECTOR MAGNIFICUS  
MR. J. E. JONKERS, HOOGLERAAR IN DE  
FACULTEIT DER RECHTSGELEERDHEID,  
PUBLIEK TE VERDEDIGEN OP DONDERDAG  
12 NOVEMBER 1959 TE 16 UUR

DOOR

**BOUWE BÖLGER**

GEBOREN TE HAARLEM IN 1928



1959

DRUKKERIJ HOLLAND N.V. - AMSTERDAM

ON THE POWER TRANSFER  
BETWEEN PARAMAGNETIC SPINS  
AND CRYSTAL LATTICE

PROCEEDINGS

Promotor :  
Prof. Dr C. J. GORTER

BOUWF. BÖLGER



PHYSIKALISCHES INSTITUT DER UNIVERSITÄT WÜRZBURG



*Aan mijn ouders*  
*Aan mijn vrouw*  
*Aan Heleen*



THE  
LIBRARY OF THE  
MUSEUM OF NATURAL HISTORY  
AND  
GEOGRAPHY  
OF THE  
SMITHSONIAN INSTITUTION  
WASHINGTON, D. C.

THE  
LIBRARY OF THE  
MUSEUM OF NATURAL HISTORY  
AND  
GEOGRAPHY  
OF THE  
SMITHSONIAN INSTITUTION  
WASHINGTON, D. C.

Teneinde te voldoen aan de wens van de Faculteit der Wis- en Natuurkunde volgt hier een kort overzicht van mijn universitaire studie.

Ik ving mijn studie aan in September 1945 aan de Technische Hogeschool te Delft en zette deze in 1946 voort te Leiden. In Maart 1949 legde ik het candidaatsexamen letter A af, waarna ik werd opgeroepen voor het vervullen der militaire dienstplicht, gedurende welke ik een opleiding kreeg tot meteoroloog.

Vanaf het verlaten van de dienst in October 1951 werkte ik, met onderbreking van het jaar 1952-1953, op het Kamerlingh Onnes Laboratorium te Leiden onder leiding van Prof. Dr C. J. GORTER.

In Juni 1954 legde ik het doctoraalexamen experimentele natuurkunde af. De tentamens in de theoretische natuurkunde en de mechanica werden mij afgenomen door Prof. Dr J. KORRINGA en Prof. Dr N. G. VAN KAMPEN.

In 1951 werkte ik onder leiding van Dr Ir N. J. POULIS aan een onderzoek betreffende de kernspinresonantie.

Gedurende het academiejaar 1952-1953 verbleef ik in de Verenigde Staten van Amerika, op verzoek van Prof. Dr J. G. ASTON, waar ik in diens laboratorium, scheikundige faculteit der Pennsylvania State University, een opstelling bouwde voor kernspinresonantie en met behulp hiervan phase overgangen in enige stoffen bestudeerde.

Na mijn terugkeer te Leiden kwam ik in de microgolfgroep en werkte hier samen met Dr H. J. GERRITSEN en R. OKKES op het gebied van anti-ferromagnetische en paramagnetische resonantie. Het onderzoek van de verzadiging der paramagnetische absorptie werd eerst later opgezet. De meeste metingen hieromtrent werden verricht in samenwerking met K. J. VAN DAMME en J. M. NOOTHOVEN VAN GOOR. Hulp ontving ik voorts o.a. van G. W. J. DREWES, A. J. SURJADI, F. E. NOMMENSEN, en de radiotechnici G. VAN DER HEIDE en H. H. PERQUIN. Met W. J. CASPERS had ik vele theoretische discussies. Onze werkgroep werd in 1957 een onderdeel van de werkgroep voor vaste stoffen der Stichting voor „Fundamenteel Onderzoek der Materie”, waarbij ik wetenschappelijk medewerker werd.

Vanaf October 1957 hield ik mij ook bezig met het construeren van een quantum mechanische microgolhversterker (MASER), samen met Dr J. UBBINK en B. J. ROBINSON Ph.D. Met een proefopstelling gelukte het ons 11 Maart 1958 versterking te krijgen, een stabiele versterker werd eerst later geconstrueerd. Dit onderzoek werd gedaan in samenwerking met de stichtingen F.O.M. en Radiostraling van Zon en Melkweg en het Natuurkundig Laboratorium der N.V. Philips' Gloeilampenfabrieken.

Tijdens mijn werkzaamheden op het Kamerlingh Onnes Laboratorium heb ik behalve van de wetenschappelijke staf, ook veel steun mogen ontvangen van de technische en administratieve staf. In het bijzonder wil ik noemen de cryogeen technicus D. DE JONG en de meester-instrumentmaker, tevens leraar van de Leidse Instrumentmakersschool J. HOOGWERF, die ook bij het construeren der microgolfapparatuur van advies diende.



# CONTENTS

	page
INTRODUCTION . . . . .	xi
CHAPTER I. ON THE GENERAL THEORY OF PARAMAGNETIC RESONANCE AND RELAXATION . . . . .	1
1.1 The energy levels of paramagnetic ions . . . . .	1
1.2 Macroscopic equations . . . . .	5
1.3 Microscopic theory. . . . .	7
1.4 Spin-spin equilibrium and the resonance line shape . . . . .	8
1.5 On the theory of the relaxation rates . . . . .	13
1.6 Equilibrium and saturation of multilevel spin systems . . . . .	21
1.7 The power transfer between spin and lattice systems . . . . .	24
1.8 The relaxation method. . . . .	29
REFERENCES . . . . .	30
CHAPTER II. EXPERIMENTAL METHODS AND TECHNIQUES . . . . .	32
2.1 Introduction . . . . .	32
2.2 Magnetic losses in resonant structures . . . . .	32
2.3 The reflection method . . . . .	34
2.4 The transmission method. . . . .	37
2.5 Apparatus for the reflection measurements . . . . .	39
2.6 Apparatus for the transmission measurements . . . . .	42
2.7 Pulse methods for determining the relaxation times . . . . .	43
2.8 The principle of operation of a three level maser . . . . .	44
2.9 The temperature behaviour of the quality factors . . . . .	47
2.10 Crystal growing . . . . .	48
2.11 Errors . . . . .	48
REFERENCES . . . . .	49
CHAPTER III. EXPERIMENTAL RESULTS . . . . .	50
A. RESULTS OBTAINED BY STEADY STATE SATURATION	
3.1 Presentation of the data . . . . .	50
3.2 Results on CrK alum . . . . .	51
3.3 Results on CuK and CuNH <sub>4</sub> tutton salt . . . . .	60
3.4 Results on CuSO <sub>4</sub> 5H <sub>2</sub> O . . . . .	66
3.5 Results on CuK <sub>2</sub> Cl <sub>4</sub> 2H <sub>2</sub> O and Cu(NH <sub>4</sub> ) <sub>2</sub> Cl <sub>4</sub> 2H <sub>2</sub> O . . . . .	69
3.6 Results on Mn (NH <sub>4</sub> ) <sub>2</sub> (SO <sub>4</sub> ) <sub>2</sub> 6H <sub>2</sub> O . . . . .	73
3.7 Results on Co (NH <sub>4</sub> ) <sub>2</sub> (SO <sub>4</sub> ) <sub>2</sub> 6H <sub>2</sub> O . . . . .	76
B. RESULTS OBTAINED BY PULSE MEASUREMENTS AND RELAXATION RATES DETERMINED BY EXPERIMENTS ON MASERS.	
3.8 Results on K <sub>3</sub> Cr(CN) <sub>6</sub> /K <sub>3</sub> Co(CN) <sub>6</sub> . . . . .	77
3.9 Results on synthetic ruby . . . . .	83
3.10 Discussion of the pulse measurements . . . . .	86
REFERENCES . . . . .	88

	page
CHAPTER IV. DISCUSSION OF THE RESULTS . . . . .	90
4.1 The connection between $\tau_1$ and $\eta$ . . . . .	90
4.2 Phenomenological description . . . . .	91
4.3 General considerations on the phonon household . . . . .	93
4.4 Application to the saturation of paramagnetic resonance . . . . .	96
4.5 The influence of spin-spin interactions on $\eta$ . . . . .	99
4.6 The influence of an inhomogeneously distributed power transfer constant . . . . .	104
4.7 Conclusion and indications for future work . . . . .	113
REFERENCES . . . . .	116
SAMENVATTING . . . . .	117

## INTRODUCTION

The establishment of equilibrium between a system of paramagnetic moments and the crystal lattice can be characterized by a spin-lattice relaxation time  $\tau_1$ . This has been the object of many investigations and recently the interest and that for related problems has gained new impetus due to the application of paramagnetic materials in low noise microwave amplifiers, so called "solid state masers".

In the usual method to determine the spin-lattice relaxation time an alternating field is applied parallel to the static magnetic field and the complex susceptibility measured as a function of the frequency. With the aid of the thermodynamical model of CASIMIR and DU PRÉ [1],  $\tau_1$  can then be found. A survey of the experimental data up to 1947 has been given by GORTER [2].

Apart from a few exceptions, the theory of VAN VLECK [3] describes the experimental results for the magnetically diluted salts fairly well. For the concentrated salts, on which most of the early measurements were carried out, the agreement at liquid helium temperatures is miserable.

With the advent of paramagnetic resonance new techniques have become available to measure the spin-lattice relaxation behaviour. The system of magnetic moments can be heated, owing to an inadequate power transfer to the lattice, by absorption of microwave power. The study of the magnetic temperature as a function of the absorbed power in the stationary state, yields a value of the power transfer constant closely related to  $\tau_1$ . This method is called the saturation method. Data obtained by ESCHENFELDER and WEIDNER [4] seemed to indicate a large discrepancy between the results obtained by the two methods.

It has been the purpose of the investigations described in this thesis to study the spin-lattice relaxation behaviour in a number of paramagnetic salts by the saturation method. A comparison is made between the results obtained by theory and by the relaxation and the saturation method. For the work carried out in connection with the construction of a maser reference is made to [5] and [6]. Only the results of that work pertaining to relaxation properties has been used.

## REFERENCES

1. CASIMIR, H. B. G. and F. K. DU PRÉ, *Physica* 5, 507 (1938); *Comm. Kamerlingh Onnes Lab. Leiden*, suppl. no. 85 a.
2. GORTER, C. J., *Paramagnetic Relaxation*. Elseviers Publ. Co. Amsterdam (1947).
3. VAN VLECK, J. H., *Phys. Rev.* 57, 426 (1940).
4. ESCHENFELDER, A. H. and R. T. WEIDNER, *Phys. Rev.* 92, 869 (1953).
5. BÖLGER, B., B. J. ROBINSON and J. UBBINK, To be published in *Physica and Commun.*
6. ——— and ———, *Arch. des Sc. Geneve* 11, 187 (1958); and *Commun. Suppl.* 114 i.

EXPERIMENTAL

The experimental work was carried out in the laboratory of the Department of Chemistry, University of Toronto, Canada. The apparatus used was a modified version of the apparatus described by [Author Name] [Year]. The details of the apparatus are given in the Appendix.

The reaction was carried out in a stainless steel bomb of 100 ml capacity. The bomb was filled with the reactants and sealed. The bomb was then heated in a water bath at the required temperature. The reaction was allowed to proceed for a certain period of time and then cooled. The products were then analysed by the method described below.

The analysis was carried out by the method of [Author Name] [Year]. The details of the method are given in the Appendix. The results of the analysis are given in Table I.

The results show that the reaction proceeds to completion. The products are [List of products]. The reaction is exothermic. The rate of reaction increases with increasing temperature. The reaction is first order with respect to [Reactant]. The activation energy of the reaction is [Value] kcal/mole.

The authors are indebted to the National Research Council of Canada for the grant which supported this work. The authors also wish to thank [Name] for his assistance in the early stages of the work.

REFERENCES

- [Author Name], [Year], [Journal Name], [Volume], [Page].

## CHAPTER I

### ON THE GENERAL THEORY OF PARAMAGNETIC RESONANCE AND RELAXATION

#### [1.1] *The energy levels of paramagnetic ions*

Paramagnetic resonance deals with the transitions caused by a magnetic high frequency field between the lowest group of energy levels of a paramagnetic ion. The splittings between these levels will first be discussed.

The case of free ions is relatively simple. The fact, however, that in crystals the energy levels are displaced by interactions with the surroundings makes paramagnetic resonance a fruitful source of problems in solid state physics.

In this thesis we shall restrict ourselves to crystals in which the effect of the crystal field is small compared to that of the Coulomb interactions of the electrons with the nucleus and with each other, so that the self consistent field method can be used to describe the ionic wave functions. In ionic crystals this condition is fulfilled to a high degree.

We shall only consider the elements belonging to the iron transition group.

[1.1.1] The Hamiltonian used to describe a paramagnetic ion in a crystal lattice can be divided into:

a. the orbital energy  $\mathcal{H}_o$  due to the coulomb energy of the electrons. This energy is mainly due to the influence of the nearest atoms. The direct effect of ions at a larger distance is negligible and their influence is mainly felt via coupling with the nearest neighbours.

b. The spin orbit coupling  $\mathcal{H}_{oS}$  will be taken to be (cf. [1])  $\mathcal{H}_{oS} = \lambda \mathbf{L} \cdot \mathbf{S}$  where  $\mathbf{L}$  and  $\mathbf{S}$  are the total angular momentum vectors of orbit and spin.

A tensor type of interaction between  $\mathbf{L}$  and  $\mathbf{S}$  has been considered by PRYCE [2].

c. The Zeeman energy

$$(1.01) \quad \mathcal{H}_z = \beta(\mathbf{H} + \mathbf{h}) \cdot (\mathbf{L} + 2\mathbf{S})$$

where  $\beta$  is the Bohr magneton,  $\mathbf{H}$  the applied static field and  $\mathbf{h}$  a radio frequency field.

d. The dipole-dipole interaction between two ions  $i$  and  $j$  can be written as

$$(1.02) \quad \mathcal{H}_d = \frac{\boldsymbol{\mu}_i \cdot \boldsymbol{\mu}_j}{r_{ij}^3} - 3 \frac{(\boldsymbol{\mu}_i \cdot \mathbf{r}_{ij})(\boldsymbol{\mu}_j \cdot \mathbf{r}_{ij})}{r_{ij}^5}$$

where  $\mathbf{r}_{ij}$  is the radius vector between ions  $i$  and  $j$  with magnetic moments  $\boldsymbol{\mu}_i$  and  $\boldsymbol{\mu}_j$ .

e. The exchange interaction

$$(1.03) \quad \mathcal{H}_{\text{ex}} = 2J_{ij} \mathbf{S}_i \cdot \mathbf{S}_j$$

is due to the overlap of the wave functions of ion  $i$  and  $j$ ; in this expression superexchange may be included. In more general considerations one has to add anisotropic exchange terms.

The interactions of the electronic spin with the nuclear spin moment have been omitted as they are generally small and are not of interest in the present work.

The terms d. and e. determine the coherence effects between the spins and will be discussed later.

As the interactions  $\mathcal{H}_O$ ,  $\mathcal{H}_{OS}$  and  $\mathcal{H}_Z$  are generally far more important than the coupling of the spins with each other, it is possible to consider the spins of different ions as being separate entities in a first approximation.

[1.1.2] The perturbation calculation starts with the largest term  $\mathcal{H}_O$ . The crystal field around an ion is expanded in Legendre polynomials and one considers how the orbital degeneracy is removed by going successively to lower orders of field symmetry. This has been done by the methods of group theory by BETHE, MULLIKEN and JAHN [3] [4] [5] and we will use their notation of designating the levels.

For the case that the lowest eigenvalue of  $\mathcal{H}_O$  is non-degenerate, the perturbation calculation can be carried out by a method given by PRYCE [6], by choosing a representation for  $\mathbf{L}$ , diagonalizing  $\mathcal{H}_O$  and the so-called spin Hamiltonian contains the operator  $\mathbf{S}$  and the matrix elements of  $\mathbf{L}$  in the specified representation, corresponding to the lowest multiplet. It is now possible to define an effective spin operator  $\mathbf{S}'$  so that  $2S' + 1$  is the degeneracy of the ground state. The spin Hamiltonian can be expressed in terms of the operator  $\mathbf{S}'$ . For the case of a degenerate lowest orbital level reference is made to the literature [7] [8].

For ions with  $L=0$  one has to go to a high order perturbation, but for other ions the second order is usually sufficient. In the derivation one makes use of a general theorem that  $\mathbf{L}$  has no diagonal elements for a singlet orbital state.

The spin Hamiltonian, when spin-spin interactions (d and e) are neglected, has the following form: (cf. [7])

$$(1.04) \quad \begin{cases} \mathcal{H}_S = 2\beta\mathbf{H} \cdot \mathbf{S} + (2\lambda)^{-1}(\beta\mathbf{H} + \lambda\mathbf{S})(\bar{g} - 2)(\beta\mathbf{H} + \lambda\mathbf{S}) = \\ = \bar{g}\beta\mathbf{H} \cdot \mathbf{S} + \mathbf{S} \cdot \bar{D} \cdot \mathbf{S} - \beta^2\mathbf{H} \bar{A} \mathbf{H}. \end{cases}$$

If the ground state orbital wave function is denoted by  $\langle o |$  and the higher ones by  $\langle n |$  then

$$(1.05) \quad (\bar{g} - 2) = \sum_n \frac{2\lambda}{E_n - E_0} \langle o | \mathbf{L}_i | n \rangle \langle n | \mathbf{L}_j | o \rangle \quad i, j = x, y \text{ or } z.$$

The factor  $g$  is a tensor and so are  $\bar{D}$  and  $\bar{A}$ .

In the third part of (1.04), the Zeeman energy is given by the first term, the second term gives the zero field splitting caused by the crystal field and the third term represents the temperature independent paramagnetism. The total spin Hamiltonian must of course show at least the same symmetry as the crystal field. One advantage of using this method is that the resonance properties of an ion can be described by a small number of constants. For a more detailed discussion of the spin Hamiltonian and the values of the constants found experimentally in the various substances, reference is made to the review articles of BLEANEY and STEVENS [7] and of BOWERS and OWEN [8].

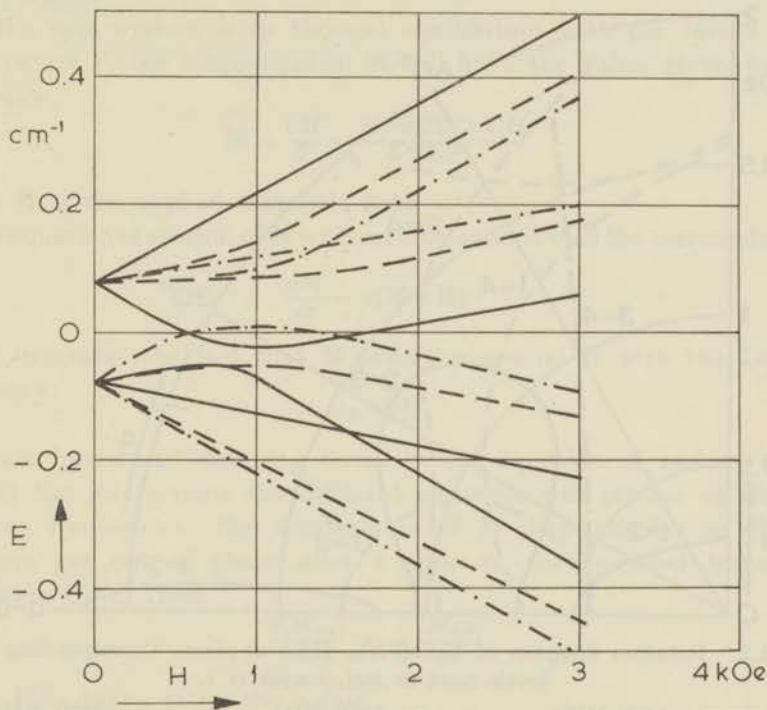


Fig. 1.1. Energy levels of  $K_3Cr(CN)_6$  as a function of  $H$ .  
 - - -  $H // x$ -axis. - · - · -  $H // y$ -axis. —  $H // z$ -axis.

[1.1.3] As an illustration we give in fig. 1.1 the energy levels of  $Cr^{+++}$  in  $CrK_3(CN)_6$  diluted with the Co salt as a function of the applied magnetic field  $H$  along the different crystal axes, as calculated from the spin Hamiltonian.  $Cr^{+++}$  has a  $S = 3/2$  and in this substance  $\mathcal{H}_S$  has the following form

$$(1.06) \quad \mathcal{H}_S = g\beta H \cdot S + D[S_z^2 - 1/3 S(S+1)] + E(S_x^2 - S_y^2)$$

where  $g$  is almost isotropic and equal to 1.99. The values of the other constants are  $D = 0.083 \text{ cm}^{-1}$  and  $E = 0.011 \text{ cm}^{-1}$ . The magnetic axes are slightly rotated with respect to the crystal axes. There are two  $Cr^{+++}$  ions in a unit cell with the  $ac$ -plane as a symmetry plane.

To find the paramagnetic spectrum at 4000 MHz (or  $0.133 \text{ cm}^{-1}$ ) for instance, one has to adjust the field so as to fit this energy between two energy levels. To show the anisotropy, a rotation diagram (fig. 1.2) in the  $ac$ -plane for the frequencies 1420, 3850 and 8500 MHz has been drawn for some of the transitions. This diagram represents the loci of the field vector for which resonance takes place as a function of the angle  $\alpha$  of  $\mathbf{H}$  with the  $a$ -axis.

The transitions are labeled by the corresponding energy levels, numbered from the lowest.

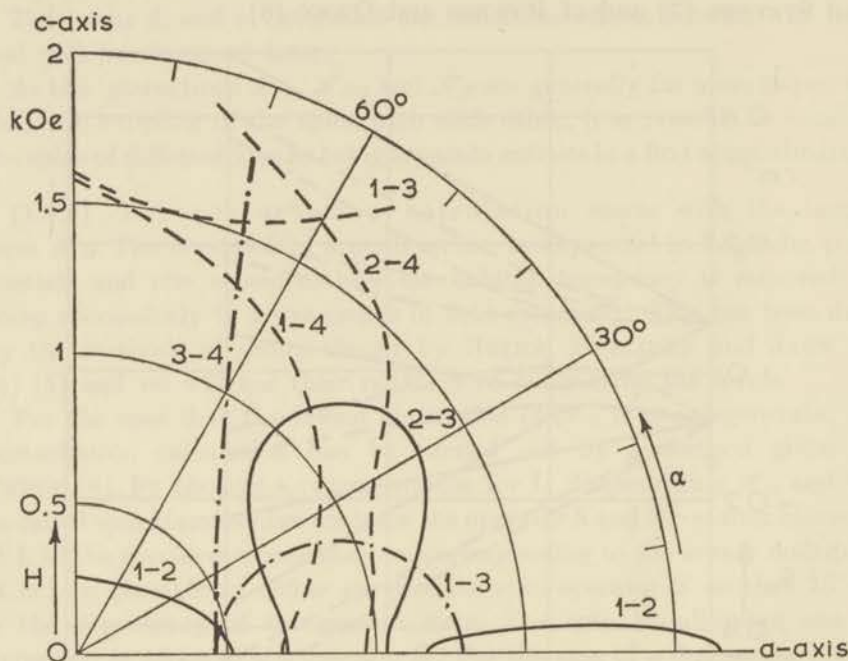


Fig. 1.2. Rotation diagram of  $\text{K}_3\text{Cr}(\text{CN})_6$ ,  $\mathbf{H}$  in  $ac$ -plane. Corresponding energy levels next to loci, lowest is 1.

— 1420 MHz.    - · - · - 3850 MHz.    - - - 9400 MHz.

[1.1.4] The terms of the Hamiltonian of the paramagnetic ion depending on the position of the ion in the lattice such as in  $\mathcal{H}_0$ , through a perturbation calculation, and in  $\mathcal{H}_a$  and  $\mathcal{H}_{\text{ex}}$  through the ion distances  $r_{ij}$  in (1.02) and (1.03), may be developed into a power series of the deviations  $\mathbf{u}_k$  and  $\mathbf{u}_j$  of ion  $k$  and  $j$  from their equilibrium positions. Limiting ourselves to terms of second order, this gives

$$(1.07) \quad \mathcal{H} = \mathcal{H}_0 + \sum_k \mathcal{H}_{1k}(u_k) + \sum_{kj} \mathcal{H}_{2kj}(u_k u_j).$$

For the first term  $\mathcal{H}_0$ , due to the ions in their equilibrium positions, we take the spin Hamiltonian (1.04) with the spin-spin interactions added, the second and third terms are respectively linear and quadratic terms in the displacement vectors  $\mathbf{u}_k$ . They give rise to the coupling of the

spin system with the thermal motions of the lattice. Their influence is several orders of magnitude smaller than  $\mathcal{H}_0$  and they can be regarded as small perturbations. To a first approximation the spins can be regarded as being decoupled from the lattice.

### [1.2] Macroscopic equations

[1.2.1] A classical description of nuclear and paramagnetic resonance has been given by BLOCH [9] for spins without zero field splitting. Consider an assembly of  $N$  spins, all with the same gyromagnetic ratio  $\gamma = g\beta/\hbar$ .

If the spin system is in thermal equilibrium with the lattice at a temperature  $T$ , the magnetization  $\mathbf{M}$  will have the value given by the Curie law,

$$(1.08) \quad \mathbf{M} = \frac{C\mathbf{H}}{T} = \frac{N\gamma^2\hbar^2 S(S+1)\mathbf{H}}{3kT}$$

where  $\mathbf{H}$  is the applied magnetic field.

The equation of motion of  $\mathbf{M}$  without interactions with the surroundings is

$$\frac{d\mathbf{M}}{dt} = \gamma(\mathbf{M} \times \mathbf{H})$$

which expresses the fact that  $\mathbf{M}$  precesses around  $\mathbf{H}$  with the Larmor frequency:

$$\omega_L = \gamma\mathbf{H}.$$

BLOCH introduced damping terms in the equation of motion of  $\mathbf{M}$ . Due to the interactions the different electrons will precess at slightly different frequencies. The components of  $\mathbf{M}$  perpendicular to  $\mathbf{H}$  will therefore get out of phase after a time  $\tau_2$ , the so-called transverse relaxation time. Then

$$(1.09) \quad \frac{d|M_{x,y}|}{dt} = -\frac{|M_{x,y}|}{\tau_2}$$

where  $\mathbf{H}$  is taken along the  $z$ -axis.

The relaxation time  $\tau_1$  of the component of  $\mathbf{M}$  parallel to  $\mathbf{H}$  will in general have a larger value than  $\tau_2$ , as a change in the  $z$ -component entails a change of the Zeeman energy and this can only happen through a coupling with the surroundings.

$$(1.10) \quad \frac{dM_z}{dt} = -\frac{M_z - M_0}{\tau_1}.$$

We shall now write down the equations of motion when a linearly polarized radio frequency field  $\mathbf{h}$  perpendicular to  $\mathbf{H}$  is applied to the sample.

$$(1.11) \quad \begin{cases} \frac{dM_{x,y}}{dt} = \gamma[\mathbf{M} \times \mathbf{H}]_{x,y} - \frac{M_{x,y}}{\tau_2} \\ \frac{dM_z}{dt} = \gamma[\mathbf{M} \times \mathbf{H}]_z - \frac{M_z - M_0}{\tau_1} \end{cases}$$

with  $H_x = h/2 (e^{i\omega t} + e^{-i\omega t})$ ;  $H_y = 0$ ;  $H_z = H$ .

The steady state solution has the following form

$$(1.12) \quad \left\{ \begin{aligned} M_x &= \frac{M_z \gamma^2 H h \tau_2^2 [(\omega_L^2 + 1/\tau_2^2 - \omega^2) - (2i\omega/\tau_2)] e^{i\omega t}}{4\omega^2 + \tau_2^2 [\omega_L^2 + 1/\tau_2^2 - \omega^2]^2} \\ M_y &= \frac{M_z \gamma h [i\omega + 1/\tau_2] e^{i\omega t}}{(i\omega + 1/\tau_2)^2 + \gamma^2 H^2} \\ M_{z_{av}} &= M_0 \frac{4\omega^2 + \tau_2^2 (\omega_L^2 + 1/\tau_2^2 - \omega^2)^2}{4\omega^2 + \tau_2^2 (\omega_L^2 + 1/\tau_2^2 - \omega^2)^2 + 1/2 \gamma^2 h^2 \tau_1 \tau_2 (\omega_0^2 + 1/\tau_2^2 + \omega^2)} \end{aligned} \right.$$

where the high frequency motions of  $M_z$  have been eliminated by averaging over many Larmor periods.

Near the resonance frequency  $\omega^2 = \omega_L^2 + 1/\tau_2^2$ , slightly displaced because of the damping, we have

$$(1.13) \quad M_x = \frac{M_0}{2} \frac{\gamma h \tau_2 (\Delta \tau_2 + i) e^{i\omega t}}{1 + (\Delta \tau_2)^2 + 1/4 \gamma^2 h^2 \tau_1 \tau_2}$$

where

$$\omega_L + 1/\tau_2^2 - \omega^2 = 2\omega \Delta.$$

Introducing the complex susceptibility  $\chi = \chi' - i\chi''$  so that  $\mathbf{M} = \chi \mathbf{H}$ , and relating this to the power  $P$  absorbed by the system from the r.f. field, one obtains

$$(1.14) \quad P = 1/2 \omega \chi'' h^2 = 1/2 \omega \mathbf{h} \cdot \text{Im } \mathbf{M}.$$

From (1.13) we find

$$(1.15) \quad P = \frac{N(\hbar\omega)^2 \gamma^2 h^2 \tau_2 S \cdot (S+1)}{12kT [1 + (\Delta \tau_2)^2 + 1/4 \gamma^2 h^2 \tau_1 \tau_2]}.$$

Upon increasing  $h$  we have initially  $P \propto h^2$  as expected, but for values of  $h^2 > \frac{1}{1/4 \gamma^2 \tau_1 \tau_2}$  (at resonance),  $P$  starts to saturate (cf. fig. 1.3) and reaches

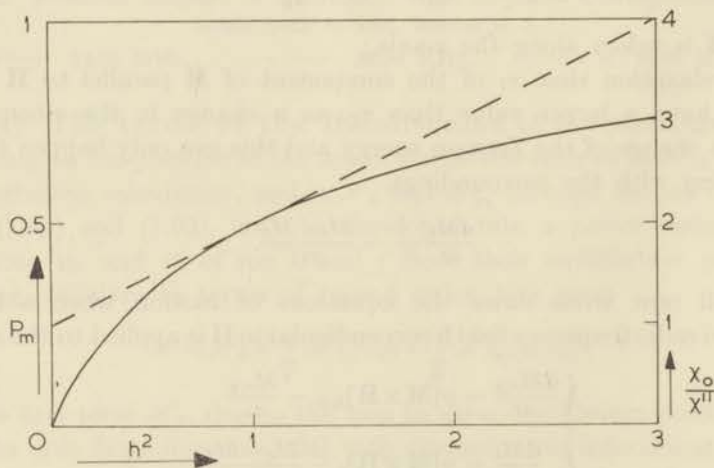


Fig. 1.3.  $P_m$  and  $\chi_0/\chi''$  as a function of  $h^2$ .

—  $P_m$       - - -  $\chi_0/\chi''$

asymptotically the value

$$(1.16) \quad P_{\infty} = \frac{N(\hbar\omega)^2 S \cdot (S+1)}{3kT\tau_1}.$$

At 4° K and  $H=3000 \text{ o}$  typical values for the relaxation constants are  $\tau_2 \approx 10^{-9}$  s. and  $\tau_1 \approx 10^{-3}$  s. requiring a r.f. field of about  $0.1 \text{ o}$  to reach half the expected saturation.

### [1.3] *Microscopic theory*

We shall now approach the subject from a microscopic viewpoint. Suppose we have an assembly of spins of which the spin Hamiltonian (1.04) is known, and that the eigenvalues and eigenfunctions have been calculated.

When a radio frequency field  $h_x \sin \omega t$  is applied as a perturbation

$$(1.17) \quad \mathcal{H}_{\text{rf}} = \gamma \hbar h_x(\omega) S_x \sin \omega t,$$

then the transition probability induced by this perturbation will be proportional to the square of the modulus of the matrix elements  $\langle i | S_x | j \rangle$ , taken between the eigenstates  $|i\rangle$  and  $|j\rangle$  of the spin Hamiltonian.

The transition frequencies  $\omega_{ij} = \frac{E_i - E_j}{\hbar}$  will have a certain width due to spin interactions and lifetime limiting processes. The shape of the transition will be characterized by the normalized shape function  $g(\omega - \omega_{ij})$  where

$$(1.18) \quad \int_{-\infty}^{+\infty} g(\omega - \omega_{ij}) \frac{d\omega}{2\pi} = 1.$$

If the transition frequencies  $\omega_{ij}$  have a separation much larger than their width, the induced transition rate  $W_{ij}$  can be written as

$$(1.19) \quad W_{ij} = \frac{1}{4} \gamma^2 \hbar^2 (\omega) g(\omega - \omega_{ij}) |\langle i | S_x | j \rangle|^2$$

with

$$(1.20) \quad W_{ij} = W_{ji}.$$

These results follow from normal time dependent perturbation theory (cf. [10]).

If the population of the  $i$ th level is called  $n_i$ , then the power absorbed by the spin system due to transitions from  $i$  to  $j$  will be

$$(1.21) \quad P_m = (n_i - n_j) \hbar \omega_{ij} W_{ij}.$$

The populations will change, partly due to transitions induced by the r.f. field and partly due to transitions induced by the lattice vibrations. (Spontaneous emission can be neglected.)

We shall now consider a two-level system and call the lattice induced transition rate  $U_{12}$ , level 1 being the lowest in energy.

Multilevel systems will be considered later as they lead to rather large formulae, masking the effects we want to discuss here.

For the rate of change of the population difference we find

$$(1.22) \quad \frac{d(n_1 - n_2)}{dt} = 2(-n_1 U_{12} + n_2 U_{21}) - 2(n_1 - n_2)W_{12}.$$

Because of the fact that the energy exchange between the spins and the lattice, which is in the thermal equilibrium at a temperature  $T$ , takes place in quanta  $\hbar\omega_{12}$ , we have

$$(1.23) \quad \frac{U_{12}}{U_{21}} = e^{+(\hbar\omega_{12}/kT)} = \frac{n_{2_0}}{n_{1_0}}$$

where  $n_{1_0}$  and  $n_{2_0}$  are the equilibrium populations, having their normal Boltzmann ratio.

The exponential may be expanded as in most cases  $\hbar\omega_{12} \ll kT$ , and (1.22) can be rewritten using the relation  $n_1 + n_2 = n_{1_0} + n_{2_0}$  as:

$$(1.24) \quad \frac{d(n_1 - n_2)}{dt} = -[(n_1 - n_2) - (n_{1_0} - n_{2_0})]2\bar{U}_{12} - (n_1 - n_2)2W_{12}$$

where

$$\bar{U}_{12} = \frac{U_{12} + U_{21}}{2}.$$

The steady state solution of (1.24) is

$$(1.25) \quad n_1 - n_2 = \frac{n_{1_0} - n_{2_0}}{1 + W_{12}/\bar{U}_{12}}.$$

If  $N$  is the total number of spins we find with (1.19)

$$n_{1_0} - n_{2_0} = \frac{N}{2S+1} \frac{\hbar\omega_{21}}{kT} \quad \text{and} \quad \frac{1}{\bar{U}_{12}} = 2\tau_1$$

$$(1.26) \quad \left\{ \begin{aligned} P_m &= (n_{1_0} - n_{2_0}) \frac{\hbar\omega_{21}W_{12}}{1 + W_{12}/\bar{U}_{12}} = \\ &= \frac{N}{2S+1} \frac{(\hbar\omega_x)^2}{kT} \frac{1/4\gamma^2 h^2(\omega) g(\omega - \omega_{12}) |\langle 1|S_x|2\rangle|^2}{1 + 1/2\gamma^2 h^2(\omega) g(\omega - \omega_{12}) \tau_1 |\langle 1|S_x|2\rangle|^2} \end{aligned} \right.$$

#### [1.4] Spin-spin equilibrium and the resonance line shape

[1.4.1] Spin-spin equilibrium. There have been many theories and experiments on the internal equilibrium in spin systems. The main body of the experimental work has been carried out by GORTER e.a. [11], using their relaxation methods. The spin system has many degrees of freedom, more or less coupled through the spin-spin interactions. If such a system is in internal equilibrium one can assign a temperature  $T_s$  to it and by using its density matrix

$$\rho_s = \frac{\exp -\mathcal{H}_s/kT_s}{\sum \exp -\mathcal{H}_s/kT_s}$$

the equilibrium properties can be described. In most cases one does not have to take the total density matrix of spin system plus lattice because the spin and lattice degrees of freedom are independent, apart from a small term causing spin lattice relaxation. To obtain  $g_S$  one can sum the total density matrix over all lattice states.

That the spin system is in internal equilibrium does not merely mean that the populations of the energy levels are in accordance with the Boltzmann factors. It means also that the non-diagonal elements of the density matrix are zero. Or, macroscopically, the transverse magnetization is zero.

Let us consider what happens macroscopically in the Bloch picture when at a certain time the magnetization  $\mathbf{M}$  is not along the magnetic field (cf. [9] and fig. 1.4). Because of the coherence disturbing effects the

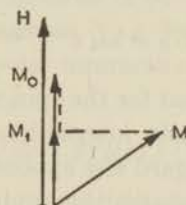


Fig. 1.4. Time behaviour of  $\mathbf{M}$  according to BLOCH.

transverse magnetization decreases according to (1.09) with a time constant  $\tau_2$ . During this process the internal energy  $\mathbf{M} \cdot \mathbf{H}$  remains constant, as in the Bloch picture a change in the spin-spin interactions is neglected. After a time of about  $\tau_2$ ,  $\mathbf{M}$  will reach the value  $M_1$  and the spin system will be in internal equilibrium at a temperature  $T_S$  which corresponds to its internal energy and the size of  $M_1$ .

According to Curie's law (1.08) we have

$$(1.27) \quad \mathbf{M}_1 = \frac{CH}{T_S} \text{ where } \frac{T_S}{T} = \frac{n_1 - n_2}{n_{1_0} - n_{2_0}}.$$

If in paramagnetic resonance the r.f. field is much smaller than the coherence disturbing internal fields, it is still legitimate to describe the situation by means of a spin temperature. To describe the saturation behaviour one has to put in (1.26):

$$(1.28) \quad T_S = T [1 + \frac{1}{2} \gamma^2 \hbar^2 g^2 (\omega - \omega_{ij}) \tau_1 \langle |S_x| \rangle^2].$$

At r.f. fields higher than the internal fields, or for times shorter than  $\tau_2$  after a shock excitation of the spin system, it is not possible to speak of a spin temperature. Phase coherence effects then play an important rôle and the state of the spin system cannot be described in terms of phaseless constants.

The studies of GORTER e.a. in this field have been mainly concerned

with the spin absorption at low frequencies which is closely connected with resonance line shapes, although no completely satisfactory analysis has yet been presented to relate them [12] [13]. Especially in the case of multilevel spin systems, as will be discussed in [1.6], and systems with exchange the theory is far from complete.

There have been many discussions as to whether it is allowed to split the spin system into a Zeeman part and an interaction part each with its own internal energy and temperature. This procedure has been followed by BLOEMBERGEN *e.a.* [14], YOKOTA [15] and ABRAGAM *e.a.* [16]. The difficulty is that the degrees of freedom are not independent. In the case of large exchange interaction they may be considered to be commuting, which is not sufficient to justify their assumptions.

According to a theory of KRONIG and BOUWKAMP [17] the rate of spin transitions due to the spin interactions in a two-level system, is

$$(1.29) \quad U_S = \omega_d e^{-\omega^2/2\omega_d^2}$$

where  $\hbar\omega$  is the energy required for the spin transition and  $\omega_d$  a frequency characterizing the dipole-dipole interactions, which will be introduced later (cf. (1.35)). One may regard the exponential as the probability that the internal field just compensates the applied field, or as the amplitude of the Fourier component at frequency  $\omega$  of a gaussian random fluctuating internal field. This probability readily becomes a very small quantity as  $\omega$  is increased, one of the reasons why this theory was originally rejected by BROER [18].

[1.4.2] The resonance line shape. Comparing the results of the quantum theory and the classical picture, it is found that (1.26) corresponds with (1.15) when

$$g(\omega - \omega_L) = \frac{2\tau_2}{1 + (\omega - \omega_L)^2 \tau_2^2}$$

This is a Lorentz line shape with a half width at half power of  $1/\tau_2$ . It is not surprising that the classical description leads to a Lorentz line shape, as it was introduced by assuming (1.09). This is one of the main drawbacks of the Bloch picture as experimentally one finds mostly an almost gaussian line shape in the absence of exchange interactions.

The shape of a paramagnetic resonance line will partly be determined by the lifetime broadening due to spin lattice relaxation. That contribution will have a Lorentz shape with a half width  $1/\tau_1$ . There are many salts in which this is the main contribution to the line width at the higher temperatures *e.g.* TiCs alum [19],  $\text{FeNH}_4$  tutton salt *etc.*

This situation arises also in salts containing ions of the rare earths group, but for the iron group we have for the ions with an odd number of spins in general  $\tau_1 \ll \tau_2$ , making the lifetime broadening negligible.

To calculate the contribution of the spin-spin interactions to the line width two widely different methods have been used. VAN VLECK applied

the method of moments to the case of identical spins [20]. He calculated

$$\int (\omega - \omega_L)^4 g(\omega - \omega_L) d\omega \text{ and } \int (\omega - \omega_L)^2 g(\omega - \omega_L) d\omega$$

by a diagonal sum and showed that  $\mathcal{H}_{\text{ex}}$  has no influence on the second moment of the absorption line, because of the commutation properties of  $\mathcal{H}_{\text{ex}}$ ,  $\mathcal{H}_Z$  and  $\mathcal{H}_{\text{rf}}$ . There are two contributions to the fourth moment, however, the first one due to dipole-dipole coupling alone, the second due to the rate of change of this coupling which, as we shall see later, is determined by  $\mathcal{H}_{\text{ex}}$ .

ANDERSON [21] and KUBO and TOMITA [22] have developed a mathematical model which allows one to calculate the actual line shape. They assume the system to absorb a single frequency, which varies in a random way over a certain range determined by the dipole-dipole interactions, but at a rate controlled by the motions or exchange coupling. This concept was first proposed by GORTER and VAN VLECK [23].

We will first split up the dipolar interaction (1.02) into terms depending on their influence on  $M_z$

$$(1.30) \left\{ \begin{aligned} \mathcal{H}_a = \sum_{i>j} AS_{zi}S_{zj} + B(S_i^+S_j^- + S_i^-S_j^+) + C(S_i^+S_{zj} + S_{zi}S_j^+) + \\ + D(S_i^-S_{zj} + S_{zi}S_j^-) + E S_i^+S_j^+ + F S_i^-S_j^- \end{aligned} \right.$$

where  $S^\pm = S_x \pm iS_y$  and  $A, B, C, D, E$  and  $F$  are dependent on the polar coordinates of ion  $i$  with respect to ion  $j$ .

ABRAGAM called these terms stop-stop, flip-flop, flip-stop etc., according to their effect on  $M_z$ .

For large static fields the terms  $A$  and  $B$  will broaden the absorption line at the Larmor frequency  $\omega_L$ , while the terms  $C, D, E$  and  $F$  introduce weak satellite lines at frequencies around  $0, 2\omega_L$  and  $3\omega_L$  (cf. fig. 1.5) [24]. The absorption near zero frequency has been the subject of many experimental studies by GORTER e.a. [11] [25] [26].

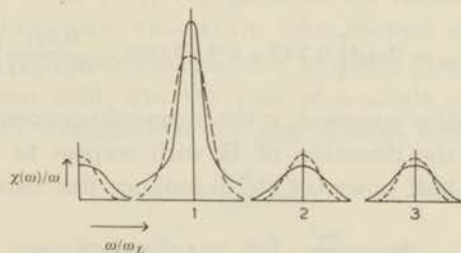


Fig. 1.5.  $\chi''(\omega)/\omega$  as a function of  $\omega/\omega_L$ .  
 ———  $\omega_d < \omega_{\text{ex}} < \omega_L$       - - -  $\omega_{\text{ex}} < \omega_d$ .

[1.4.3] The influence of exchange coupling. A brief outline of Anderson's theory [21] [27] will now be given.

We take as the Hamiltonian

$$(1.31) \quad \mathcal{H} = g\beta H \sum_j S_{zj} + \mathcal{H}_a + 2 \sum_{j>k} J_{jk} \mathbf{S}_j \cdot \mathbf{S}_k + g\beta h \sum_j S_{xj}$$

The absorption spectrum as measured by the last perturbing term is given by the Fourier integral of the time dependent operator  $S(t)$

$$(1.32) \quad I(\omega) = \text{Trace} \left| \int S_z(t) e^{i\omega t} dt \right|^2$$

where

$$(1.33) \quad i\hbar \frac{dS_z}{dt} = [\mathcal{H}, S_z].$$

Since  $\mathcal{H}_{\text{ex}}$  commutes with  $\mathcal{H}_Z$  and with  $\sum_j S_{z_j}$ , the exchange interaction causes no broadening as it does not directly change the energy levels nor interrupt the radiation, but we do have

$$(1.34) \quad i\hbar \dot{\mathcal{H}}_a = [\mathcal{H}_Z + \mathcal{H}_{\text{ex}}, \mathcal{H}_a] \approx [\mathcal{H}_{\text{ex}}, \mathcal{H}_a].$$

The omission of  $\mathcal{H}_Z$  in the commutator expresses the assumption that  $\mathcal{H}_a$  is so small as to have no appreciable matrix elements between the eigenstates of  $\mathcal{H}_Z$  and also that we are only interested in the line near the Larmor frequency.

This assumption is the much discussed truncation and only valid when

$$\mathcal{H}_{\text{ex}} \ll \mathcal{H}_Z \text{ and } \mathcal{H}_a \ll \mathcal{H}_Z.$$

We thus retain only the secular terms  $A$  and  $B$  of  $\mathcal{H}_a$  which results in a frequency shift of the resonance. This shift has a time variation due to (1.34) at a rate of the order of  $\mathcal{H}_{\text{ex}}/\hbar$ , to the effect that  $\mathcal{H}_a$  is partly averaged out during the time that resonance is observed.

The assumption now is that this time variation is a gaussian random one.

The results of calculations on this basis are that the second moment has for a simple cubic lattice the value

$$(1.35a) \quad \omega_d^2 = \langle |\omega - \omega_L|^2 \rangle_{\text{av}} = 12.3 \gamma^4 \hbar^2 S \cdot (S+1) (\lambda_1^4 + \lambda_2^4 + \lambda_3^4 - 0.187) cd^{-6}$$

and the fourth moment for  $\mathbf{H}$  along the (100) axis.

$$(1.35b) \quad \langle |\omega - \omega_L|^4 \rangle_{\text{av}} = 3\omega_d^4 \left[ 0.742 + c^{-1} \left\{ 0.098 - \frac{0.021}{S(S+1)} \right\} + \frac{\pi}{6} \left( \frac{\omega_{\text{ex}}}{\omega_d} \right)^2 \right]$$

where  $d$  is the lattice constant,  $c$  the magnetic concentration and  $\lambda_{1,2,3}$  the cosines fixing the direction of  $\mathbf{H}$  with respect to the crystal axes. The half width at half power of the resonance line becomes

$$(1.36) \quad \begin{aligned} \Delta\omega &= \frac{\omega_d^2}{\omega_{\text{ex}}} \quad \text{for } \omega_d \ll \omega_{\text{ex}} \ll \omega_L \\ \Delta\omega &= \omega_d \quad \text{for } \omega_{\text{ex}} \ll \omega_d \end{aligned}$$

with

$$(1.37) \quad \omega_{\text{ex}}^2 = \frac{8.48}{3} \left( \frac{J}{\hbar} \right)^2 S(S+1).$$

For the case that  $\omega_{\text{ex}} \gg \omega_L$  the truncation performed in (1.34) is no longer permitted as the energies for transitions induced by the non-

secular terms of  $\mathcal{H}_a$  are now available from the interactions. In the calculation of  $\mathcal{H}_a$  retaining all the terms of (1.30) multiplies (1.35a) by the factor  $\frac{10}{3}$ .

We get

$$(1.38) \quad \Delta\omega = \frac{10}{3} \frac{\omega_a^2}{\omega_{\text{ex}}} \quad \text{for} \quad \omega_{\text{ex}} \gg \omega_L.$$

[1.4.4] Inhomogeneously broadened lines. It may be that, upon diluting a substance magnetically,  $\mathcal{H}_a$  becomes smaller than variations from ion to ion in the zero field splitting or static local fields, due to ions of another kind or field inhomogeneities. For the so-called inhomogeneously broadened lines then occurring one has to modify the absorbed power (1.26). For  $g(\omega - \omega_l)$  the single ion absorption shape is taken, but as the ions are spread over a wider line, one has to multiply the whole expression (1.26) by  $\frac{g^*(\omega - \omega_0)}{g(\omega - \omega_L)}$ , the ratio of the observed shape  $g^*(\omega - \omega_0)$  to the single ion shape, and integrate over the distribution of the Larmor frequencies of the different ions. If  $g^*(\omega - \omega_0)$  only varies slowly over the region where  $g(\omega - \omega_L)$  is appreciable, then the magnetic absorption becomes:

$$(1.39) \quad P_{\text{inh}} = \frac{N}{2S+1} \frac{(\hbar\omega)^2}{kT} \frac{1/4 \gamma^2 \hbar^2 \langle 1|S_x|2 \rangle^2 g^*(\omega - \omega_0)}{|1 + 1/2 \gamma^2 \hbar^2 g(0) \tau_1 \langle 1|S_x|2 \rangle^2}$$

where  $g$  is assumed to have a Lorentzian shape [28] [29].

#### [1.5] *On the theory of the relaxation rates*

The energy transfer from a spin system to its environment has been the subject of many controversies, and the different mechanisms that have been proposed will be reviewed in this chapter. We shall limit ourselves to the case of non-conducting ionic crystals.

[1.5.1] Spontaneous emission. An excited spin can return to its ground state by spontaneous emission, in which case it gives a quantum  $\hbar\omega$  to the radiation field. For the case of a single excited spin in free space the Einstein coefficient  $A$  for spontaneous emission is:

$$(1.40) \quad A = \frac{4\omega^3}{\hbar c^3} |\mu_{mn}|^2$$

where  $\mu_{mn}$  is the matrix element of the component  $\gamma\hbar S_x$  of the magnetic moment perpendicular to the static magnetic field  $\mathbf{H}$ . At frequencies  $\omega/2\pi$  around  $10^{10}$  Hz the value of  $A$  is about  $10^{-12}$  giving a lifetime of  $10^{12}$  s. or  $10^5$  years.

In resonance experiments, however, the conditions for the calculation of  $A$  are not fulfilled, and this rate will be enhanced for two reasons.

The first is that the spins are not in empty space but in an electromagnetic resonator with a quality factor  $Q$  and a volume  $V_e$ . PURCELL [30]

has pointed out that in this case the energy density of the field per unit frequency range and unit volume is increased by a factor  $\beta = \lambda^3 Q / 8\pi^2 V_c$  making the rate for spontaneous emission

$$(1.41) \quad W_{em} = \frac{4\pi Q}{\hbar V_c} |\mu_{mn}|^2.$$

In our experiments  $\beta$  ranged from 50 to 500.

The second reason is that we are not dealing with a single spin, but a great number of spins, constricted within a space with dimensions smaller than the velocity of light  $c$  divided by the frequency width  $\Delta\omega/2\pi$  of the transition band. In such aggregates of spins coherence effects become important and states exist with radiation rates far greater than normal [31] [32]. However, the factor by which the radiation is increased is for paramagnetic materials in saturation experiments of no importance.

[1.5.2] Lattice induced transitions. For the lattice vibrations there are two ways to influence the magnetic moment. One way is through modulation of the spin-spin interactions, the other through modulation of the electric crystal field near a magnetic ion.

In spin lattice relaxation, one spin quantum is used to excite lattice states, and as these states have a continuous spectrum, one can apply time dependent perturbation theory; the calculations differ from spin-spin relaxation ones, in which one cannot describe the relaxation mechanism in terms of a coupling between one spin and the spin system as a whole.

WALLER [33] has pointed out that two essentially different processes are possible by which the lattice vibrations can take or give up the energy for the spin transition. When the spin jumps from level  $i$  to level  $j$  the energy

$$(1.42) \quad E_i - E_j = \hbar\omega_{ij}$$

is in the direct process compensated by the emission or absorption of one elastic quantum  $\hbar|\omega_{ij}|$  and is induced by the part of the spin Hamiltonian linear in the displacement vectors  $u_k$ , the term  $\mathcal{H}_{1k}$  in (1.07).

In indirect processes two lattice quanta play a rôle. One  $\hbar\omega_l$  is absorbed while another  $\hbar\omega_k$  is emitted so that

$$(1.43) \quad \hbar|\omega_{ij}| = \hbar\omega_k - \hbar\omega_l.$$

This is called a quasi Raman process and has its origin in the quadratic terms  $\mathcal{H}_{2kl}$  in (1.07).

The lattice will be considered to behave according to the Debye theory. We are interested in the part of the frequency spectrum below 1/200th of the Debye temperature when dealing with the direct process. So this assumption is not a real restriction. For the indirect processes the whole frequency spectrum plays a rôle, and so the optical branch as discussed

by BLACKMANN [34] may have an important influence at the higher temperatures.

In the Debye theory, according to the procedure of SOMMERFELD and BETHE [35], the normal modes of the lattice are quantized. The lattice states are described by a set of quantum numbers  $p_k$  for each of the  $k$ th modes of the elastic vibrations. The energy of the mode is given by

$$(1.44) \quad E_k = (p_k + 1/2)\hbar\omega_k.$$

The normal coordinates  $q_k$  will have matrix elements

$$(1.45) \quad \langle p_k | q_k | p_k + 1 \rangle = \left\{ \frac{\hbar(p_k + 1)}{M\omega_k} \right\}^{1/2}$$

where  $M$  is the total mass of the crystal. As VAN VLECK remarked [36] this is a weak point in the theory as it assumes that the amplitude of vibration is the same for all atoms regardless of their mass, although in first approximation one can neglect the particle structure for long phonon wave lengths.

The number of oscillator modes in a frequency interval between  $\omega$  and  $\omega + d\omega$  for the longitudinal waves with velocity  $v_l$  is given by

$$(1.46) \quad \rho_l(\omega)d\omega = \frac{\omega^2 V d\omega}{2\pi^2 v_l^3}$$

and for the transverse waves with velocity  $v_t$  by

$$(1.47) \quad \rho_t(\omega)d\omega = \frac{\omega^2 V d\omega}{2\pi^2 v_t^3}$$

where  $V$  is the volume of the crystal. These formulae are valid for  $\omega \ll \omega_c$ , the cut-off or Debye frequency.

If  $N$  is the number of atoms in the crystal, there are  $N$  longitudinal and  $2N$  transverse modes of vibration, so

$$\int_0^{\omega_{cl}} \rho_l(\omega)d\omega = N \quad \text{and} \quad \int_0^{\omega_{ct}} \rho_t(\omega)d\omega = 2N$$

giving

$$(1.48) \quad \omega_{cl} = \left( 6\pi^2 v_l \frac{N}{V} \right)^{1/3} \quad \text{and} \quad \omega_{ct} = \left( 6\pi^2 v_t \frac{N}{V} \right)^{1/3}.$$

We can write the displacement vectors  $\mathbf{u}_i$  as a linear combination of the normal modes  $\mathbf{q}_k$  of the lattice,

$$\mathbf{u}_i = \sum_k a_k \mathbf{q}_k \sin \omega_k(t - r_i/v_a + \varphi_k)$$

where  $v_a = v_l$  for the longitudinal modes and equals  $v_t$  for the transverse ones.

The relative displacement between the atoms  $i$  and  $j$  for waves propagating along  $\mathbf{r}_{ij}$ , if the wave length  $\lambda_k \gg |r_{ij}|$ , is

$$(1.49) \quad \mathbf{u}_{ij} = \mathbf{u}_i - \mathbf{u}_j = \mathbf{r}_{ij} \sum_k a_k \frac{\omega_k}{c} \mathbf{q}_k \cos \omega_k(t - r/v_a + \varphi_k).$$

For the direct process we are interested in matrix elements of the linear part of (1.07) corresponding to the creation or destruction of one phonon:

$$(1.50) \quad \langle p_k, i | \mathcal{H}_1(\mathbf{q}_k, \mathbf{S}_l, \mathbf{S}_m) | p_k + 1, j \rangle$$

with the condition (1.42) due to conservation of energy.

The rate  $U_{ij_d}$  at which transitions are induced in the spin system by this direct process will be

$$(1.51) \quad U_{ij_d} = \int_0^{\omega_c} \varrho(\omega_k) |\langle \mathcal{H}_1 \rangle|^2 d\omega_k \propto \int_0^{\omega_c} (\hbar\omega_k)^\alpha |\langle \mathcal{H}_1' \rangle|^2 g(\omega_k - \omega_{ij}) \langle p_k + 1 \rangle_{av} d\omega_k$$

where the exponent  $\alpha$  gives the frequency dependence of  $\varrho(\omega_k) |\langle \mathcal{H}_1 \rangle|^2$ , and  $\langle \mathcal{H}_1' \rangle$  contains the matrix elements of the spin operators in  $\langle i | \mathcal{H}_1 | j \rangle$ .

The integrand of the second integral, which extends over all possible lattice vibrations, contains the distribution function of the spin transition centered at  $\omega_{ij}$ .

If the lattice is in equilibrium at a temperature  $T$ , then the average number of phonons at a frequency  $\omega$  is

$$(1.52) \quad \langle p_k \rangle_{av} = \frac{1}{e^{\hbar\omega/kT} - 1}$$

Combining (1.51) and (1.52) one obtains for  $\omega_{ij} \gg \omega_a$

$$(1.53) \quad U_{ij_d} \propto \omega_{ij}^{\alpha-1} \cdot T \text{ for } \hbar\omega_{ij} \ll kT.$$

thus at very low temperatures, the zero point vibrations determine the relaxation rates.

For the indirect process we are interested in the matrix elements of  $\mathcal{H}_2$  in (1.07), quadratic in the normal coordinates:

$$(1.54) \quad \langle p_k, p_l, i | \mathcal{H}_2(\mathbf{q}_k, \mathbf{q}_l, \mathbf{S}_m, \mathbf{S}_n) | p_k + 1, p_l - 1, j \rangle$$

with (1.43) as a condition. The transition rate due to this indirect process will be

$$(1.55) \quad U_{ij_{ind}} = \int_0^{\omega_c} \int_0^{\omega_c} \varrho(\omega_k) \varrho(\omega_l) |\langle \mathcal{H}_2 \rangle|^2 g(\omega_k - \omega_l - \omega_{ij}) d\omega_k d\omega_l.$$

The main contribution to this integral will come from phonons around  $kT$  or  $\hbar\omega_c$ , depending on which is smaller. One has to go to a higher order perturbation calculation but the decrease in the matrix element is more than offset by the large increase in the number of lattice vibrations that can take part in the process at higher temperatures.

We substitute  $\omega_k - \omega_l = \omega$  into (1.55) and find:

$$(1.56) \quad U_{ij_{ind}} \propto \int_0^{\omega_c} \int_0^{\omega_c} \omega_k^2 g(\omega - \omega_{ij}) |\langle \mathcal{H}_2' \rangle|^2 \langle p_k + 1 \rangle_{av} \langle p_k \rangle_{av} d\omega_k d\omega$$

where  $\langle \mathcal{H}_2' \rangle$  contains the matrix elements of the spin operators in  $\langle \mathcal{H}_2 \rangle$ .

With (1.52) one finds for (1.56)

$$(1.57) \quad U_{ij\text{ind}} \propto T^2 \text{ when } kT \gg \hbar\omega_c$$

$$(1.58) \quad U_{ij\text{ind}} \propto T^{\alpha+1} \text{ when } kT \ll \hbar\omega_c.$$

The case  $\omega_{ij} > \omega_c$  can be neglected.

[1.5.3] The energy transfer by means of modulation of the spin-spin interactions has first been considered by WALLER [33] for systems without exchange interactions. One may include the exchange interactions by considering the magneto-elastic interactions as a perturbation which causes spin transitions because of lattice strains (magnetostriction).

The dipolar coupling  $\mathcal{H}_d$  (1.02) depends on the radius vector  $\mathbf{r}_{ij}$  between ion  $i$  and  $j$  and will therefore be affected by the lattice vibrations.

In (1.07) the linear part becomes proportional to  $\gamma^2 \hbar^2 / r_{ij}^4$  and the quadratic part to  $\gamma^2 \hbar^2 / r_{ij}^5$ . The non-secular terms of these perturbations come from the corresponding ones in  $\mathcal{H}_d$  in (1.30), and are derivatives of the terms  $C$ ,  $D$ ,  $E$  and  $F$ , which can cause transitions in the spin system. WALLER arrived at values for the relaxation rate of about  $10^{-1} \text{ s}^{-1}$  at liquid air temperatures and  $10^{-11} \cdot H^2 \text{ s}^{-1}$  in the liquid helium range. As the observed values for a typical salt such as CrK alum are  $10^6 \text{ s}^{-1}$  and  $10^2 \text{ s}^{-1}$  resp. this mechanism is too weak to explain the observed values. When there are inequivalent ions in the unit cell, as is the case for most salts, the terms  $A$  and  $B$  will also contribute to the relaxation. This, however, does not much reduce the large discrepancy.

The exchange integral  $J$  is a sensitive function of the radius vector  $\mathbf{r}_{jk}$ . If ions  $j$  and  $k$  are equivalent, however, the exchange interaction between them commutes with the Zeeman energy and  $\mathcal{H}_{\text{ex}}$  will not be able to change the magnetization.

In [1.4.3] and the subsequent discussion we have seen that the exchange produces a random frequency modulation of  $\mathcal{H}_d$ , and one could therefore imagine a perturbation  $\mathcal{H}_Z \rightarrow \mathcal{H}_d \rightarrow \mathcal{H}_{\text{ex}} \rightarrow \text{lattice}$ . I have made an estimate of the relaxation probability due to this process, assuming that the exchange constant  $J_{ij}$  in (1.03) is an exponentially decreasing function of the distance  $r_{ij}$  between  $i$  and  $j$ , and that  $\omega_{\text{ex}} < \omega_L$ .

The amplitude of the Fourier component at frequency  $\omega_L$  in  $\mathcal{H}_d$ , due to the modulation of  $\mathcal{H}_{\text{ex}}$  by the lattice vibrations, can be calculated by using (1.34), (1.49) and the above-mentioned assumption. The effect of this Fourier component on the spin operators is found by using (1.33). For the direct effect it is found that  $U_{ij_d} \propto \omega_{\text{ex}}^2 T$  where  $\omega_{\text{ex}}$  is defined by (1.37). For  $\omega_{\text{ex}} \approx 3 \cdot 10^{10} \text{ s}^{-1}$  a rough estimate makes  $U_{ij_d} \approx 10^{-5} \text{ s}^{-1}$  at  $1^\circ \text{ K}$ . As this rate is quite slow, this mechanism seems not to be the most important one.

BLOEMBERGEN and WANG [14] indicated that another situation arises, however, when the exchange frequency (cf. 1.37) is much larger than

the Larmor frequency. For this case the 10/3 effect comes into play. The energy for a spin transition is now available in the dipole term because of the strong modulation by  $\mathcal{H}_{\text{ex}}$ . An analogous situation arises in the case of nuclear resonance, where the dipole term is modulated by the random velocities of the nuclei. Up to a cut-off frequency  $\bar{\omega}$  one finds a white spectrum there and  $\tau_1$  becomes about equal to  $\tau_2$  if  $\bar{\omega} \gg \omega_L$ .

When  $\omega_{\text{ex}} \gg \omega_L$  the energy exchange between "exchange system" and lattice is at a high rate, as it can take place in large quanta  $\hbar\omega_{\text{ex}}$ . The bottleneck for the energy transfer will presumably be between the "Zeeman" and "exchange" system. With respect to the random frequency modulation picture cf. [1.4.3] and the above-mentioned analogy, BLOEMBERGEN *e.a.* expect  $\tau_1 \approx \tau_2$ .

An example of this case is the free radical diphenyl peryl hydrazyl. BLOEMBERGEN and WANG report a value of  $\tau_1$  of  $6.4 \times 10^{-8}$  s. at  $300^\circ$  K and  $77^\circ$  K with  $\tau_2 \approx 6 \times 10^{-8}$  s, while MEYER [37] found  $\tau_1 \approx 10^{-7}$  s. at  $4.2^\circ$  K. VERSTELLE (to be published) has recently studied this effect in more detail.

As this type of relaxation is determined by the spin-spin interactions and independent of the lattice vibrations one would expect  $U$  not to depend on temperature.

[1.5.4] The influence of spin orbit interactions. Relaxation probabilities due to the modulation of the crystal electric fields are essentially single ion processes. HEITLER and TELLER [38] considered the case of substances with a spin splitting at zero magnetic field. The lattice vibrations modulate the value of  $D$  in the spin Hamiltonian (1.04) and induce transitions in the spin system accordingly. They considered only the direct process. FIERZ [39] extended these calculations to the case of indirect processes. Their results are similar to those of WALLER's when  $g\beta\mathbf{H}$  is replaced by  $2D$  and they find for the direct process

$$U_{ij} \approx 3.3 \times 10^6 \omega_{ij}^2 kT / \hbar \omega_c^3.$$

KRONIG [40] was the first to recognize the important possibility for heat transfer via the orbit lattice coupling. VAN VLECK [36] independently carried out similar, more detailed calculations for the special cases of Cr and Ti alum.

In the alums the paramagnetic ions  $X$  are surrounded by a near octahedron of watermolecules  $Y$ .

VAN VLECK [41] considers the influence of the normal modes of vibration  $Q_i$  of the cluster  $XY_6$  and their effect on the orbital momentum  $\mathbf{L}$  of  $X$ . The modes  $Q_i$  can again be developed into linear combinations of the lattice modes  $\mathbf{q}_i$ .

The crystal field of the cluster  $XY_6$  around the center ion  $X$  will generally contain only terms quadratic in the  $Q$ 's. Our case differs, however, from the general situation in two ways. If an orbital state of the

central ion is degenerate, the Jahn-Teller theorem [42] states that the octahedron will become distorted, so as to lift this degeneracy. The atoms around the cluster will partly oppose this distortion. Through this Jahn-Teller effect terms linear in the  $Q$ 's with even symmetry will appear in the field.

Another way to obtain linear terms is by the so-called indirect effect of atoms not belonging to the cluster  $XY_6$ . In an early analysis VAN VLECK [43] comes to the conclusion that the direct effect of distant atoms is not very important, but the influence of them on the octahedron of water-molecules is quite large and will bring linear terms in the field acting on  $X$ . More recently many paramagnetic resonance experiments have shown that this indirect effect can be large. The constants in the spin Hamiltonian of a paramagnetic ion are found to depend on temperature, magnetic dilution, pressure and the size of the other ions present. It may be that this indirect effect of distant atoms is coupled with the Jahn-Teller effect. Only the even normal modes produce linear terms in the crystal field. They are (cf. [41])  $Q_1$  (total symmetric vibration, representation  $\Gamma_{1g}$ ),  $Q_2$  and  $Q_3$  (tetragonal distortion,  $\Gamma_{3g}$ ),  $Q_4$ ,  $Q_5$  and  $Q_6$  (trig. dist.  $\Gamma_{5g}$ ) and  $Q_{19}$ ,  $Q_{20}$  and  $Q_{21}$  (rotation,  $\Gamma_{4g}$ ).

Considering (1.04) and (1.05), there are two different ways for the lattice vibrations to influence the  $g$ -factor:

#### A. The adiabatic terms.

These are present when considering the change in the orbital wave functions  $|n\rangle$  by the  $Q$ 's only. The perturbation calculation can be carried out by keeping  $S$  and  $Q$  as operators, but as  $(E_n - E_0)$  in (1.05) retains the same value, the second order perturbation becomes zero because of the Hermitian property of any element and the pure imaginary values of the matrix elements of  $\mathcal{H}_{SO}$ , while those of  $\mathcal{H}_{OL}$  are real.

VAN VLECK [36] showed that one has to go to a third order perturbation to get non-vanishing terms. A good example of these terms being predominant is  $\text{Cr}^{+++}$  in  $\text{CrK alum}$ . In equilibrium the water octahedron is slightly distorted along a body diagonal of the cubic alum crystal, thus producing a crystal field of trigonal symmetry with this diagonal as a symmetry axis. By taking the  $x$ ,  $y$ ,  $z$ -axes along the principle cubic axes, VAN VLECK finds for the interaction between  $S$  and  $Q$

$$(1.59) \left\{ \begin{aligned} \mathcal{H}_{SL} = \epsilon_1 [Q_3(2S_z^2 - S_x^2 - S_y^2) + \sqrt{3} Q_2(S_y^2 - S_z^2)] + \\ + \epsilon_2 [Q_4(S_x S_y + S_y S_x) + Q_5(S_x S_z + S_z S_x) + Q_6(S_y S_z + S_z S_y)] \end{aligned} \right.$$

where  $\epsilon_1$  and  $\epsilon_2$  are constants proportional to  $\lambda^2/(E_n - E_0)^2$ .

After expressing the normal coordinates of the cluster in the normal modes of the lattice and multiplying the square of the modulus of the matrix elements by the phonon density, the relaxation rates become:

$$(1.60) \quad U_{ij_a} = 1/\hbar^2 \langle \rho(\omega_{ij}) | \mathcal{H}_{SL}(i p_k, j(p_k + 1)) |^2 \rangle_{av}$$

With (1.51), (1.52) and (1.53) one has  $U_{ij} \propto T\omega_{ij}^2$ . At low fields and at  $T = 1.4^\circ\text{K}$  it is found that  $U \approx 50 \text{ s}^{-1}$ .

To obtain the power which the spin system is able to transfer towards the lattice from the values of  $U_{ij}$ , one has to take a suitable average over all energy levels.

We will postpone this calculation to [1.7] where a more general discussion of the power transfer will be given.

The values of  $U_{ij\text{ind}}$  calculated with (1.55) are independent of  $\omega_{ij}$ . The value of the exponent  $\alpha$  for the adiabatic processes equals 6, made up of an  $\omega^4$  dependence of the number of lattice vibrations taking part in the process, and an  $\omega^2$  factor due to (1.49).

One of the underlying assumptions for calculating  $U_{ij\text{ind}}$  is that the phonon wave length is large compared to the dimensions of the water octahedron, a condition which is only fulfilled at temperatures well below the Debye temperature, which is about  $80^\circ\text{K}$  for the alums.

#### B. The non-adiabatic terms.

If one takes into account the contribution of the energy of the phonon or spin jump  $\hbar\omega_{ij}$  to the energy difference in the denominator of (1.05), the second order perturbation of the lattice vibrations on the spins does not become zero, and can be relatively large in cases where the energy difference of the orbital levels between which  $\mathbf{L}$  has non-vanishing matrix elements, is small so that one cannot neglect  $\hbar\omega_{ij}$  compared to  $E_n - E_0$ .

An example of this case is TiCs alum where this splitting is about  $400 \text{ cm}^{-1}$  which is small compared to the corresponding value of about  $23000 \text{ cm}^{-1}$  for  $\text{Cr}^{+++}$  in CrK alum.

When developing the energy denominator, in which because of energy conservation the phonon frequency has to be  $\omega_{ij}$ , one finds for the matrix element of  $\mathcal{H}_{SL}$  by perturbation with the orbital levels  $n$

$$(1.61) \quad \begin{aligned} \langle 0, i, p_k | \mathcal{H}_{SL} | 0, j, p_k + 1 \rangle = \\ = \sum_n \frac{-2\hbar\omega_{ij}}{(E_n - E_0)^2} \langle 0, i | \mathcal{H}_{SO} | n, j \rangle \langle n, p_k | \mathcal{H}_{OL} | 0, p_k + 1 \rangle. \end{aligned}$$

The relaxation rate will have the same form as in (1.59), but due to the appearance of  $\omega_{ij}$  in (1.60), one finds  $U_{ij} \propto \omega_{ij}^4 T$  for  $\hbar\omega_{ij} \ll kT$ .

For the indirect processes the exponent  $\alpha$  in (1.56) will be 8, which is 2 higher than for the adiabatic terms for the same reason why  $\omega_{ij}$  appeared in (1.61).

For  $\text{Cu}^{++}$  in CuK tutton salt calculations have been made by NAGAOKA [44] on the same basis as those of VAN VLECK. The five orbital levels in the lowest multiplet are, in a cubic crystal field, split into a lower lying doublet and a triplet with a separation  $\Delta$  of  $15500 \text{ cm}^{-1}$ .

The rhombic component in the electric field splits the doublet with a separation of say  $\Delta'$ . This last splitting has no influence on the  $g$ -factor

in first order, but does influence the relaxation rates. The adiabatic and non-adiabatic terms seem to be of about equal importance. NAGAOKA expects a highly anisotropic  $U_d \propto H^4$  depending on  $(\Delta'/\Delta)^2$ . This rate is expected to become extremely small when  $\mathbf{H}$  is parallel to one of the axes of the crystal field.

[1.5.5] The Temperley effect. It has been known for a long time that the discrepancies between these theories and experiments are quite serious in the liquid helium range. The relaxation rates in that range for the concentrated salts are usually found to be a decreasing instead of an increasing function of  $\omega_{ij}$  while the temperature dependence is stronger than expected for the direct process, but not strong enough for the indirect ones. So for undiluted CrK-alum it is found that  $U \propto T^3$  and for undiluted FeNH<sub>4</sub>-alum  $U \propto T^5$ . The diluted salts seem to behave more according to VAN VLECK's theory.

TEMPERLEY [45] attempted to explain these discrepancies by supposing that by spin-spin interactions a number of spins jump at the same time, creating a phonon with the total energy. This effect could explain the field dependence of the relaxation probabilities. To explain also the temperature dependence one has to assume that a large number of spins jump together making the excited phonon frequency  $\omega \gg kT/\hbar$ .

VAN VLECK [36] doubted whether this effect is large enough. We shall discuss it later in more detail.

### [1.6] *Equilibrium and saturation of multilevel spin systems*

[1.6.1] The attainment of equilibrium in spin systems with  $S > 1/2$  can be different from the case of  $S = 1/2$  in this respect, that in addition to the processes considered there, the separations of the energy levels may be such as to allow flip-flip or flop-flop processes requiring no energy. These processes become possible because of energy splittings at zero magnetic field.

GORTER, DREWES and VERSTELLE [12] used this picture for the description of their experimental results, but did not work it out so that it explains the experimental results quantitatively.

BLOEMBERGEN e.a. [46] considered the possibility that a multiple effect of the spin-spin interactions is important. The idea is that at points where the resonance lines of different spin transitions overlap, flip-flop processes ( $\propto B^2$  in (1.30)) between neighbouring ions occur. They call the rate at which this takes place the cross relaxation rate  $U_{cr}$ .

Jumps in which more than two spins take part, may sometimes increase  $U_{cr}$  considerably, and for LiF it is possible to explain the short times required to establish spin equilibrium [47] by considering triple spin processes.

For the overlap they take the product of the shape functions of the two resonance lines. If these lines are far apart compared to the line

width, this overlap will be small, reducing the cross relaxation rate considerably.

When saturating a single resonance line of the absorption spectrum  $U_{cr}$  becomes important when comparable with the spin lattice relaxation rate. Calculations for similar processes have been made by ANDERSON [21] when he considered the effect of the exchange on the fine structure of resonance lines. The jump rates he considered were of the order of  $\omega_d$ . At this moment we are interested in much smaller rates, of the order of  $10^{-6} \omega_d$ .

The resonance transitions can be considered as weakly coupled oscillators. In the case considered by ANDERSON the coupling is strong and one therefore gets an appreciable distortion of the initial resonance lines. In the case considered here, however, the distortion will be too small to be observable. The exact values of  $U_{cr}$  will be difficult to calculate, but there is no doubt that in concentrated salts the interactions are usually so large as to produce saturation of the total spin system when saturating a single resonance line with a radio frequency field.

[1.6.2] No cross relaxations. We will consider first the case of low magnetic concentrations without cross relaxation. At times much longer than the spin-spin relaxation time  $\tau_2$  after applying a r.f. magnetic field to a sample in a static magnetic field, the transverse magnetization will be damped out, and the spin system can be described by the population densities  $n_i$  of levels  $i$ . There are  $2S+1$  levels and we have always

$$(1.62) \quad \sum_1^{2S+1} n_i = N$$

the total number of ions present. We shall discuss the rates of change of  $n_i$  and the influence on  $n_i$  of radio frequency fields at the various resonances. This can be done by setting up equations of the type (1.22).

The transition rates from level  $i$  to level  $j$  due to interaction with the surroundings are called  $U_{ij}$  and those due to r.f. fields  $W_{ij}$  the sum being  $V_{ij} = U_{ij} + W_{ij}$ .

Because of (1.23) we have

$$(1.63) \quad U_{ij} = U_{ji} e^{\hbar\omega_{ij}/kT}$$

with  $\hbar\omega_{ij} = E_i - E_j$  and also we have  $W_{ij} = W_{ji}$ .

We will now use a treatment analogous to that of LLOYD and PAKE [48].

$$(1.64) \quad \frac{dn_i}{dt} = \sum_j' -n_i V_{ij} + n_j V_{ji} \quad (i, j = 1 \dots (2S+1))$$

where the prime means that the sum is taken for all values of  $j \neq i$ . Of the  $2S+1$  equations (1.64) there are  $2S$  independent ones, from which one variable can be eliminated with (1.62). We are left with  $2S$  simultaneous differential equations with  $2S$  independent variables.



For the difference between the populations of level  $j$  and  $k$  one can write with (1.68)

$$(1.70) \quad \Delta_{jk} = N \frac{C_{j1} - C_{k1} + W_{12}(C_{j1,12} - C_{k1,12})}{D + W_{12}C_{12}}$$

The powers absorbed at the various frequencies in the case of well-separated resonances is found from

$$(1.71) \quad P_{ij} = \Delta_{ij} \hbar \omega_{ij} W_{ij}$$

Relations between the various cofactors can be obtained by realizing the in equilibrium

$$(1.72) \quad (\Delta_{jk})_{W=0} = \frac{N}{2S+1} \frac{\hbar \omega_{jk}}{kT}$$

The cases pertaining to the experimental conditions will be calculated in the appropriate places.

[1.7] *The power transfer between spin and lattice systems*

The relaxation rates as discussed in [1.5] enable us to calculate the power transfer between spin and lattice systems. For the case of cross relaxation rates faster than the spin lattice relaxation rate, the spin system will come into equilibrium at a temperature  $T_S$  in a time  $1/U_{cr}$ , short compared to  $\tau_1$ . The spin lattice relaxation will then take place according to a simple exponential decay  $e^{-t/\tau_1}$ , and is due to the power transfer of all transitions. To express the power transfer between spins and lattice we will not use the populations  $n_i$  of the different levels. This can be done for the case where the spectrum consists of well-separated lines, but if these are overlapping ones, individual level populations lose their meaning.

For the power absorbed from a r.f. magnetic field by the magnetic material, we have (cf. (1.26))

$$(1.73) \quad P_m = QW/T_S$$

where  $W$  is the induced transition rate  $W_{ij}$ , summed over all possible Larmor frequencies present in the material. The distribution of the spins over their energy levels is described by the density matrix.

$$(1.74) \quad \rho_S(E_i) = \frac{\exp -E_i/kT_S}{\sum_i \exp -E_i/kT_S}$$

where  $E_i$  are the eigenvalues of the spin Hamiltonian  $\mathcal{H}_{sp}$  with interactions.

[1.7.1] *Direct processes.* For the lattice induced transition rates due to the direct processes, we take the integrant of (1.51), without the shape factor. Integration over the shape of the transition as was performed there, is not necessary as we include here the spin-spin interactions in the spin Hamiltonian.

The energy transferred from the spin system in temperature equilibrium to the lattice, by the direct process will be:

$$(1.75) \quad P_{\text{tr}} = \sum_{ij} \hbar \omega_{ij} [U_{ija} \rho_S(E_i) - U_{jia} \rho_S(E_j)].$$

Due to conservation of energy we have  $\omega_k = \omega_{ij}$  and with (1.51) formula (1.75) becomes

$$(1.76) \quad P_{\text{tr}_d} = \sum_{ij} (\hbar \omega_{ij})^{\alpha+1} |\langle i | \mathcal{H}'_1(\mathbf{S}) | j \rangle|^2 \{ \rho_S(E_i) (p_{ij} + 1) - \rho_S(E_j) p_{ij} \}.$$

The factor in brackets contains the part dependent on spin and lattice temperature  $T_L$ .

For  $T_S \rightarrow \infty$  it is seen that, when  $p_{ij}$  stays finite, the power transfer becomes independent of  $p_{ij}$  and is proportional to the number of ions in the upper state. The power transfer then found could be called spontaneous emission of phonons analogous to the situation with photons.

For the case  $\hbar \omega_{ij} \ll kT_L$ , (1.76) can be rewritten with (1.52) as:

$$(1.77) \quad P_{\text{tr}_d} = \sum_{ij} \eta_{ija} T_L \left( \frac{1}{T_L} - \frac{1}{T_S} \right) = \eta_d T_L \left( \frac{1}{T_L} - \frac{1}{T_S} \right)$$

where the power transfer constant  $\eta_d$  for the direct process equals

$$(1.78) \quad \eta_d = \sum_{ij} \eta_{ija} = \sum_{ij} (\hbar \omega_{ij})^{\alpha+1} |\langle i | \mathcal{H}'_1(\mathbf{S}) | j \rangle|^2.$$

The summation in (1.78) may be performed by a diagonal sum.

For the case of  $\text{Cr}^{+++}$  in CrK alum we found (cf. [1.5.4]) that  $\alpha$  equals 3 for the adiabatic terms in the direct process. For  $\eta_d$  we then find:

$$(1.79) \quad \eta_d \propto \text{Tr}[[\mathcal{H}'_1 \mathcal{H}_{\text{sp}}] \mathcal{H}_{\text{sp}}]^2.$$

The non-adiabatic terms would require the calculation of a sixth moment.

[1.7.2] Indirect processes. To calculate the power transfer due to the indirect processes, the same procedure as above is followed. For the transition rates we take the integrand of (1.55) again without the shape factor  $g(\omega - \omega_{ij})$ . The power transferred is then found to be

$$(1.80) \quad \left\{ \begin{aligned} P_{\text{tr}_{\text{ind}}} &= \sum_{ij} \int_0^{\omega_0} \int_0^{\omega_0} \rho(\omega_k) \rho(\omega_l) |\langle i | \mathcal{H}'_2 | j \rangle|^2 \rho_S(E_i) \frac{(\hbar \omega_{ij})^2}{k} \left( \frac{1}{T_L} - \frac{1}{T_S} \right) d\omega_k d\omega_l = \\ &= \sum_{ij} \eta_{ij_{\text{ind}}} T_L \left( \frac{1}{T_L} - \frac{1}{T_S} \right). \end{aligned} \right.$$

The power transfer constant  $\eta_{\text{ind}}$  due to the indirect processes becomes

$$(1.81) \quad \eta_{\text{ind}} = \sum_{ij} \eta_{ij_{\text{ind}}} = \sum A (\hbar \omega_{ij})^2 |\langle i | \mathcal{H}'_2 | j \rangle|^2 T_L^\alpha$$

where  $A$  is a constant and  $\alpha$  depends on whether adiabatic or non-adiabatic terms are important, and on the integration over the densities of the

lattice vibrations (cf. (1.56)). The summation can again be performed by a diagonal sum

$$(1.82) \quad \eta_{\text{ind}} \propto \text{Tr}[\mathcal{H}_2' \cdot \mathcal{H}_{\text{sp}}]^2.$$

[1.7.3] The influence of exchange interactions on the power transfer for the case of  $S=1/2$  is different for the direct and indirect processes. For  $S=1/2$ ,  $\mathcal{H}_1$  and  $\mathcal{H}_2$  can only contain the spin operators linearly. In section [1.4] (cf. (1.33)) we have discussed that the fourth moment of the spin operators  $\sum_i S_{x,y,z_i}$  is influenced by the exchange but because of commutation properties the second moment is not. Therefore  $\eta_d$  will be influenced by exchange interactions. If  $\omega_{\text{ex}} \gg \omega_L$  the lattice vibrations up to the frequency  $\omega_{\text{ex}}$  can be excited.

The value of  $\eta_{\text{ind}}$  does not depend on exchange interactions when all ions are equivalent. For  $S > 1/2$  each salt has to be considered separately.

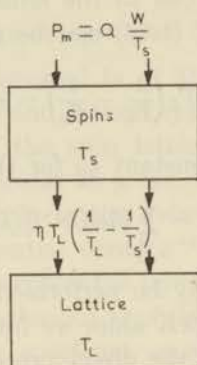


Fig. 1.6. Model for the energy balance.

[1.7.4] The power balance equations are obtained by combining (1.73) and (1.77) or (1.80). The situation is sketched in fig. 1.6. The rate of change of the internal energy  $U_S$  of the spin system is:

$$(1.83) \quad \frac{dU_S}{dt} = \frac{QW}{T_S} - \eta T_L \left( \frac{1}{T_L} - \frac{1}{T_S} \right).$$

And the steady state solution:

$$(1.84) \quad T_S = T_L + \frac{QW}{\eta}$$

which with (1.73) results in:

$$(1.85) \quad P_m = \frac{QW}{T_L + QW/\eta}$$

and for the case where (1.26) is valid

$$(1.86) \quad \tau_{1st} = \frac{Q}{2\eta T_L} = \frac{N(h\omega)^2}{2k(2S+1)\eta T_L}$$

To solve for the transient solution of (1.83) we realize that for  $\mathbf{H}$  kept constant

$$(1.87) \quad \frac{dU_s}{dt} = \frac{b+CH^2}{T_s^2} \frac{dT_s}{dt}$$

where  $(b+CH^2)/T_s^2$  is the spin specific heat at constant magnetic field (cf. [11]), and  $C$  is the Curie constant. The term  $b$  is made up of the various spin interactions and the zero field splitting.

Solving (1.83) and (1.87) for the case that after  $t=0$  the induced transition rate has the value  $W$  and at  $t=0$  the spin temperature is  $T_s(0)$ :

$$(1.88) \quad \left( \frac{1}{T_s(t)} - \frac{\eta}{QW + \eta T_L} \right) = \left( \frac{1}{T_s(0)} - \frac{\eta}{QW + \eta T_L} \right) e^{-\frac{QW + \eta T_L}{b + CH^2} t}$$

The magnetization  $\mathbf{M} = \mathbf{CH}/T_s$  will thus show an exponential change towards equilibrium with a relaxation time

$$(1.89) \quad \tau_{1tr} = \frac{b + CH^2}{QW + \eta T_L}$$

The ratio between the relaxation times as found by the steady state method using formula (1.26) and by the transient method with  $W=0$  is with respect to (1.86) and (1.89)

$$(1.90) \quad \frac{\tau_{1tr}}{\tau_{1st}} = \frac{2}{3} S \cdot (S+1)(2S+1) \gamma^2 \frac{(b/C + H^2)}{\omega^2}$$

At high magnetic fields ( $H^2 \gg b/C$ ) when the relation  $\omega = \gamma H$  holds, this factor becomes 1, 4, 10, 20, 35 for  $S = 1/2, 1, 3/2, 2, 5/2$  respectively.

The background for the difference between  $\tau_{1tr}$  and  $\tau_{1st}$  lies in the derivation of the equation (1.26) which was obtained by considering only the relaxation probability at the saturated transition, while one actually has to consider the total power transfer between spin system and lattice as was done in formulas (1.77) and (1.83) leading to (1.85).

[1.7.5] For the case  $W=0$  the values of  $\tau_{1tr}$  in (1.89) due to the direct process are calculated by VAN VLECK [36] for CrK alum and are:  $\tau_{1tr} = 11; 9; 6.7; \text{ and } 3$  ms for  $H$  equal to 0; 0.5; 1 and 3 K $\theta$  respectively.

The order of magnitude compares well with the experimental data; however, the temperature and field dependence for concentrated substances are completely different. This will be discussed later. For the indirect processes VAN VLECK finds

$$(1.91) \quad \tau_{1tr} = \tau_0 \frac{b + CH^2}{b + pCH^2}$$

This formula is identical with the formula used earlier by BRONS [49] to describe the experimental results at liquid air temperatures. The value of  $p$  for CrK alum is expected to be between 0.6 and 0.4, dependent on which of the normal modes  $Q_i$  of the water octahedron is the most effective

to produce relaxation, but independent of the values assigned to the cubic field splitting of the orbits and the zero field spin splitting. The value of  $p$  depends on the commutator (1.82) and is expected also not to depend on temperature. For most salts this is found not to be the case, however (cf. [11]). This discrepancy is rather serious and must not be dismissed lightly. To obtain more insight into the processes involved it seems advisable to determine experimentally and theoretically the anisotropy of  $p$  (or  $\eta_{\text{ind}}$ ) and the influence of the exchange interactions.

VAN VLECK has averaged his values of the power transfer over a gaussian distribution of the magnetic field, thus taking into account the effect of dipolar fields. It is better, however, to take in the commutators for calculating  $\eta$ , the total spin Hamiltonian with spin-spin interactions, making the calculations exact. This will be considered more fully in Chapter IV.

[1.7.6] Deviations from Curie's law. For the case that the spin splittings become of the order of  $kT_s$ , we have to contain the density matrix in (1.76) and (1.80). The magnetic absorption is most easily found by using one of the KRAMERS-KRONIG relations [50] [51]

$$(1.92) \quad \chi'(\omega_1) - \chi'(\infty) = \frac{2}{\pi} \int_0^{\infty} \frac{\omega \chi''(\omega)}{\omega^2 - \omega_1^2} d\omega.$$

This relation only holds when the magnetization is a linear function of  $h$ , so at low r.f. fields.

For the static susceptibility one finds

$$\chi_0 - \chi_{\infty} = \frac{2}{\pi} \int_0^{\infty} \frac{\chi''(\omega)}{\omega} d\omega.$$

When the line width of the transition is temperature independent we see that the temperature dependence of  $\chi''$  and  $\chi_0$  are the same.

For many salts the Curie-Weiss law holds

$$(1.93) \quad \chi_0 \propto \chi'' \propto \frac{1}{T_s - \theta} \text{ for } T_s \gg \theta.$$

At higher r.f. fields one can in first approximation insert  $T_s$  instead of the bath temperature as is done in (1.93).

When short range order effects are neglected, the curves  $\chi_0/\chi''$  vs.  $h^2$  as drawn in fig. 1.3 will still be straight lines, with the same slope, but having the ordinate  $(1 - \theta/T_L)$  at  $h^2 = 0$ . So for an antiferromagnetic coupling they are higher, and for a ferromagnetic one lower. We assumed the line width to be temperature independent but this is not realised for  $T_L \approx \theta$ .

[1.8] *The relaxation method*

When the field applied to a paramagnetic substance is changed, the magnetization will be able to follow this change if the rate is slow enough. At higher rates  $M$  will have a phase lag, with subsequent absorption and dispersion. This provides a method for determining  $\tau_1$ , the so-called relaxation method. The technique has been developed mainly by GORTER e.a. [11] [52].

The spin system is again regarded as an ensemble in internal equilibrium at a temperature  $T_S$ , which was first done by CASIMIR and DU PRÉ [53]. We can start therefore with (1.77) setting  $W = 0$

$$(1.94) \quad \Delta U_S = -\eta/T_L \Delta T dt.$$

We are interested in cases where  $T_S \approx T_L$ , as the relative variations in  $H$  are kept small. Changing  $H$  will change the internal energy by an amount

$$(1.95) \quad \Delta U_S = C_H \left( \frac{\partial T}{\partial M} \right)_H \Delta M + C_M \left( \frac{\partial T}{\partial H} \right)_M \Delta H$$

where  $C_H$  and  $C_M$  are the specific heats of the spin system at constant field and constant magnetization respectively.

On the other hand we have

$$(1.96) \quad \Delta T = T_S - T_L = \left( \frac{\partial T}{\partial M} \right)_H \Delta M + \left( \frac{\partial T}{\partial H} \right)_M \Delta H.$$

From equations (1.93), (1.94) and (1.95)  $\Delta T$  can be eliminated and one arrives at the following equation

$$(1.97) \quad \left( C_H + \frac{\eta}{T} dt \right) \left( \frac{\partial T}{\partial M} \right)_H \Delta M + \left( C_M + \frac{\eta}{T} dt \right) \left( \frac{\partial T}{\partial H} \right)_M \Delta H = 0.$$

We now superpose on  $H$  a parallel sinusoidal component and look for the corresponding component in  $M$  and  $T_S$

$$(1.98) \quad \begin{cases} H = H_c + h e^{i\omega t} \\ M = M_c + m e^{i\omega t}. \end{cases}$$

The static and the complex susceptibility are defined as resp.

$$\chi_0 = \left( \frac{\partial M_c}{\partial H_c} \right)_T \quad \text{and} \quad \chi = \chi' - i\chi'' = m/h.$$

Inserting these definitions in (1.96) results in the equation for the frequency dependent susceptibility.

$$(1.99) \quad \chi/\chi_0 = \frac{i\omega C_M + \eta/T}{i\omega C_H + \eta/T}$$

or with

$$(1.100) \quad F = \frac{C_H - C_M}{C_H} = \frac{CH^2}{b + CH^2}$$

$$(1.101) \quad \tau_1 = \frac{C_H T}{\eta} = \frac{b + CH^2}{\eta T} = \frac{C_H \cdot T}{\eta}$$

one finds

$$(1.102) \quad \chi/\chi_0 = (1-F) + \frac{F}{1+i\omega\tau_1}.$$

At low frequencies one finds normally  $\chi = \chi_0$ , and at high frequencies

$$\chi_{ad} = (1-F)\chi_0 = \frac{C_M}{C_H}\chi_0,$$

the so-called adiabatic susceptibility. At these high frequencies the spin system is supposed to be still in internal equilibrium.

#### REFERENCES

1. VAN VLECK, J. H., *The Theory of Electric and Magnetic Susceptibilities*, Oxford Univ. Press. (1932).
2. PRYCE, M. H. L., *Phys. Rev.* **80**, 1107 (1950).
3. BETHE, H., *Ann. Phys.* **V** 3, 133 (1929).
4. MULLIKEN, R., *Phys. Rev.* **43**, 279 (1933).
5. JAHN, H. A., *Proc. Roy. Soc.* **164**, 117 (1938).
6. PRYCE, M. H. L., *Proc. Phys. Soc. A* **63**, 25 (1950).
7. BLEANEY, B. and K. W. H. STEVENS, *Rep. Prog. Phys.* **16**, 107 (1953).
8. BOWERS, K. D. and J. OWEN, *Rep. Prog. Phys.* **18**, 304 (1955).
9. BLOCH, F., *Phys. Rev.* **70**, 460 (1946).
10. KRAMERS, H. A., *Quantentheorie des Elektrons und der Strahlung*, Leipzig (1938), P. 216.
11. GORTER, C. J., *Paramagnetic Relaxation*, Elsevier Publ. Co., Amsterdam (1947).
12. VERSTELLE, J. C., G. W. J. DREWES and C. J. GORTER, *Physica* **24**, 632 (1958). *Commun. Kamerlingh Onnes Lab. Leiden No. 311b.*
13. SMITS, L. J., H. E. DERKSEN, J. C. VERSTELLE and C. J. GORTER, *Physica* **22**, 773 (1956). *Commun. no. 304d.*
14. BLOEMBERGEN, N. and S. WANG, *Phys. Rev.* **93**, 72 (1954).
15. YOKOTA, M., *J. Phys. Soc. Jap.* **10**, 762 (1955).
16. ABRAGAM, A. and W. G. PROCTOR, *Phys. Rev.* **109**, 1441 (1958).
17. KRONIG, R. and C. J. BOUWKAMP, *Physica* **6**, 290 (1939).
18. BROER, L. J. F., Thesis, Amsterdam (1945).
19. BLEANEY, B., G. S. BOGLE, A. H. COOKE, R. J. DUFFUS, M. C. M. O'BRIEN and K. W. H. STEVENS, *Proc. Phys. Soc. A* **68**, 57 (1955).
20. VAN VLECK, J. H., *Phys. Rev.* **74**, 1168 (1948).
21. ANDERSON, P. W., *J. Phys. Soc. Jap.* **9**, 316 (1954).
22. KUBO, R. and K. TOMITA, *J. Phys. Soc. Jap.* **9**, 888 (1954).
23. GORTER, C. J. and J. H. VAN VLECK, *Phys. Rev.* **72**, 1128 (1947), *Comm. Suppl. No. 97a.*
24. WRIGHT, A., *Phys. Rev.* **76**, 1826 (1949).
25. VOLGER, J., F. W. DE VRIJER and C. J. GORTER, *Physica* **13**, 653 (1947).
26. BROER, L. J. F. and J. KEMPERMAN, *Physica* **13**, 465 (1947).
27. ANDERSON, P. W. and P. R. WEISS, *Rev. Mod. Phys.* **25**, 269 (1953).
28. BLOEMBERGEN, N., Thesis, Leiden (1948).
29. PORTIS, A. M., *Phys. Rev.* **91**, 1071 (1953).
30. PURCELL, E. M., *Phys. Rev.* **69**, 681, (A) (1946).
31. DICKE, R. H., *Phys. Rev.* **93**, 99 (1954).
32. BLOEMBERGEN, N. and R. V. POUND, *Phys. Rev.* **95**, 8 (1954).
33. WALLER, I., *Z. Phys.* **79**, 370 (1932).

34. BLACKMAN, M., Proc. Roy. Soc. A 149, 117 (1935).
35. SOMMERFELD, A. and H. BETHE, Handbuch der Physik, Springer Verlag Berlin (1933) sec. ed. Vol 24/2, p. 500 ff.
36. VAN VLECK, J. H., Phys. Rev. 57, 426 (1940).
37. MEYER, J. W., Thesis, M.I.T. (1955).
38. HEITLER, W. and E. TELLER, Proc. Roy. Soc. A 155, 629 (1936).
39. FIERZ, M., Physica 5, 433 (1938).
40. KRONIG, R., Physica 6, 33 (1939).
41. VAN VLECK, J. H., J. Chem. Phys. 7, 72 (1939).
42. JAHN, H. A. and E. TELLER, Proc. Roy. Soc. A 161, 220 (1937).
43. VAN VLECK, J. H., J. Chem. Phys. 7, 61 (1939).
44. NAGAOKA, Y., J. Phys. Soc. Jap. 13, 1328 (1958).
45. TEMPERLEY, H. N. V., Proc. Camb. Phil. Soc. 35, Pt. II, 256 (1939).
46. BLOEMBERGEN, N., S. SHAPIRO, P. S. PERSHAN and J. O. ARTMAN, Cross relaxations in spinsystems, Harvard Univ. Technical report no. 285.
47. ABRAGAM, A. and W. G. PROCTOR, Phys. Res. 109, 1441 (1958).
48. LLOYD, J. P. and G. E. PAKE, Phys. Rev. 94, 579 (1954).
49. BRONS, F., Thesis, Groningen (1939).
50. KRAMERS, H. A., Atti Congr. Fis., Como 545 (1927).
51. KRONIG, R., J. Opt. Soc. Amer. 12, 547 (1926).
52. MAREL, L. C. VAN DER, Thesis, Leiden (1958).
53. CASIMIR, H. B. G. and F. K. DU PRE, Physica 5, 507 (1938). Comm. Suppl. No. 85a.

## CHAPTER II

### EXPERIMENTAL METHODS AND TECHNIQUES

#### [2.1] *Introduction*

In this chapter we shall discuss some specific techniques for determining the spin lattice relaxation time by means of paramagnetic resonance. There are two in principle different methods, which have been used up till now. With the first method, the steady state saturation technique, the decrease in relative energy absorption is measured as the microwave field strength is increased. The power transfer constant  $\eta$  or the relaxation time  $\tau_1$  is determined by making use of (1.85) and (1.86).

The second method displays with a low power r.f. signal the magnetic absorption and its return to equilibrium after being saturated with a pulse of high r.f. field. With the equations (1.88) or (1.65) the relaxation behaviour can be determined.

Steady state saturation is a heat transfer problem and the spins have a forced motion. The pulse method is more analogous to the relaxation method; a kind of  $RC$  time is measured. During the time the high power pulse is off, the spins describe a free-running precession. In the pulse method one can choose the saturating frequency to be different from the sensing frequency so that one transition is saturated and its influence on the energy level populations of other transitions is measured. These methods will be discussed at the end of this chapter.

#### [2.2] *Magnetic losses in resonant structures*

To increase the effects of magnetic resonance the samples are placed in a low loss resonant structure. Maxwell's equations for the electromagnetic field inside the resonator have therefore to be combined with the equations for the magnetization of the sample.

An elegant method of describing the behaviour of resonant structures has been given by PANNENBORG [1], by making use of the scattering matrix. The scattering matrix  $\bar{S}$  of a junction relates the vectors of the incoming to those of the outgoing waves. One of its most important properties is that for a lossless junction  $\bar{S}$  is unitary. By lumping the losses inside a resonator into an extra output line with a matched termination, its scattering matrix becomes unitary. The coupling of this line has to be made variable when the magnetic losses are changed. When non-linear effects of the magnetization become important, such as in parametric amplifiers etc., one has to go back to Maxwell's equations.

If the modes of vibration of the resonator are well separated, one can make fruitful use of the equivalent circuit method, where all the distributed losses and stored energies are concentrated in resistances and reactances. One of the disadvantages of this method is that one has to assign a specific location to the distributed circuit parameters. At another point along the transmission line, transformation of the impedance  $Z$  takes place, due to the finite wavelength and according to the well-known transmission line equations [2]. Therefore all circuit representations will from now on refer to a certain reference plane in the transmission line. For the details of microwave theory we refer to the current handbooks [3].

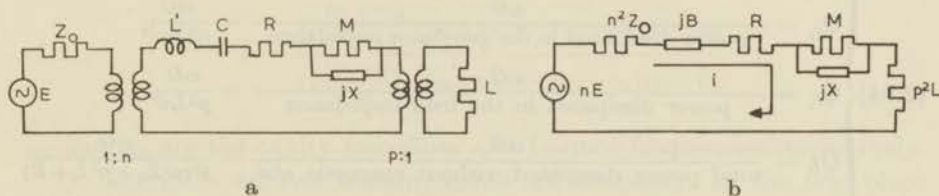


Fig. 2.1. a) Equivalent circuit of resonator with magnetic material.  
b) Transformed equivalent circuit.

The resonator without magnetic material can be represented as a simple series  $RLC$  circuit (cf. fig. 2.1) with a resistance  $R$  due to the losses in cavity walls and dielectric materials present. The reactance at frequency  $\omega$  equals

$$(2.01) \quad jB = j\left(\frac{\omega}{\omega_c} - \frac{\omega_c}{\omega}\right) Q_0 R$$

where  $\omega_c$  is the cavity resonance frequency  $1/\sqrt{L'C}$  and  $Q_0 = \omega L'/R$  the quality factor.

The influence of the magnetic material can be represented by the parallel combination of resistance  $M$  and reactance  $jX$ , due to the magnetic absorption and dispersion, in series with  $R$ .

If the paramagnetic resonance line has a Lorentzian shape we can with (1.13) write for the total impedance of the magnetic material,

$$(2.02) \quad Z_m = M/1 + j(\omega - \omega_L)\tau_2.$$

The cavity is coupled to a generator and a load. This coupling can be represented by transformers with transformation ratios of  $1:n$  and  $p:1$  resp. The generator with voltage  $E$  at frequency  $\omega$  is supposed to be matched to the input transmission line with a characteristic impedance  $Z_0$ . The load and the generator mesh can be transformed into the cavity mesh (fig. 2.1b).

Some of the power falling on the cavity will be reflected towards the generator, some will be transmitted towards the load, both depending on  $Z_m$ . This provides two ways of measuring magnetic r.f. susceptibilities. by transmission and by reflection.

Quantities more accessible to physical interpretation than impedances are quality factors. Taking for the energy stored in the volume  $V_c$  of the resonator

$$(2.03) \quad G = \frac{1}{16\pi} \int_{V_c} (\epsilon' E^2 + \mu' h^2) dV = \frac{1}{8\pi} \int_{V_c} \mu' h^2 dV$$

then the quality factors are defined as:

$$(2.04) \quad \left\{ \begin{array}{l} Q_0 = \frac{\omega \times \text{energy stored}}{\text{power diss. inside the cav. without magnetic abs.}} = \frac{\omega G}{i^2 R} \\ Q_{e_1} = \frac{\omega G}{\text{power dissipated in the generator impedance}} = \frac{\omega G}{n^2 Z_0 i^2} \\ Q_{e_2} = \frac{\omega G}{\text{power dissipated in the load impedance}} = \frac{\omega G}{p^2 L i^2} \\ Q_L = \frac{\omega G}{\text{total power dissipated without magnetic abs.}} = \frac{\omega G}{i^2 (n^2 Z_0 + p^2 L + R)} \\ Q_m = \frac{\omega G}{\text{power dissipated in the magnetic material}} = \frac{\omega G}{i^2 M} \end{array} \right.$$

As the inverse of the  $Q$ 's we define  $u = 1/Q$  with the same indices. As adding of inverse  $Q$ 's has often a simple physical meaning (adding of losses) we shall use mainly the  $u$ 's in the following.

The magnetically dissipated power is according to (1.14)

$$(2.05) \quad P_m = \frac{1}{2} \omega \chi'' \int h^2 dV_m,$$

integrated over the volume  $V_m$  of the magnetic material and so we have with (2.03) and (2.04);

$$(2.06) \quad u_m = \frac{1}{Q_m} = 4\pi f \chi''$$

where the filling factor  $f$  equals:

$$(2.07) \quad f = \frac{\int_{V_m} h^2 dV}{\int_{V_c} \mu' h^2 dV}.$$

### [2.3] The reflection method

[2.3.1] The reflection method to detect paramagnetic resonance and saturation will first be dealt with. The reflection coefficient  $\Gamma$  at a certain reference plane is defined as the ratio of the vector of the electric field of the backwards travelling wave to that of the forwards travelling wave, both waves in the same mode of propagation of the transmission line. For a transmission line with characteristic impedance  $Z_0$  terminated by an impedance  $Z$  we have by standard microwave theory

$$(2.08) \quad \Gamma = \frac{Z - Z_0}{Z + Z_0}$$

in the plane of  $Z$  or equally

$$(2.09) \quad \frac{Z}{Z_0} = \frac{1+\Gamma}{1-\Gamma}.$$

In fig. 2.1b the load impedance can be omitted and is taken zero. For  $\Gamma$  one obtains:

$$(2.10) \quad \Gamma = \frac{jB+R+M/[1+j(\omega-\omega_L)\tau_2]-n^2Z_0}{jB+R+M/[1+j(\omega-\omega_L)\tau_2]+n^2Z_0}.$$

Multiplying numerator and denominator by  $i^2/\omega W$ , and using the definitions of the  $u$ 's:

$$(2.11) \quad \Gamma = \frac{j2\frac{(\omega-\omega_c)}{\omega} + u_0 + u_m\{1-j(\omega-\omega_L)\tau_2\} - u_e}{j2\frac{(\omega-\omega_c)}{\omega} + u_0 + u_m\{1-j(\omega-\omega_L)\tau_2\} + u_e}.$$

$\omega_c$  and  $\omega_L$  are the cavity resonance and Larmor frequencies respectively.

To determine  $u_m$  two measurements are necessary. In the first place a determination of the reflection coefficient  $\Gamma_m$  with the magnetic field adjusted to the centre of the magnetic transition to be studied. Secondly the reflection coefficient  $\Gamma_0$  with the magnetic field at a high value, making  $u_m=0$ . This provides a determination of the relative external loading. When for both measurements the cavity is adjusted to resonance, then  $\Gamma_0$  and  $\Gamma_m$  are real numbers. In the following this adjustment is always supposed to be made. We keep the sign for  $\Gamma$ , however, and so  $\Gamma_0$  is negative when  $u_e > u_0$  corresponding to an overcoupled cavity, and  $\Gamma_0$  is positive when  $u_e < u_0$  for undercoupling. When  $u_m$  is positive we have  $\Gamma_m > \Gamma_0$  for both cases.

From the above-mentioned two measurements  $u_m$  can be calculated as we have with (2.11);

$$(2.12) \quad \frac{u_m}{u_e} = \frac{P_m}{P_{\text{ext}}} = \frac{1+\Gamma_m}{1-\Gamma_m} - \frac{1+\Gamma_0}{1-\Gamma_0} = \frac{2(\Gamma_m-\Gamma_0)}{(1-\Gamma_0)(1-\Gamma_m)}$$

where  $P_{\text{ext}}$  is the power dissipated in the external loading of the generator impedance, while there is also magnetic absorption.

Of the power  $P_i$ , incident on the iris, the part  $P_{\text{cav}}$  dissipated inside the cavity is, whilst there is also magnetic absorption,

$$P_{\text{cav}} = (1 - \Gamma_m^2)P_i$$

and the reflected power is

$$(2.13) \quad P_r = \Gamma_m^2 P_i.$$

The power dissipated externally can be found from (2.11) if  $\omega = \omega_c = \omega_L$  to be:

$$(2.14) \quad P_{\text{ext}} = \frac{u_e}{u_0 + u_m} (1 - \Gamma_m^2) P_i = (1 - \Gamma_m)^2 P_i.$$

If  $E$  is the electric field strength of the incident wave, then  $(1-\Gamma)E$  is the electric field inside the cavity. As the external loading does not change during the two experiments discussed above, we have with (2.14), (2.03) and (2.04) that  $P_{\text{ext}} \propto W \propto h^2$ . The proportionality factor between  $P_{\text{ext}}$  and  $h^2$  is only a geometrical one.

When the r.f. field is uniform over the sample dimensions the final form of the equations becomes:

$$(2.15) \quad \frac{P_{\text{ext}}}{P_m} = \frac{T_L P_{\text{ext}}}{QW_{ij}} + \frac{P_{\text{ext}}}{\eta}$$

$$(2.16) \quad \frac{P_{\text{ext}}}{P_m} = \frac{(1-\Gamma_m)(1-\Gamma_0)}{2(\Gamma_m - \Gamma_0)}$$

$$(2.17) \quad P_{\text{ext}} = (1-\Gamma_m)^2 P_t.$$

[2.3.2] Determination of  $\eta$ . A fast method of determining the reflection coefficients is to measure the power  $P_r$  reflected by the cavity with a microwave bridge. If  $P_t$  is the incident power,  $\Gamma$  follows from (2.13).

The first term of the right hand side of (2.15) is independent of  $h$  because  $W_{ij} \propto P_{\text{ext}} \propto h^2$ , giving a straight line for the  $P_{\text{ext}}/P_m \propto 1/\chi''$  versus  $P_{\text{ext}}$  plot if  $\eta$  and  $T_L$  are independent of  $h$ . The slope is  $1/\eta$ .

To calculate  $\tau_1$  with (1.86) or (1.101) one only has to know, moreover, the weight of the sample and the frequency  $\omega$ .

For the case of inhomogeneously broadened resonance lines the saturation behaviour becomes different (cf. [1.4.4]).

The determination of  $\tau_1$  by the method of BLOEMBERGEN, PURCELL and POUND reduces to measuring the r.f. field  $h_{1/2}$  at which  $\chi''$  has dropped to half its initial value. This occurs when the first and second terms on the right side of (2.15) become equal so that  $\eta = QW_{1/2}/T_L$  or with (1.26)

$$(2.18) \quad \frac{1}{2} \gamma^2 h_{1/2}^2 g(0) |\langle i | S_x | j \rangle|^2 = \frac{1}{\tau_1}.$$

This method involves a calibration of  $h$ , — which is difficult to obtain more precise than 30 %, — and knowledge of  $g(0)$  the matrix element. A serious disadvantage of Bloembergen's method is that when  $\eta$  or  $T_L$  depend on  $h$ , of which we shall see examples later, one does not use all the information available in the measurements.

[2.3.3] The polar impedance diagram. We shall briefly sketch what happens in the polar impedance diagram (cf. [2]). This diagram or Smith chart (fig. 2.2) represents the complex  $\Gamma$  plane. The loci of constant resistance and constant reactance form two families of orthogonal circles. The constant reactance circles, dotted-dashed in fig. 2.2, have centres on  $\text{Re } \Gamma = 1$ ; the constant resistance ones, the solid lines in fig. 2.2, their centres on the real  $\Gamma$  axis.

When varying the frequency of the generator, the impedance presented by an empty resonator without any other resonances nearby will, at

a certain reference plane, be a locus of constant resistance, as only the reactance is varied. The reflection coefficient is the vector drawn from the origin to the locus. Curve (a) corresponds to total reflection,  $R=0$ , curve (b)  $R < Z_0$  corresponds to an overcoupled cavity, curve (c)  $R = Z_0$ , to a matched cavity and curve (d)  $R > Z_0$  to an undercoupled cavity.

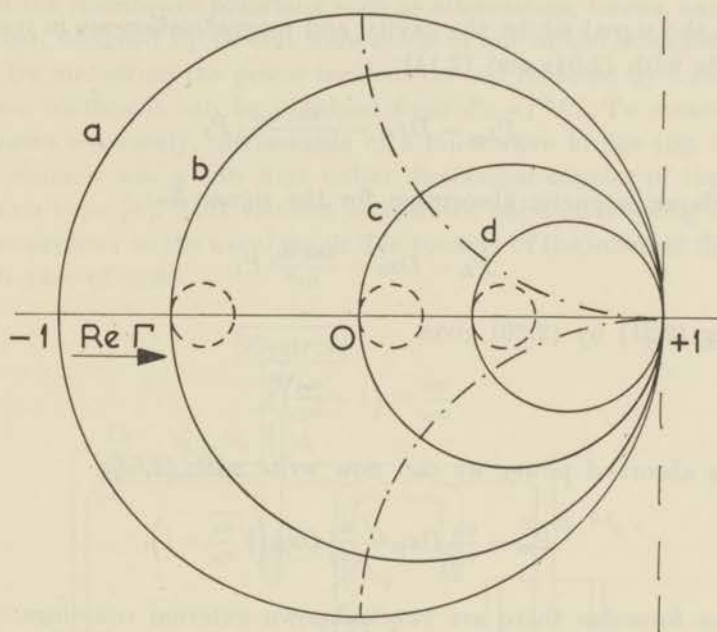


Fig. 2.2. Polar impedance diagram.

—	resistance circles.	a	$R = 0$
- · - · -	reactance circles.	b	$R < Z_0$
- - -	magnetic effect, $H$ varied.	c	$R = Z_0$
		d	$R > Z_0$

Suppose now the cavity is at resonance ( $\Gamma$  real), then varying  $\omega L$  ( $H$ ) will change  $Z$  according to the dashed circles due to the influence of the magnetic material. The reactance part is due to dispersion, the resistance to absorption. One observes that magnetic absorption increases the reflected power for undercoupled and matched cavities and decreases it for overcoupled cavities. As long as the magnetic material is dissipative, its impedance locus has of course to stay inside the cavity locus. Magnetic materials can be brought into an emissive state. Their locus is then inverted with the cavity resonance point as the centre of inversion.

#### [2.4] *The transmission method*

The calculating labour involved to obtain the saturation curves with the reflection method is quite substantial and we therefore tried to find another method which required less calculating time. We should like a formula like (2.15) where instead of  $P_{\text{ext}}$  a variable is used, proportional

to the square of the radio frequency field and directly accessible to measurement. Inspecting fig. 2.1 one sees that by inserting for the load a square law detector with detector sensitivity  $D$  the signal  $x$  becomes:

$$(2.19) \quad Dx = P_L = i^2 L \propto h^2.$$

If  $x_m$  is the signal whilst the cavity and magnetization are in resonance, one finds with (2.04) and (2.11):

$$(2.20) \quad P_{Lm} = Dx_m = \frac{4u_{e_1}u_{e_2}}{(u_L + u_m)^2} P_i$$

and without magnetic absorption for the signal  $X_0$ :

$$(2.21) \quad P_L = Dx_0 = \frac{4u_{e_1}u_{e_2}}{u_L^2} P_i.$$

Dividing (2.21) by (2.20) gives

$$\frac{x_0}{x_m} = \left(1 + \frac{u_m}{u_L}\right)^2.$$

For the absorbed power we can now write with (2.04)

$$(2.22) \quad P_m = \frac{u_m}{u_{e_2}} Dx_m = \frac{u_L}{u_2} Dx_m \left(\sqrt{\frac{x_0}{x_m}} - 1\right).$$

In these formulae there are two unknown external couplings, one can be eliminated, however, by varying the generator coupling with fixed load coupling so as to maximize  $P_L$  (2.21). This makes  $u_L = 2u_{e_1}$  and

$$(2.23) \quad P_L = x_0 D = \frac{u_{e_2}}{u_{e_1}} P_i.$$

Together with (2.22) follows

$$(2.24) \quad \frac{x_m P_i/x_0}{P_m} = \frac{1}{2} \left(\sqrt{\frac{x_0}{x_m}} - 1\right)^{-1}$$

which is the formula to be used for calculating the saturation graphs.  $P_i/x_0$  is an easily calibrated constant and  $x_m \propto h^2$ . If the difference  $x_0 - x_m = \delta \ll x_0$  we may expand the root:

$$(2.25) \quad \frac{x_m P_i/x_0}{P_m} = \frac{x_m}{\delta}.$$

As  $\delta$  and  $x_m$  are directly accessible to measurement, the calculations take very little time. The power dissipated by the magnetic material is then found to be

$$(2.26) \quad P_m = \frac{P_i}{x_0} \delta.$$

## [2.5] Apparatus for the reflection measurements

The experiments on the steady state saturation have been carried out at microwave frequencies around 10 KMHz. For the general theory and techniques of microwaves reference is made to the current handbooks on the subject, especially those of the M.I.T. series nos. 8, 9, 10 and 11. Most of the microwave plumbing such as attenuators, tuners, cavities etc. have been designed by us and were made in one of the laboratory workshops. By measuring the power incident on and reflected by a cavity, the reflection coefficient can be obtained from  $P_L = \Gamma^2 P_i$ . To measure these two powers separately, use is made of a microwave bridge (fig. 2.3). The bridge element was a 3db four outlet directional coupler of the RIBLET and SAAD type [4]. This element consists of pairs of coupling slots and is by far superior to the usual magic Tee because of the inherent directivity of each pair of slots.

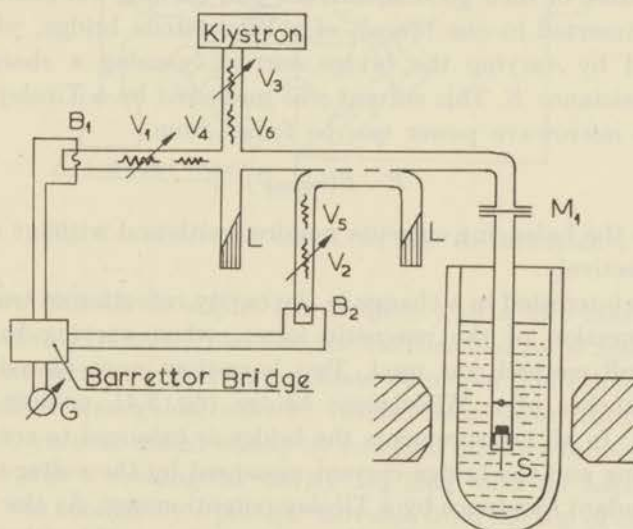


Fig. 2.3. Apparatus for measurements of reflection coefficients.

$B_1$  and  $B_2$  barrettors;  $V_1 \dots V_6$  attenuators;  $L$  matched load;  $M_1$  vacuum seal;  $S$  sample in  $2\lambda_g$  long cavity.

Initially a magic Tee has been used but sliding screw tuners were needed to obtain satisfactory behaviour of this bridge element.

For the high power microwave source was used a Philips 55395, a two cavity klystron, able to deliver 140 to 200 Watt C.W. power in the X band [5].

Because of the high powers used, special care has to be taken to prevent burning out of attenuators and detectors. For  $V_3$  we constructed a water attenuator, while the fixed attenuators  $V_4$ ,  $V_5$  and  $V_6$  were made of a ceramic caslode. Their size was chosen so as to keep the power dissipation in the calibrated variable attenuators  $V_1$  and  $V_2$  below the burning out level.

These variable attenuators contained a platinized glass vane as dissipative element. They were calibrated 3 times at three frequencies far apart with the aid of a barrettor bridge and also compared to each other. The reproducibility was within 0.1 db.

The matched terminations were made from double tapered caslode and had a voltage standing wave ratio below 1.1 in the frequency range used. A handy sliding match was made from a long piece of tapered oak just fitting inside the wave guide ( $V.S.W.R. < 1.08$ ).

For power detection we used silicon crystals or barrettors. Barrettors contain as sensitive element a very thin platinum wire which changes its resistance upon heating. Power measurements are made by using the equivalence of heating by microwaves or by a direct current. The barrettors were of the 821 type (Sperry or Narda Co.) with an operating resistance of  $200 \Omega$ . For power detection, barrettors compare favourably with crystals because of their good square law and burning out characteristics. They were inserted in one branch of a Wheatstone bridge, which could be balanced by varying the bridge current, causing a change in the barrettor resistance  $B$ . This current was measured by a Tinsley potentiometer. The microwave power can be found from

$$(2.27) \quad P = B(i_0^2 - i^2).$$

$i$  and  $i_0$  are the balancing currents required with and without microwave power respectively.

As we are interested in a change in the cavity reflection or transmission, due to saturation of the magnetic losses, when varying the incident power, a null method was used. Two barrettors were placed in neighbouring branches of a Wheatstone bridge (fig. 2.4), passing the same d.c. current. In all measurements the bridge is balanced to zero galvanometer reading and the bridge current measured by the voltage drop over the  $1 \Omega$  standard resistance by a Tinsley potentiometer. As the barrettors may need slightly different heating powers one could either give one barrettor an additional heating, by for instance a 100 KHz signal, or take the following procedure. Set switches  $S_1$  and  $S_2$  to the  $200 \Omega$  standard resistances  $R_1$  and  $R_2$ , adjust  $G$  to zero by  $R_5$ . Set  $S_1$  to barrettor  $B_1$  and balance with bridge current by  $R_7$  or  $R_8$ . This makes  $B_1$  equal to  $200 \Omega$ . Set  $S_2$  to  $B_2$  and balance with  $R_5$  keeping the bridge current the same. The bridge is now ready for power measurements. The incident microwave power  $P_i$  is measured by  $B_1$  (in fig. 2.3), when setting  $S_1$  to  $B_1$  and  $S_2$  to  $R_2$  and balancing by changing the bridge current. The difference between  $P_r$  and  $P_i$  is measured by setting  $S_1$  to  $B_1$  and  $S_2$  to  $B_2$  and balancing with the attenuator  $V_2$  in fig. 2.3.

A calibration for the difference in attenuation in the microwave bridge arms and the difference in the detecting sensitivities of  $B_1$  and  $B_2$  is obtained by replacing the cavity with a total reflection. To take measurements in quick succession it is necessary to heat the barrettors also to

about  $200 \Omega$  when not passing the bridge current. The time constant involved is of the order of one or two minutes and not at all the generally used time constant characterizing the ability of a barrettor to follow a modulation of the microwave power, which is of the order of 1 ms. The time constant involved here is much longer as it is determined by the establishment of a temperature distribution along the barrettor wire and holder after changing the wire dissipation.

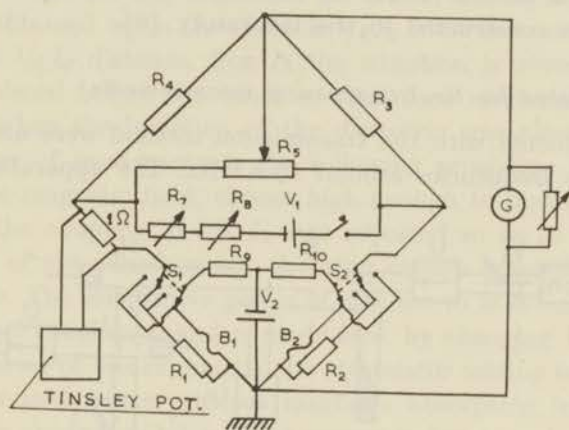


Fig. 2.4. Barrettor bridge.  $B_1$  and  $B_2$  barrettors.

It is more difficult to adjust the frequency of a two-cavity klystron than of a reflex klystron. Therefore the cavities had to be made tunable. Two different cavities with their cryostats were used. For the first cryostat a german silver waveguide, silvered inside, went down into the liquid helium bath, vacuum sealed on top by two thin mica windows  $\frac{1}{4} \lambda_g$  apart. At the end was a rectangular cavity  $2\lambda_g$  long with an adjustable iris. The cavity was tunable by a plunger movable from the top of the cryostat. The coupling could be adjusted before cooling to the desired value by placing a small capacitive screw in the middle of the iris. By screwing it in one initially increases the coupling, which decreases again after the iris has become resonant.

As it is not possible to adjust this coupling during a run and as sometimes the plunger stuck because of freezing, a different cavity of about 80 cm, or about  $18 \lambda_g$  long was constructed. This cavity was tunable with a teflon flap and the iris consisted of a movable copper sheet. Iris and tuner were located above the vacuum seal. Since the filling factor of the paramagnetic sample decreased more than the  $Q$  increased, there was a loss in sensitivity, but having ample sensitivity to start with we could spare some in exchange for convenience. The movable iris in this case provided, when closed, the total reflection needed for calibration of the barrettor sensitivities as discussed before. For the first cavity  $\Gamma=1$  was obtained by detuning the cavity far from resonance. That this really

provided a total reflection had been checked before by interchanging the detuned cavity by a total reflection. The unloaded cavity  $Q$ 's were of the order of 2800. This low value of  $Q_0$  was taken so as to make the whole set up not too frequency-sensitive. To prevent boiling bubbles of the helium inside the cavity to change the resonant frequency, this one was filled with foamplastic. The low temperature techniques used were those customary in our laboratory. The magnet had a resistance of  $2 \Omega$  and provided a field of  $10 \text{ K}\phi$  at  $100 \text{ A}$  current within a gap of about  $9 \text{ cm}$  and was constructed in the laboratory [6].

[2.6] *Apparatus for the transmission measurements*

The experiments with the transmission method were also carried out at microwave frequencies around  $10 \text{ KMHz}$ . The apparatus is sketched in fig. 2.5.

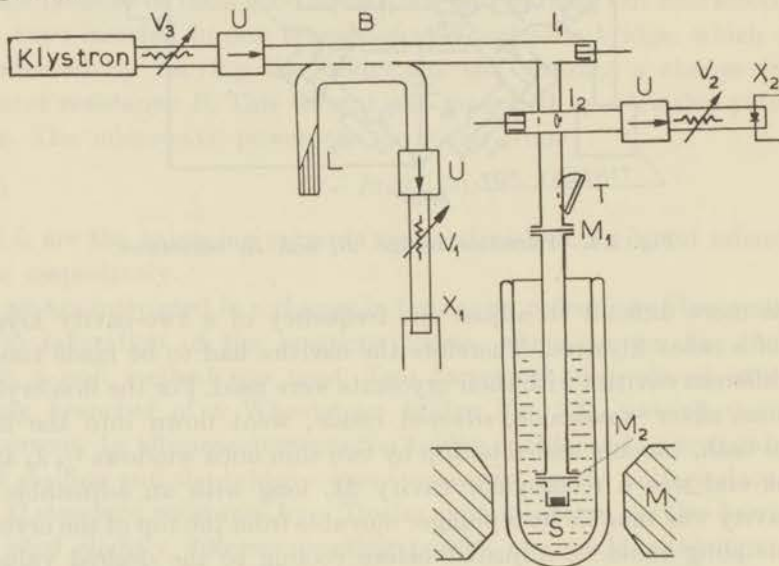


Fig. 2.5. Apparatus for transmission measurements.

$B$  directional coupler;  $I_1, I_2$  input, output coupling;  $L$  matched load;  $M_1, M_2$  vacuum seals;  $S$  sample;  $U$  unilines;  $V$  attenuators;  $X_1, X_2$  detecting crystals.

The same power source was used as with the reflection measurements. The power was detected by two carefully selected silicon crystals. The requirements for the selection were: a very close to square law detection and a difference in output between the two of less than  $0.1 \text{ mV}$  in the range from  $0$  to  $20 \text{ mV}$ , the difference being made zero at  $20 \text{ mV}$ .

In fig. 2.5 the incident power is sampled by crystal  $X_1$ , through a  $3 \text{ db}$  directional coupler [2.5] and the transmitted power by  $X_2$ . Their output voltages will be called  $x_1$  and  $x_2$  respectively from now on. The outputs were always kept below or equal to  $20 \text{ mV}$  and were measured by a Philips d.c. millivoltmeter G.M. 6010.

The cavity was about 80 cm long and tunable by a dielectric vane of teflon ( $Q_0 \approx 2800$ ). The irises had to be made variable, the input iris  $I_1$  in order to match the cavity to the generator, a condition set to the validity of equation (2.24), the output iris  $I_2$  in order to be able to work in a convenient range of  $V_2$ .

An easy way of doing this is by a movable shorting plunger in the output waveguide [7] as shown in fig. 2.5. The coupling takes place through the magnetic h.f. fields and for iris  $I_1$  for instance, maximum coupling is obtained when the short is  $1/4 \lambda_g$  from the centre of the iris, minimum at  $1/2 \lambda_g$  distance. For  $I_2$  the situation is reversed. The two irises were placed before the tuner so that their electrical distance did not change when the insertion of the dielectric was altered.

For a series of measurements the following procedure was used.

At a static magnetic field, chosen high enough to make the magnetic losses zero, the coupling of iris  $I_1$  was adjusted so as to maximize the transmission of the tuned cavity,  $I_2$  being chosen beforehand to a convenient value. The microwave power is now set to make  $x_2 = 20$  mV and the difference  $\delta$  between  $x_1$  and  $x_2$  made zero, by changing  $V_1$ . During the rest of this series of measurements the attenuator setting is not changed.

The transmitted power without magnetic absorption is given by  $x_1$ , with magnetic absorption by  $x_2$ . They correspond to  $x_0$  and  $x_m$  respectively in formulae (2.24) and (2.25) and can be simultaneously measured. This can most conveniently be done by a X-Y recorder. Most of the time we measured  $x_2 - x_1 = \delta$  and  $x_2$ , as they enter directly into equation (2.25). When the tracking of  $X_1$  and  $X_2$  was not according to the requirements set, a correction was made. The value of the detector sensitivity  $P_t/x_1$  in mW/mV is calibrated by substituting a barrettor for the cavity at the input branch. If this sensitivity is  $C$  db, then the input power during a run is  $P_t = C + V_1 + 10 \log x_1$  dbm, db above the 1 mW level.  $V_1$  is the attenuator setting in db.

#### [2.7] *Pulse methods for determining the relaxation times*

The principle of this method has been indicated in [2.1]. The approach of the magnetization towards its steady state value during or after a pulse of saturating power will depend on the transition observed and the initial situation. For the case of non-important cross relaxations, the considerations in [1.6.2] provide the necessary relations for interpreting the observations. For the case of internal spin equilibrium (cf. (1.88)), or one of the time constants  $1/\lambda_k$  (cf. (1.65)) much larger than the others, the change of the magnetization is according to a simple exponential.

The magnetization can be observed by a microwave signal of frequency  $\omega_s$  near the transition to be studied and an intensity so low as not to disturb the system appreciably. We will call this microwave field the sensing or signal field. The magnetization can be made to deviate from its equilibrium value by a pulse of high microwave power, called the

pump power, at frequency  $\omega_p$ . The pump may saturate the signal transition or one of the others when present. Observation of the fall of the magnetization during the high power pulse may provide information about the cross relaxations.

The situation where  $\omega_p = \omega_s$  has been employed by BOWERS and MIMS [8] and also by DAVIS and STRANDBERG [9]. An apparatus for this type of measurements is under test in our group, but only preliminary measurements have been made with it. In our set up  $\omega_s/2\pi$  can be changed in steps of about 100 MHz to other cavity resonances in the range of 8.3 to 11 KMHz. The apparatus is essentially the same as used for the transmission measurements. The signal frequency is generated by a low power klystron and is detected by a superheterodyne receiver with a sensitivity of about  $10^{-12}$  W.

Experiments with  $\omega_s/2\pi = 1420$  MHz and  $\omega_p/2\pi = 4000$  MHz or 10 KMHz were made in connection with the construction of a low noise microwave amplifier. From the characteristics of some types of these amplifiers it is possible to obtain information about the relaxation processes. We shall therefore mention briefly the principle of a so called three level maser as constructed by our group.

### [2.8] *The principle of operation of a three level maser*

[2.8.1] Introduction. In conventional microwave amplifiers (traveling wave tubes and klystron amplifiers) the source of energy is the kinetic energy of an electron beam which introduces a certain amount of noise into the amplifier. Recently it has been found possible to amplify a microwave signal by converting the internal energy of an atomic system directly into microwave energy. When the equilibrium of the system is disturbed in a particular manner it is possible to obtain an emissive condition, and when the medium is stimulated by a microwave signal, the energy thus stored can be emitted coherently. GORDON, ZEIGER and TOWNES [10] have coined the term "maser" to describe such "microwave amplification by stimulated emission of radiation". The small probability of spontaneous emission at radio frequencies (the main source of noise) makes it possible for such an amplifier to have a very low noise figure.

Of the many types of masers (discussed by WITTKÉ [11]) the only one giving continuous emission is the three level maser (BLOEMBERGEN [12]) using a paramagnetic material as the working substance.

For a detailed analysis of the characteristics of three level masers reference is made to the papers by BUTCHER [13] and for the work on this subject by our group to [14].

[2.8.2] Principle of operation. In section [1.6] we discussed the influence of microwave fields on the energy level populations of a multi-level spin system with negligible cross relaxations. Inspecting formula (1.70) it is seen that the difference in population  $\Delta_{jk}$  of level  $j$  and  $k$  can

become negative when  $C_{k1,12} \gg C_{j1,12}$  and  $W_{12}$  (at the pump frequency) is large enough, while levels 1 and 2 have to be non-adjacent ones. The power absorbed by the  $j$  to  $k$  transition also becomes negative when  $\Delta_{jk}$  becomes negative (cf. (1.71)) or in other words we have attained emission.

The frequency of the  $j$  to  $k$  transition will be taken to be the signal frequency  $\omega_s$ . Suppose the sample is placed in a reflection cavity. When the frequencies in formula (2.11) are so adjusted that  $\omega = \omega_L = \omega_s$ , it is seen that the reflected power becomes larger than the incident power when  $-u_m > u_0$  ( $\Gamma_m < -1$ ) so when the emitted power is larger than that dissipated in the cavity walls ( $u = 1/Q$  were defined in (2.04)). For this case we have obtained amplification. The bandwidth can be obtained from the total quality factor ( $Q_m$  is negative). Under certain conditions the power emitted by the sample will be so large that the amplifier breaks into oscillation.

Under the conditions of oscillation the signal intensity will build up, until the transition is so far saturated that the power emitted by the sample just compensates for the losses in the cavity and external coupling. The level of oscillation can be obtained from this condition

$$(2.28) \quad u_m + u_0 + u_e = 0.$$

In (1.70)  $\Delta_{jk}$  is determined by the pump intensity for small signal powers. For large signals, however,  $\Delta_{jk}$  will also depend on its intensity due to the presence of  $V_{jk} = U_{jk} + W_{jk}$  in  $D$  and  $C$ 's in (1.69). For a spin system with only three levels calculation of (1.70) becomes easy. Numerating the levels from the lowest and pumping between levels 1 and 3 results for high pump powers ( $W_{13}$  large) in an induced absorption at  $\omega_{23}$  of

$$(2.29) \quad P_{23} = \frac{N\hbar^2\omega_{32}}{3kT} W_{23} \frac{\omega_{32}\bar{U}_{23} - \omega_{21}\bar{U}_{12}}{\bar{U}_{21} + U_{23} + W_{23}}$$

where  $2\bar{U}_{ij} = U_{ij} + U_{ji}$ .

The condition for obtaining negative values of  $P_{23}$  is seen to be

$$(2.30) \quad \omega_{21}\bar{U}_{12} > \omega_{32}\bar{U}_{23}.$$

At low signal powers ( $W_{23} \ll U_{21} + U_{23}$ ) the ratio of the emitted power when  $W_{13} \rightarrow \infty$  to the absorbed power when  $W_{13} = 0$  is, when  $W_{23}$  is the same for both cases:

$$(2.31) \quad \frac{P_{23\text{em}}}{P_{23\text{ab}}} = \frac{u_{m\text{em}}}{u_{m\text{ab}}} = \frac{\omega_{21}\bar{U}_{12} - \omega_{32}\bar{U}_{23}}{\omega_{32}(U_{21} + U_{23})}$$

which depends only on the ratios of relaxation rates and frequencies of transitions 23 and 12, but not on filling factors, cavity  $Q$ 's, sample weight etc. In case of oscillations, we have mostly  $W_{23} \gg U_{21} + U_{23}$ . When this

condition is fulfilled over the dimension of the sample the maximum power emitted becomes, still with  $W_{13} \rightarrow \infty$ ;

$$(2.32) \quad P_{23\max} = \frac{N \hbar^2 \omega_{32}}{3 kT} (\omega_{21} \bar{U}_{12} - \omega_{32} \bar{U}_{23}).$$

It is noted that this expression does neither depend on line width, when homogeneously broadened, nor on matrix element and filling factor.

[2.8.3] In the experimental arrangement the crystals were placed in cavities resonant simultaneously at the signal and pump frequencies, and cooled by a refrigerant in a Dewar-glass. For the best amplifying characteristics the  $Q_0$  of the cavity must be high at the signal frequency and preferably also at the pump frequency. The filling factor  $f$  for the signal frequency must be as high as is consistent with the requirement to saturate throughout the crystal with the pump field.

A number of cavities has been used to obtain a variety of field configurations for the different frequencies, needed for the substances tested. Cavities used for 1420 and 3850 MHz were:

(1) A coaxial cavity  $\lambda/2$  long at 1420 MHz with a  $TE_{111}$  mode at 3850 MHz, and the  $3\lambda/2$  coaxial mode for 4260 MHz. This cavity had a high  $Q_0$  but the filling factor was poor. To increase  $f$  we tried:

(2) A double reentrant cavity approximately  $\lambda/4$  at 1420 MHz and  $3/4\lambda$  at 3850 MHz. To obtain the right electrical length for both frequencies, a disc of teflon or quartz was inserted at the electrical antinode of the 3850 MHz mode. As the 1420 MHz electric field was small in that region the disc mainly influenced the pump field pattern.  $Q_0$  was 4000 at 1.3 °K. Some unwanted modes were difficult to eliminate, and also because of another experiment to be described, the following cavity was also used.

(3) A resonant strip  $\lambda/2$  long at 1420 MHz placed in a rectangular cavity with either a  $TE_{103}$  or  $TE_{104}$  resonance near 3850 MHz. The strip was supported by two rectangular quartz rods which also shortened the  $\lambda_g$  of the 3850 MHz mode.

The cavity used for 1420 MHz and the pump frequency between 8500 and 10700 MHz was:

(4) A resonant strip  $\lambda/4$  long at 1420 MHz at the base of a long rectangular cavity as described in [2.6] (cf. fig. 2.5), carrying a  $TE_{10n}$  mode.

In each of the cavities the  $Q_0$  at 1420 MHz was between 5000 and 7000 at room temperature and the filling factors were about 30 %, except for the first one.

[2.8.4] The reflection characteristics were measured with a microwave bridge. The arrangement is sketched in fig. 2.6. The determination of cavity quality factors and amplifier characteristics is most easily performed by using a frequency swept source. This was not available in the laboratory, so we mixed the output of a sweep generator ( $f \approx 50$  MHz) with that of a signal generator ( $f = 1370$  MHz). Ample

signal strength was obtained in this way. The frequency calibration was obtained from markers provided by the sweep generator. For the bridge element a hybrid ring was constructed as described in [15]. The two cross branches with a characteristic impedance of  $\sqrt{2}Z_0$  have to be slightly shorter than  $\lambda_g/4$  (because of fringing fields). The isolation obtained was 30 db at 1420 MHz. Cavity number 3 is sketched in figure 2.6. Detection took place by a superheterodyne receiver (noise figure 9 db) preceded by a low pass filter F (cut-off 2000 MHz).

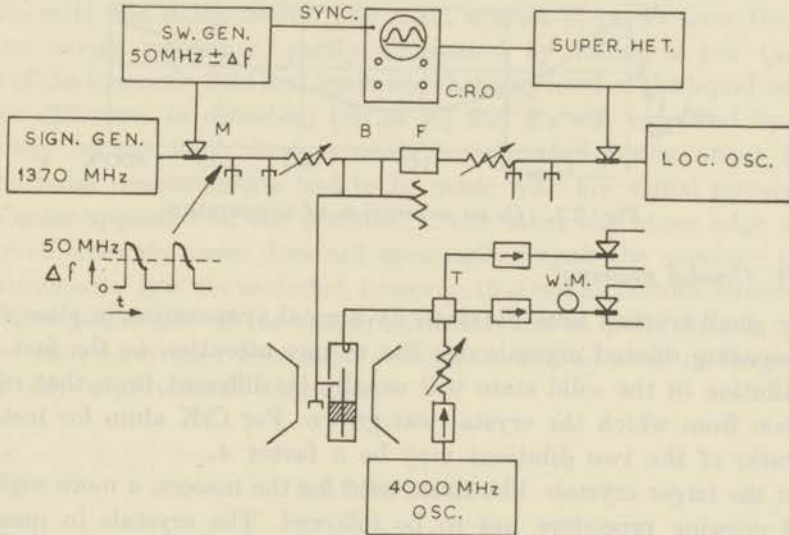


Fig. 2.6. Apparatus for experiments with two different frequencies. B bridge element for 1420 MHz; F filter; T Magic Tee for 4000 MHz.

The 4000 MHz source was a triode oscillator (EC 57) which could be pulse modulated. The rest of the apparatus at this frequency was a straightforward magic Tee bridge.

The 10 KMHz apparatus has been discussed before in [2.6]. The klystron power supply was slightly changed so as to allow pulse modulation.

### [2.9] *The temperature behaviour of the quality factors*

The temperature behaviour of the cavity quality factors was peculiar. Fig. 2.7 shows the unloaded  $Q_0$  of a reentrant test cavity, measured as a function of temperature. This cavity was silver plated on the inside. The same behaviour was observed on normally polished copper cavities. Decreasing the temperature from 300 K on,  $u_0$  behaves as expected and decreases also. Below the temperature where the electron mean free path becomes larger than the skin depth, PIPPARD [16] has shown that the  $u_0$  has to stay constant. This temperature is about 70° K for pure annealed copper at 1420 MHz. The increase of  $u_0$  at lower temperatures to about the same value as at 300° K is most unexpected. We should like to explain

this behaviour by supposing that the surface irregularities become larger than the skin depth at lower temperatures, thus increasing the losses. A check on this hypothesis was made by polishing a copper cavity with the finest emery available ( $0.4 \mu$ ). The increase of  $u_0$  was not present anymore and it stayed constant below  $20^\circ \text{K}$  (dashed line in fig. 2.7).

Of the cavities tried at low temperatures those made of oxygen free electrolytic copper (no pores) with highly polished surfaces, and with silver soldered joints, had the highest quality factors.

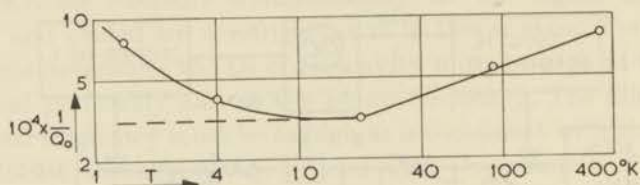


Fig. 2.7.  $Q_0$  as a function of temperature.

#### [2.10] *Crystal growing*

The small crystals were obtained by normal evaporation in glass discs. In preparing diluted crystals one has to pay attention to the fact that the dilution in the solid state will usually be different from that of the solution from which the crystal was grown. For CrK alum for instance the ratio of the two dilutions may be a factor 4.

For the larger crystals, like those used for the masers, a more sophisticated growing procedure has to be followed. The crystals in question were  $\text{K}_3(\text{Co}(\text{CN})_6)$  with a small content of  $\text{K}_3\text{Cr}(\text{CN})_6$  ( $\approx 1\%$ ). This last substance is rather unstable and the solution may not be heated too much.

The crystals, hanging in the solutions, were rotated back and forth while cooling slowly in a thermostat from  $32^\circ \text{C}$  to about  $25^\circ \text{C}$  in one week. Rotating the crystals in one direction only, decreased the growing speed considerably. The solutions (without the crystals) had been saturated by placing them in a separate thermostat at about  $35^\circ \text{C}$  for some time. The difference between the starting temperature ( $32^\circ \text{C}$ ) and the solution preparation temperature should not be too large, the oversaturation will otherwise become too high and the solution will crystallize out immediately. Crystals weighing about 100 g. were obtained in this way without too much difficulty.

#### [2.11] *Errors*

The attenuators used were calibrated to within 0.1 db at the frequencies used. The detecting sensitivities of the crystals were calibrated by using a barrettor, the voltage standing wave ratio of which was measured. From repeated measurements the accuracy of this calibration is estimated to be of the order of 0.1 db.

When using the reflection method the value of  $T_0$  was determined for

every point separately by applying a high magnetic field (10 K $\phi$ ). The  $I_0$  chosen for calculating (2.16) was the average of these values. To prevent boiling of the liquid helium to upset the measurement, the cavity and waveguides inside the Dewar were filled with foam plastic. Nevertheless the changing helium level impaired the accuracy. The resulting accuracy of  $\eta$  or  $\tau_1$  from these measurements is estimated to be within 30 %.

In the transmission method more effort was put into eliminating the errors, and the reproducibility of the later measurements (cf. CoNH<sub>4</sub>tutton salt) was much better. The main sources of errors were the drift of the cavity resonance, partly eliminated by taking a low  $Q_0$ , the drift of the magnetic field and again the changing level of the liquid helium.

The difference in detecting law of  $X_1$  and  $X_2$  was corrected for. The accuracy of the later measurements is estimated to be about 15 %.

The pulse measurements had to be made with low signal powers and thus noise appeared on the pictures. If one takes the upper edge of the observed trace the noise does not necessarily impair the accuracy of the measurements. It is not excluded, however, that not all factors determining the time behaviour of the magnetization (such as pulse length, pump power etc.) have been controlled sufficiently and so some of the results have only a provisional character.

#### REFERENCES

1. PANNENBORG, A. F., Thesis, Delft (1952).
2. BRONWELL, A. B. and R. E. BEAM, Theory and Application of Microwaves. McGraw-Hill, New York, (1947) ch. 8.
3. M.I.T. Radiation Lab. series. Vol. 8, 9, 10 and 11. McGraw-Hill, New York.
4. RIBLET, H. J. and T. S. SAAD, Proc. I.R.E. 36, 61 (1948).
5. I am very much indebted to the N.V. PHILIPS Gloeilampenfabrieken for the generous loan of this klystron and its power supply.
6. This magnet was designed by Prof. Dr K. W. TACONIS.
7. I am very indebted to Ir H. G. BELJERS for suggesting this solution.
8. MIMS, W. B. and K. D. BOWERS, Kam. Onnes Conf. 1958. Physica 24, 166 (1958).
9. DAVIS, C. F. and M. W. P. STRANDBERG, Bull. Am. Phys. Soc. Ser. II 2, 226 (1957).
10. GORDON, J. P., H. J. ZEIGER and C. H. TOWNES, Phys. Rev. 99, 1264 (1955).
11. WITTKÉ, J. P., Proc. I.R.E. 45, 291 (1957).
12. BLOEMBERGEN, N., Phys. Rev. 104, 324 (1956).
13. BUTCHER, P. N., Proc. I.R.E. 105 B (1958).
14. BÖLGER, B., B. J. ROBINSON and J. UBBINK, to be published in Physica.
15. REED, J. and G. J. WHEELER, Proc. I.R.E. Trans M.T.T. 4, 246 (1956).
16. PIPPARD, A. B., Proc. Roy. Soc. A 191, 385 (1947).

## CHAPTER III

### EXPERIMENTAL RESULTS

#### A. Results obtained by steady state saturation

##### [3.1] Presentation of the data

The steady state saturation measurements were all made at a frequency around 9400 MHz. Graphs have been made of  $P_{\text{ext}}/P_m$  vs  $P_{\text{ext}}$  as calculated from the measurements with formulas (2.15) to (2.17) or (2.24). The relation of  $P_{\text{ext}}/P_m$  to better known quantities is that

$$\frac{P_{\text{ext}}}{P_m} \propto \frac{1}{\chi'} \propto T_{\text{spin}}.$$

$P_m$  is taken for one gram ion of magnetic ions.  $\eta$ , the molar power transfer constant, is the reciprocal of the slope of the graphs

$$(3.01) \quad \eta = \frac{dP_{\text{ext}}}{d(P_{\text{ext}}/P_m)}.$$

$\eta$  was expected to be a constant but mostly, however, this is found not to be realized. Therefore  $\eta$  at low values of  $P_{\text{ext}}$  is called  $\eta_s$ , and for high values  $\eta_f$ . These as well as the coordinates of the saturation graphs will then be given. Also are given the coordinates of the point at which  $\eta = 2\eta_s$  in the column "coord.  $\eta = 2\eta_s$ ". When the range of  $P_{\text{ext}}$  was not large enough to observe a definite curvature for a series no index will be assigned to the corresponding  $\eta$ . To convert the values of  $\eta$  to relaxation times one has to use (1.89) with  $W = 0$  in case of internal spin equilibrium.

Since the saturation graphs were expected to be straight lines instead of the curved ones found, different experimental methods (reflection and transmission) with different cavities have been tried out to exclude an instrumental error. Also the apparatus was tested by experiments on CuK tutton salt and CrK alum diluted with AlK alum. Apart from CuK tutton salt at the lowest power levels, nice straight lines were obtained for these salts up to a very high degree of saturation, indicating that no instrumental error was involved.

Where possible a comparison is made with the results obtained by other experiments, especially with those obtained by the (non-resonant) relaxation method. The values of  $\eta$  (called  $\eta_{\text{rel}}$ ) derived from those results are calculated on the assumption that the spin system is in internal equilibrium, using (1.91).

Our measurements have all been made on single crystals while the relaxation measurements were mostly performed on powders. As in



The largest resonance at 3340  $\text{\AA}$  was first saturated and it was found that the saturation graphs were curved instead of straight. However, at very high and very low powers these graphs were practically straight lines. Some examples can be found in fig. 3.1, where only a few of the measured points could be plotted due to typographical difficulties. In table I the averaged coordinates of the graphs are given, converted to the values as would have been found for one gram ion of  $\text{Cr}^{+++}$ , together with the magnetically absorbed powers at minimum and maximum  $P_{\text{ext}}$ . The unit of  $P_{\text{ext}}$  is Watt and of  $P_m$  and  $\eta$  Watt/mole.

The values of  $P_{\text{ext}}/P_m$  at  $P_{\text{ext}}=0$  are extrapolated and therefore somewhat uncertain. Their relative values differ in some cases from the expected proportionality with temperature. This is due partly to the observed experimental conditions. The values of the maximum  $P_{\text{ext}}$  are given between brackets below the corresponding  $P_{\text{ext}}/P_m$  values. Doubtful values of  $\eta$  are put in brackets.

TABLE I  
CrK alum H // (111)

$P_{\text{ext}}$ W T °K	$10^5 \times P_{\text{ext}}/P_m$							$P_m$ min	$\eta_s$	$P_m$ max	$\eta_f$	Coord. $\eta = 2\eta_s$		
	0	0.020	0.050	0.100	0.200	0.400	max				$P_{\text{ext}}$ W	$10^5$ $P_{\text{ext}}$ $P_m$		
1.39	36	68	112	148	198	339		12	67	118	161	0.11	155	
1.49	36	68	102	158	246	376		626	10	73	128	159	0.17	225
							(0.800)							
1.78	62	94	134	192	236	400		10	68	108	147	0.10	192	
1.94	50	72	102	142				16	78			0.09	134	
2.52	158	194	248	300	382	472		586	10	67	170	423	0.12	315
							(1.000)							
2.55	90	122	156	196	249	300		2.5	65	154	480	0.08	180	
3.00	122	150	154	182	228	292		416	18	68	385	515	0.28	250
							(1.600)							
3.03	92	118	150	188	248			14	(75)	81		0.05	150	
3.15	130	146	168	200	274	336		15	68	165	340	0.25	305	
3.22	72	96	132	184	268	358		23	78	125	315	0.18	260	
3.36	120	146	182	220	260	316		400	14		475	715	0.12	230
							(1.900)							
3.76	116	136	172	196	246	300		372	5	68	350	920	0.16	225
							(1.300)							
4.20	124	144	170	208	266	342		400	14	67	200	(785)	0.15	237
							(0.800)							
1.91												257		
2.28												300-		
												380		
2.40												380		
2.71												490		

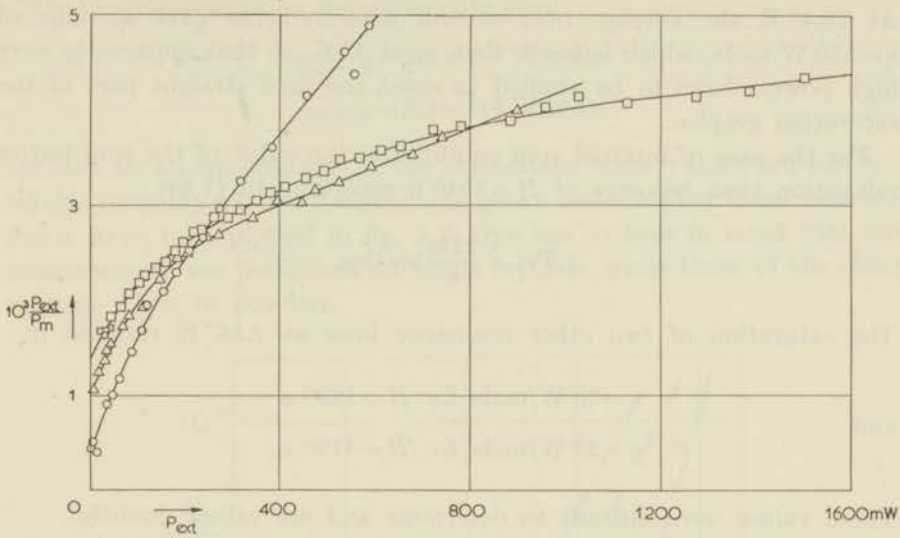


Fig. 3.1. Saturation graphs of CrK alum;  $\mathbf{H} // (111)$

□  $T = 3.36^\circ \text{K}$     △  $T = 2.55^\circ \text{K}$     ○  $T = 1.49^\circ \text{K}$

In fig. 3.2 the values of  $\eta_s$  and  $\eta_f$  are plotted as a function of temperature, on a double logarithmic scale and give the results:

$\eta_s = 68 \text{ W/mole}$ , and  $\eta_f = 77 \times T^{1.9} \text{ W/mole}$  for  $1.39^\circ \text{K} < T < 4.2^\circ \text{K}$ .

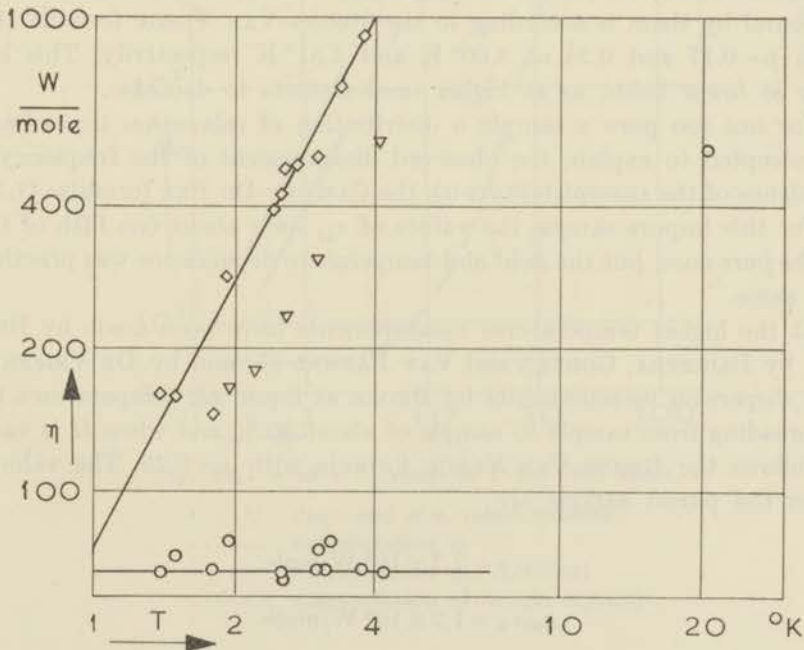


Fig. 3.2.  $\eta$  as a function of  $T$  for CrK alum;  $(\mathbf{H} // (111))$

◇  $\eta_f$     ○  $\eta_s$     ▽  $\eta_{rel}$

At 20.4° K the average over several measurements gave a value of  $\eta = 530$  W/mole, which is lower than  $\eta_f$  at 4° K, so that apparently very high powers have to be applied to reach the final straight part of the saturation graphs.

For the case of internal spin equilibrium the value of the spin lattice relaxation time becomes at  $H = 3340 \text{ } \sigma$  according to (1.89)

$$T\tau_1 = \frac{2270}{\eta} \text{ ms.deg.}$$

The saturation of two other resonance lines at 2.55° K resulted in

$$\eta = 20 \text{ W/mole for } H = 1990 \text{ } \sigma$$

and

$$\eta = 29 \text{ W/mole for } H = 4760 \text{ } \sigma.$$

These values were difficult to determine and are rather doubtful.

The experiments on the main resonance line were repeated by using the transmission method. Essentially the same behaviour of the saturation graphs and of  $\eta_s$  and  $\eta_f$  was found.

The values of  $\eta_{\text{rel}}$  for  $H = 3340 \text{ } \sigma$  as derived from the relaxation measurements on powdered specimens of CrK alum by KRAMERS, BIJL and GORTER [5] have also been plotted in fig. 3.2. They found a temperature dependence which is practically the same as of our  $\eta_f$  while the absolute values are also very close. The dependence of  $\tau$  on the magnitude of  $H$  as found by them is according to the BRONS-VAN VLECK formula (1.91) with  $p = 0.17$  and  $0.24$  at  $3.00^\circ \text{ K}$  and  $2.51^\circ \text{ K}$  respectively. This holds only at lower fields, as at higher ones  $\tau$  starts to decrease.

For not too pure a sample a distribution of relaxation times had to be accepted to explain the observed disagreement of the frequency dependence of the susceptibility with the CASIMIR-DU PRÉ formulas (1.102).

For this impure sample the values of  $\tau_{\text{av}}$  were about one fifth of those of the pure ones, but the field and temperature dependence was practically the same.

At the higher temperatures measurements have been made by BROER [6], by DIJKSTRA, GORTER and VAN PAEMEL [7] and by DE VRIJER [8]. The dispersion measurements by BROER at liquid air temperatures have a spreading from sample to sample of about 30 % and when  $H$  is varied,  $\tau_1$  follows the BRONS-VAN VLECK formula with  $p = 0.25$ . The values of  $\eta$  for the purest sample are:

$$\eta_{77^\circ \text{ K}} = 7.7 \times 10^4 \text{ W/mole}$$

$$\eta_{90^\circ \text{ K}} = 1.2 \times 10^5 \text{ W/mole.}$$

The phase transition in the crystal structure near these temperatures will influence  $\eta$ .

De Vrijer's absorption measurements gave:

$$\eta_{14.3^\circ \text{K}} = 3.2 \times 10^3 \text{ W/mole}$$

$$\eta_{20.4^\circ \text{K}} = 3.3 \times 10^3 \text{ W/mole}$$

but due to an uncertainty in the corrections these values are not too reliable (possibly a factor 2 higher). To give a better survey these measurements have been plotted in fig. 3.3. One has to bear in mind that our measurements are performed on single crystals, while those of the other workers relate to powders.

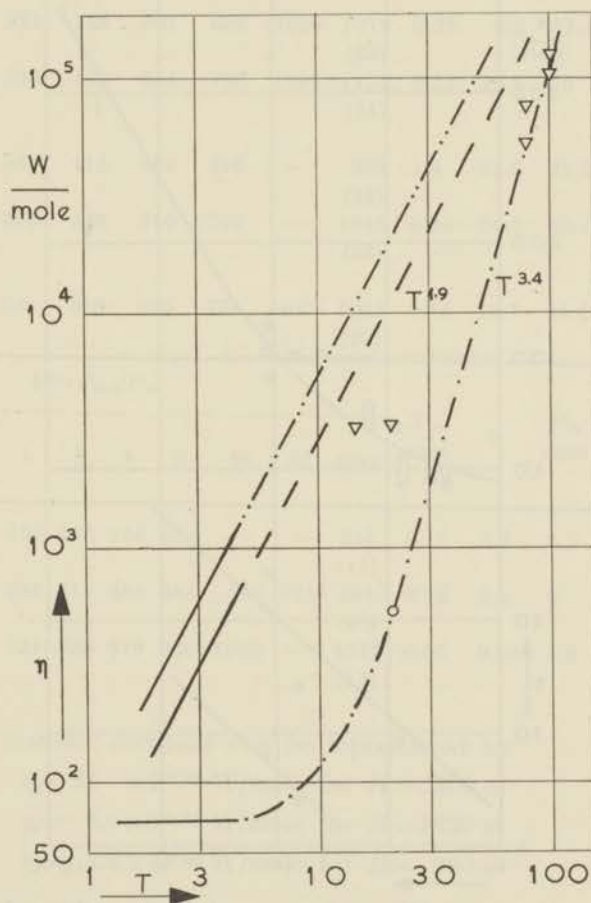


Fig. 3.3.  $\eta$  as a function of  $T$  for CrK alum

- $\nabla$  disp. and abs. measurements
- · - · - · extrapolation  $\eta_s$
- — — — — extrapolation  $\eta_{rel}$  (powder)
- · - · - · extrapolation  $\eta_f$  (single crystal)

[3.2.3] Undiluted CrK alum;  $\mathbf{H} \parallel (100)$  direction. For this direction of the magnetic field all ions are magnetically equivalent and

their symmetry axis makes an angle of about  $55^\circ$  with  $\mathbf{H}$ . The spectrum consists mainly of three peaks at about  $3300 \text{ \AA}$ ,  $1630 \text{ \AA}$  and  $990 \text{ \AA}$ . At all three resonances saturation measurements were performed by the reflection as well as by the transmission method. Initially the saturation graphs were thought to be straight lines, but in later experiments extending the range of  $P_{\text{ext}}$  to the lower side all three lines proved to be curved. The coordinates of some of them with the values of  $\eta_f$  are given in table II.  $\eta_f$  is plotted as a function of temperature in fig. 3.4.

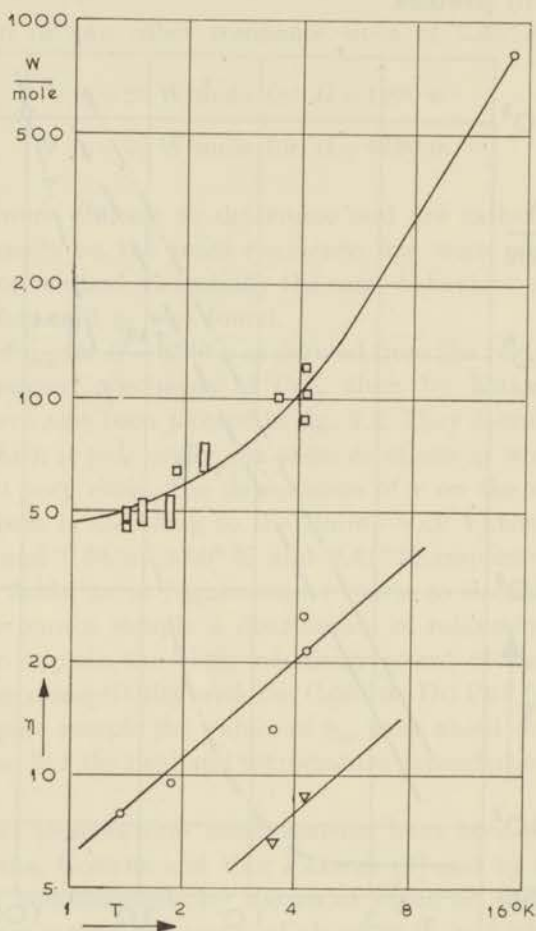


Fig. 3.4.  $\eta$  as a function of  $T$  for CrK alum;  $\mathbf{H} // (100)$

□  $H = 3340 \text{ \AA}$       ○  $H = 1630 \text{ \AA}$       ▽  $H = 990 \text{ \AA}$

To obtain reasonable values of  $\eta_s$ , still lower powers ought to be applied. At the minimal power applied their values were of the order of 16 W/mole for  $H = 3300 \text{ \AA}$  up to  $4^\circ \text{K}$ . In the liquid helium range the temperature dependence of  $\eta_f$  is about  $T^{0.88}$  for the two higher field resonances.

TABLE II  
 KCr(SO<sub>4</sub>)<sub>2</sub>·12H<sub>2</sub>O; H // (100)

H =		10 <sup>6</sup> · P <sub>ext</sub> /P <sub>m</sub>								P <sub>m</sub>	η <sub>s</sub>	P <sub>m</sub>	η <sub>s</sub>	coord.
3300 ø		0	1	2	4	8	16	32	max	min		max		η = 2η <sub>s</sub>
$\frac{P_{ext}}{mW}$	$\frac{T}{^\circ K}$													
1.38	174	234	270	355	477	666	1005	1093	0.23	14.2	32.9	45.3	4.5/372	
								(36)						
1.54	211	279	321	388	501	688	1020	1079	0.23	9.9	32.4	—	0.9/277	
								(35)				48		
1.82	259	317	363	440	564	763	1099	1134	0.23	16.3	30	54	6.6/524	
								(34)				66		
2.25	300	333	363	415	494	616	—	862	1.4	22.2	37.2	—	4.5/426	
								(32)				74		
2.99	410	463	503	559	640	789	—	1042	0.24	24.7	30.7	63	5.1/581	
								(32)				120		
4.25	448	492	509	560	625	734	947	1044	0.11	16.7	35.4	104	1.1/497	
								(37)				91		

H ø		10 <sup>6</sup> · P <sub>ext</sub> /P <sub>m</sub>								P <sub>m</sub>	η <sub>s</sub>	P <sub>m</sub>	η <sub>f</sub>	coord.
1630		0	1	2	4	8	16	32	max	min		max		η = 2η <sub>s</sub>
$\frac{P_{ext}}{mW}$	$\frac{T}{^\circ K}$													
1.38	78	104	125	156	209	—	—	245	0.11	5.5	4.5	8.0	—	
								(11)						
4.25	365	394	415	445	485	543	625	661	0.03	3.4	6	21.4	3.0/432	
								(40)				26.7		
990	4.25	621	721	803	879	960	1052	—	1071	0.05	0.99	1.6	9.9	2.2/816
								(17)						

The power transfer constant can be represented by:

$$\eta_f = 34 \times T^{0.88} \text{ W/mole for } H = 3300 \text{ ø}$$

$$\eta_f = 6.0 \times T^{0.88} \text{ W/mole for } H = 1630 \text{ ø}$$

$$\eta_f = 2.4 \times T^{0.88} \text{ W/mole for } H = 990 \text{ ø}$$

These values of  $\eta_f$  when plotted against  $b/C + H^2$  on a double logarithmic scale lie on a straight line:

$$\eta_f = 1.1(b/C + H^2)^{1.4}.$$

The power transfer might perhaps be due to two or more parallel transfer coefficients, each with a different temperature dependence. We tried a compound curve  $\eta_f = 42.5 + 4.5 T^{1.9}$  W/mole as for the (111) direction the  $\eta_f$  has a  $T^{1.9}$  law. This curve has been drawn in fig. 3.4 and seems to fit the experimental points of the line at  $H = 3300 \text{ ø}$  rather well.

[3.2.4] CrK alum diluted with AlK alum. To find the dependence of  $\eta$  on magnetic dilution, two samples have been measured with Cr : Al ratios of 1 : 2.28 and 1 : 40. The direction of  $\mathbf{H}$  was parallel (111).

ESCHENFELDER and WEIDNER [9] obtained values for a 1 : 10 diluted sample, namely  $\eta_{1:10} = 66$  W/mole independent of temperature between 2° K and 4° K. They saturated the spin system to a very high degree ( $\approx 22$  times), but their data were only obtained from selected straight saturation graphs, and no information was given about the curvature.

The results of our measurements can be found in table III and in fig. 3.5. In this figure we have also drawn  $\eta_{1:10}$  of ESCHENFELDER and WEIDNER.

The Cr<sup>+++</sup> concentrations were determined by the polarographic method \*) [29].

TABLE III  
(Cr/Al)K alum;  $\mathbf{H} // (111)$

Cr:Al = 1:2.28				Cr:Al = 1:40			
$T$	$\eta$	$P_m$ min	$P_m$ max	$T$	$\eta$	$P_m$ min	$P_m$ max
1.89	133	5.7	110	2.00	58.2	35	51
2.74	218	5.0	111	2.99	58.2	20	43
3.47	$\approx 377$	15	141	4.2	55	14	47
4.22	445	26	162	14.6	$\approx 117$	27	74
				20.0	$\approx 123$	16	41

a) Dilution Cr : Al = 1 : 2.28.

All saturation graphs are curved at low input powers. The curved part was small, so that reasonable values of the starting slope could not be determined. The main part of the graphs is straight, with reciprocal slopes as given in table III.

The absorbed power at which the curves become straight is about 15 W/mole which is much less than for the undiluted substance with  $\mathbf{H} // (111)$ . We find:

$$\eta_{1:2.28} = 51 \times T^{1.58} \text{ W/mole.}$$

By the relaxation method VAN DER MAREL e.a. [10] find practically the same temperature dependence ( $T^{1.6}$ ) for a sample diluted to the same ratio. The absolute value of  $\eta_{\text{rel}}$  as found by them is anomalous, as they are smaller than for any other concentration used at most of the magnetic fields and temperatures.

\*) We are very much indebted to Dr W. L. Groeneveld and A. P. Zuur of the Chem. Dept. of the Leiden Univ. for the use of their equipment and their advice on these matters.

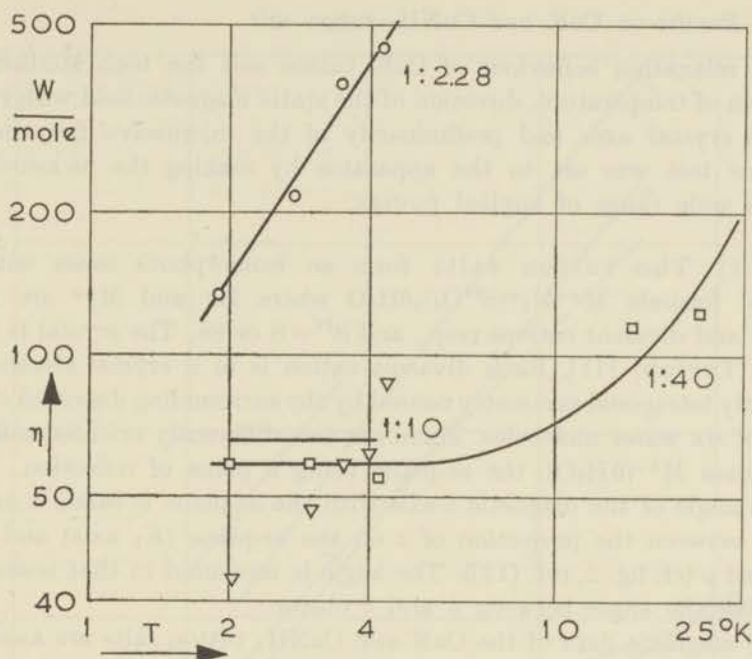


Fig. 3.5.  $\eta$  as a function of  $T$  for diluted CrK alum;  $\mathbf{H} // (111)$

- Cr:Al = 1:2.28
- Cr:Al = 1:40
- ▽ Cr:Al = 1:2 relaxation measurements
- Cr:Al = 1:10 ESCHENFELDER and WEIDNER.

b) Dilution Cr : Al = 1 : 40.

The saturation graphs are straight lines. The molar power transfer constant is found to be (cf. fig. 3.5)

$$\eta_{1:40} = 58 \text{ W/mole for } 2^\circ \text{ K} < T < 4^\circ \text{ K.}$$

At two hydrogen temperatures measurements were made (fig. 3.5). The highest dilution measured by VAN DER MAREL is 1 : 20 for which he found  $\eta_{\text{rel}} = 62 \text{ W/mole}$  at  $2.9^\circ \text{ K}$  and  $H = 3375 \text{ O}$  and a  $T^{1.6}$  law at low magnetic fields. At higher magnetic fields this dependence becomes somewhat smaller.

[3.2.5] The conclusion drawn from the above mentioned experiments is that for CrK alum  $\eta_f$  equals  $\eta_{\text{rel}}$  whilst  $\eta_s$  behaves as theoretically expected. From the measurements with  $\mathbf{H} // (111)$  and  $\mathbf{H} // (100)$  an average value of  $\eta_f$  is derived, very close to the value of  $\eta_{\text{rel}}$  for powders. From fig. 3.3 it is seen that the values of  $\eta_f$  extrapolate nicely from the liquid helium range to liquid air temperatures with a  $T^{1.9}$  law. Extrapolation of  $\eta_s$  would result in a  $T^{3.4}$  dependence. Both powers of  $T$  are much lower than the theoretically expected value of 6 for a purely indirect process.

[3.3] *Results on CuK and CuNH<sub>4</sub> tutton salt*

The relaxation behaviour of CuK tutton salt has been studied as a function of temperature, direction of the static magnetic field with respect to the crystal axes and preliminarily of the microwave frequency. A rigorous test was set to the apparatus by making the measurements over a wide range of applied powers.

[3.3.1] The tutton salts form an isomorphous series with the general formula  $M^{++}M_2^{+}(S^{IV}O_4)_2 \cdot 6H_2O$  where  $M^{+}$  and  $M^{++}$  are monovalent and divalent cations resp., and  $S^{IV} = S$  or Se. The crystal is monoclinic (TUTTON) [11]. Each divalent cation is in a crystal electric field of nearly tetragonal symmetry caused by the surrounding distorted octahedron of six water molecules. There are two differently oriented magnetic complexes  $M^{++}(6H_2O)$ , the *ac*-plane being a plane of reflection.

The angle of the magnetic *z*-axis with the *ac*-plane is called  $\alpha$  and the angle between the projection of *z* on the *ac*-plane ( $K_1$  axis) and *c*-axis is called  $\psi$  (cf. fig. 2, ref. [12]). The angle is measured in that sense so as to make the angle between *a* and *c* obtuse.

The magnetic data of the CuK and CuNH<sub>4</sub> tutton salts are assembled in table IV. The *g* values and  $\alpha$  and  $\psi$  have been found to be temperature dependent [13]. This is interpreted as due to a change in the crystal field which brings a different orbital level to the bottom [14]. POLDER's [15] calculations on the *g*-factor are in fair agreement with experiments.

TABLE IV  
Units of  $CT^2/R$  are (degrees)<sup>2</sup>  $\times 10^{-4}$ .

	$g_x$	$g_y$	$g_z$	$\alpha$	$\psi$	$C_M T^2/R$	$C_{nuc} T^2/R$	$C_{dip} T^2/R$	$C_{ex} T^2/R$
CuK <sub>2</sub> (SO <sub>4</sub> ) <sub>2</sub> · 6H <sub>2</sub> O	2.31	2.07	2.25	41°	105°	6.0	1.1	1.3	3.6
CuNH <sub>4</sub> (SO <sub>4</sub> ) <sub>2</sub> · 6H <sub>2</sub> O	2.32	2.09	2.25	39°	77°	8.7	1.1	1.3	6.3

He assumed a tetragonal field of the same order as the cubic one and showed that the sequence of the orbital levels starting from the lowest one, must be  $I_3$ ,  $I_1$ ,  $I_4$  and  $I_5$  and that the energy level separation of  $I_4$  and  $I_3$  is 15400 cm<sup>-1</sup> and that of  $I_5$  and  $I_3$  is 26600 cm<sup>-1</sup>. It has been shown, however, that a rhombic term in the crystal field is present [13]. The spin specific heat contains a nuclear, dipolar and an exchange part and has been analysed by BENZIE and COOKE [16].

[3.3.2] CuK<sub>2</sub>(SO<sub>4</sub>)<sub>2</sub> · 6H<sub>2</sub>O. Some typical saturation graphs are shown in fig. 3.6, and the coordinates of some of the graphs are given in table V. The plotted curves contained about three times as many points which could not be inserted in the drawing. The reproducibility of the apparatus is demonstrated here by the fact that some points of repeated series are three fold coinciding. The curvature of the graphs is seen (from fig. 3.6 and table V) to depend on the direction of the magnetic field.

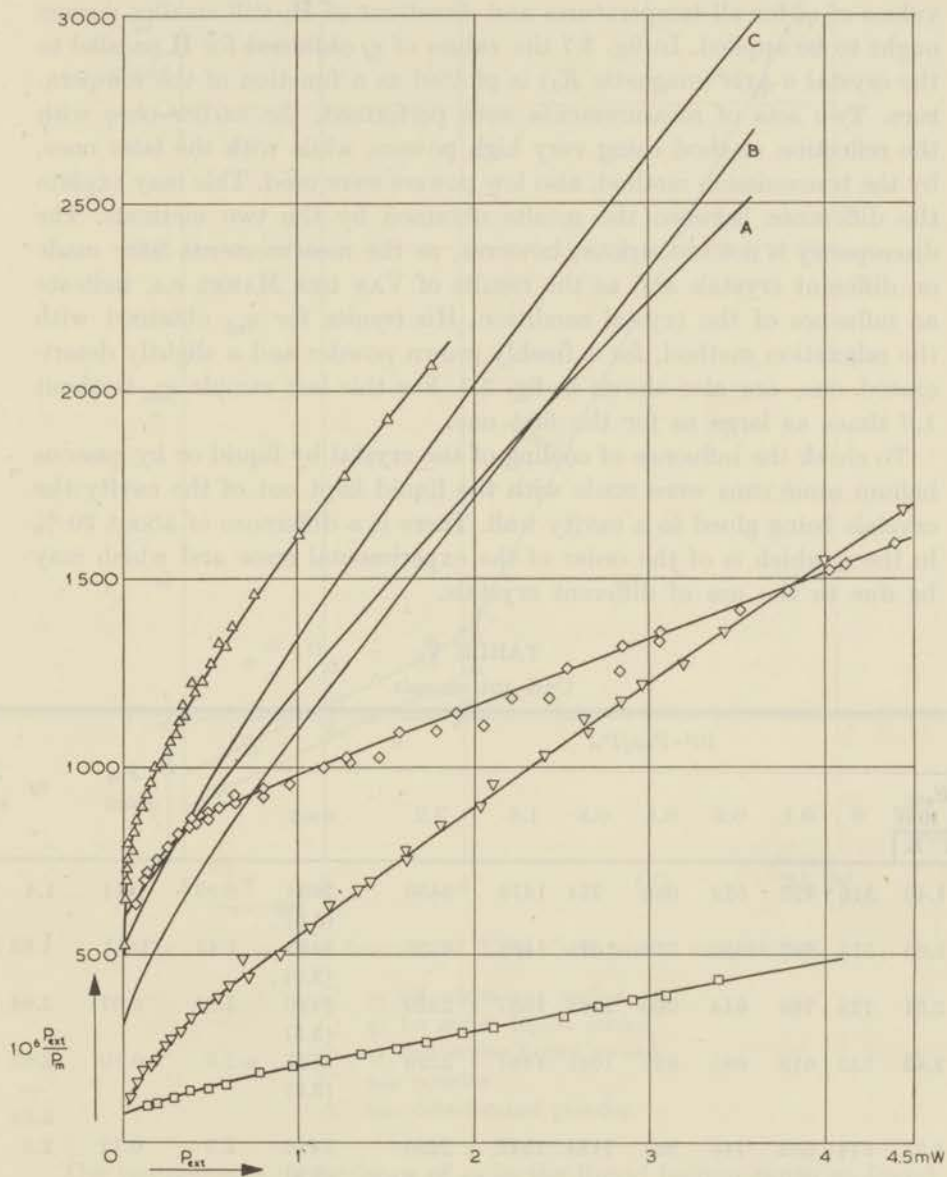


Fig. 3.6. Saturation graphs of CuK tutton salt.

- $\triangle$   $T = 1.97^\circ \text{K}$   $\mathbf{H} // K_1$
- $\nabla$  continuation of  $\triangle$ ; multiply scales by 10
- $\diamond$   $T = 1.97^\circ \text{K}$   $\angle \mathbf{HK}_1 = 22^\circ$  in  $K_1K_2$  plane. Divide horizontal scale by 10
- $\square$  continuation of  $\diamond$ ; multiply vertical scale by 10
- A  $T = 3.43^\circ \text{K}$   $\mathbf{H} // K_1$
- B  $T = 1.46^\circ \text{K}$   $\mathbf{H} // K_1$
- C  $T = 1.97^\circ \text{K}$   $\angle \mathbf{HK}_1 = 50^\circ$  in  $K_1K_2$  plane.

The minimum  $P_{\text{ext}}$  used was of the order of 5 to 10  $\mu\text{W}$ , but to obtain values of  $\eta_s$  for all temperatures and directions of  $\mathbf{H}$ , still smaller powers ought to be applied. In fig. 3.7 the values of  $\eta_f$  obtained for  $\mathbf{H}$  parallel to the crystal  $a$ -axis (magnetic  $K_1$ ) is plotted as a function of the temperature. Two sets of measurements were performed, the earlier ones with the reflection method using very high powers, while with the later ones, by the transmission method, also low powers were used. This may explain the difference between the results obtained by the two methods. The discrepancy is not too serious, however, as the measurements were made on different crystals and as the results of VAN DER MAREL e.a. indicate an influence of the crystal condition. His results for  $\eta_{\text{rel}}$  obtained with the relaxation method, for a freshly grown powder and a slightly deteriorated one, are also shown in fig. 3.7. For this last sample  $\eta_{\text{rel}}$  is about 1.6 times as large as for the first one.

To check the influence of cooling of the crystal by liquid or by gaseous helium some runs were made with the liquid kept out of the cavity the crystals being glued to a cavity wall. There is a difference of about 20 % in the  $\eta$  which is of the order of the experimental error and which may be due to the use of different crystals.

TABLE V  
CuK tutton salt

		$10^6 \cdot P_{\text{ext}}/P_m$								$\eta_s$	$P_m$ min	$\eta_f$	$P_m$ max	
		$\frac{P_{\text{ext}}}{T^\circ \text{K}}$	0	0.1	0.2	0.4	0.8	1.6	3.2	max				
$\mathbf{H} \parallel (100) \rightarrow \theta$	90°	1.46	318	425	522	688	974	1478	2450	2694 (3.6)	0.93	0.11	1.4	1.3
		2.03	515	582	650	778	1019	1465	2256	2460 (3.5)	1.49	0.11	1.88	1.4
		2.51	728	786	844	960	1185	1607	2329	2490 (3.5)	1.81	0.07	2.04	1.4
		3.43	535	615	685	821	1061	1487	2226	2523 (3.6)	$\approx 2.5$	0.10	2.62	1.4
		4.25	614	682	748	881	1134	1542	2295	2486 (3.5)	2.5	0.12	2.5	1.4
												2.25		
		$\frac{P_{\text{ext}}}{\theta}$	0	1	2	4	8	16	32	max	$\eta_s$	$P_m$ min	$\eta_f$	$P_m$ max
$T = 1.97^\circ$		22°	794	1079	1337	1819	2636	4069	—	5079 (2.2)	0.21	$1.3 \times 10^{-3}$	5.9	3.8
		90°	556	1635	2323	3351	4920	7549	$1.32 \times 10^4$	$1.76 \times 10^4$ (4.5)	0.39	$1.4 \times 10^{-3}$	2.9	2.5
		112°	603	2047	2959	—	—	—	—	4387 (3.5)	0.13	$9.2 \times 10^{-3}$	1.05	8
		140°	524	1270	2016	3224	—	—	—	4653 (6.5)	1.05	$1.9 \times 10^{-3}$	1.74	1.4

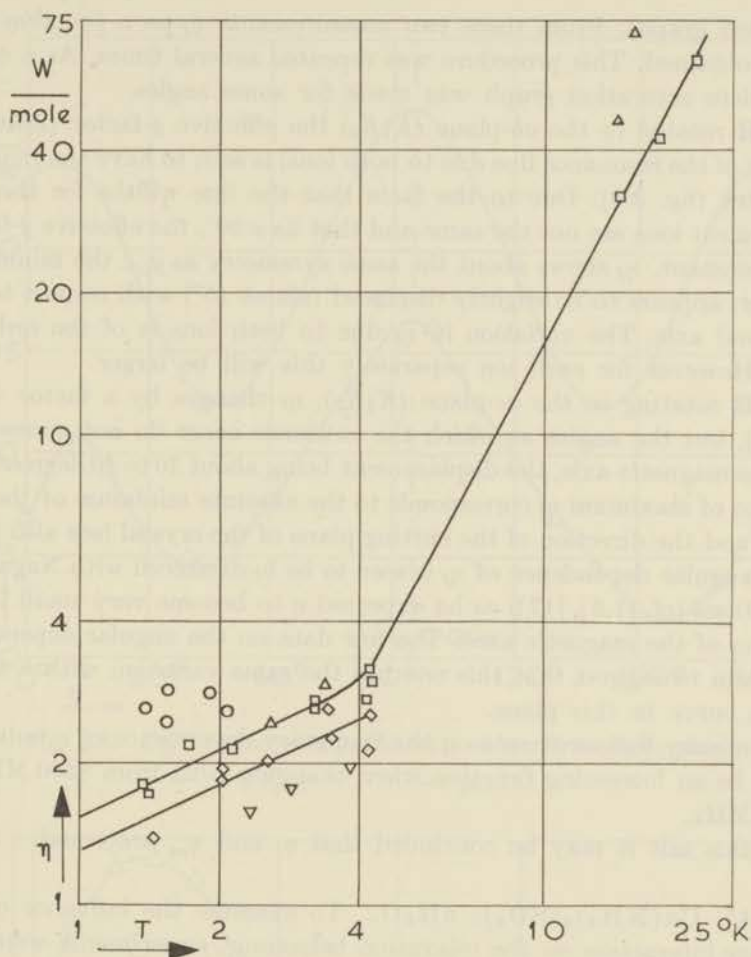


Fig. 3.7.  $\eta$  as a function of  $T$  for CuK tutton salt;  $\mathbf{H} \parallel K_1$

- $\eta_f$  1st series gas cooled
- $\eta_f$  1st series liquid cooled
- ◇  $\eta_f$  2nd series liquid cooled
- ▽  $\eta_{rel}$  powder
- △  $\eta_{rel}$  deteriorated powder.

The temperature dependence of  $\eta_f$  in the liquid helium range as found by us, with  $\mathbf{H} \parallel (100)$  direction, is  $T^{0.48}$  which is the same as for  $\eta_{rel}$ . This temperature dependence of  $\eta_f$  seems to change to  $T^{1.9}$  above 4° K.

The dependence of  $\eta_f$  on the direction of the magnetic field with respect to the crystal axis, was measured in the following way (transmission method). With a fixed applied power the values of  $x_2$  and  $\delta$  were measured as a function of the angle  $\theta$  between  $\mathbf{H}$  and the crystal axes,  $\mathbf{H}$  being rotated in a plane perpendicular to the magnetic r.f. field. This was performed at a very high value of  $P_{ext}$  and at an intermediate one. This last level was taken so as to be well in the final straight part of the

saturation graphs. From these two measurements  $\eta_f$  as a function of  $\theta$  can be obtained. This procedure was repeated several times. As a check a complete saturation graph was made for some angles.

For  $\mathbf{H}$  rotated in the  $ab$ -plane ( $K_1K_3$ ) the effective  $g$ -factor (from the position of the resonance line due to both ions) is seen to have the required symmetry (fig. 3.8). Due to the facts that the line widths for the two inequivalent ions are not the same and that  $2\alpha \neq 90^\circ$ , the effective  $g$ -factor is not constant.  $\eta_f$  shows about the same symmetry as  $g_{\text{eff}}$ , the minimum, however, appears to be slightly displaced (about  $15^\circ$ ) with respect to the tetragonal axis. The variation in  $\eta_f$  due to both ions is of the order of 15%. However for each ion separately this will be larger.

For  $\mathbf{H}$  rotating in the  $ac$ -plane ( $K_1K_2$ ),  $\eta_f$  changes by a factor 4 (cf. fig. 3.9), but the angles at which the extremes occur do not correspond with the magnetic axis, the displacement being about 30 to 40 degrees. The direction of maximum  $\eta_f$  corresponds to the absolute minimum of the line width, and the direction of the cutting plane of the crystal (see also [13]).

The angular dependence of  $\eta_f$  is seen to be in disaccord with Nagaoka's calculations (cf. [1.5], [17]) as he expected  $\eta$  to become very small in the direction of the magnetic axes. The few data on the angular dependence of  $\eta_s$  seem to suggest that this one has the same variation with  $\theta$  as the  $g$ -value curve in this plane.

Preliminary measurements on the frequency dependence of  $\eta$  indicated this to be an increasing function when changing  $\omega/2\pi$  from 8300 MHz to 10 500 MHz.

For this salt it may be concluded that  $\eta_f$  and  $\eta_{\text{rel}}$  are equal.

[3.3.4]  $\text{Cu}(\text{NH}_4)_2(\text{SO}_4)_2 \cdot 6\text{H}_2\text{O}$ . To examine the influence of the exchange interaction on the relaxation behaviour, experiments were performed on  $\text{CuNH}_4$  tutton salt, where this interaction is nearly twice as high as in  $\text{CuK}$  tutton salt, the dipole dipole interaction being equal (cf. table IV). The saturation graphs are curved and shown in fig. 3.10, where only a few of the measured points could be inserted.

The magnetic field was parallel to the crystal  $a$ -axis. At  $1.46^\circ \text{K}$  and  $1.83^\circ \text{K}$  the cavity  $Q_0$  was differing from the value for the other temperatures, reasons why the ordinates of their saturation graphs are relatively higher with respect to the other curves, for which the ordinates are proportional to  $T$  for a low value of  $P_{\text{ext}}$ .

The values derived for  $\eta$  would have been more satisfactory if the range of  $P_{\text{ext}}$  had been larger especially on the lower side. The results are plotted in fig. 3.11. Little value has to be attached to the results of  $\eta_s$ .

At temperatures below  $2.4^\circ \text{K}$   $\eta_f$  is seen to have the value of 2.26 W/mole, independent of temperature. This value is about a factor two lower than for  $\text{CuK}$  tutton salt at  $1.4^\circ \text{K}$ , whilst  $\eta_f$  is less dependent on temperature. The different orientation of the magnetic axes makes comparison difficult, however.

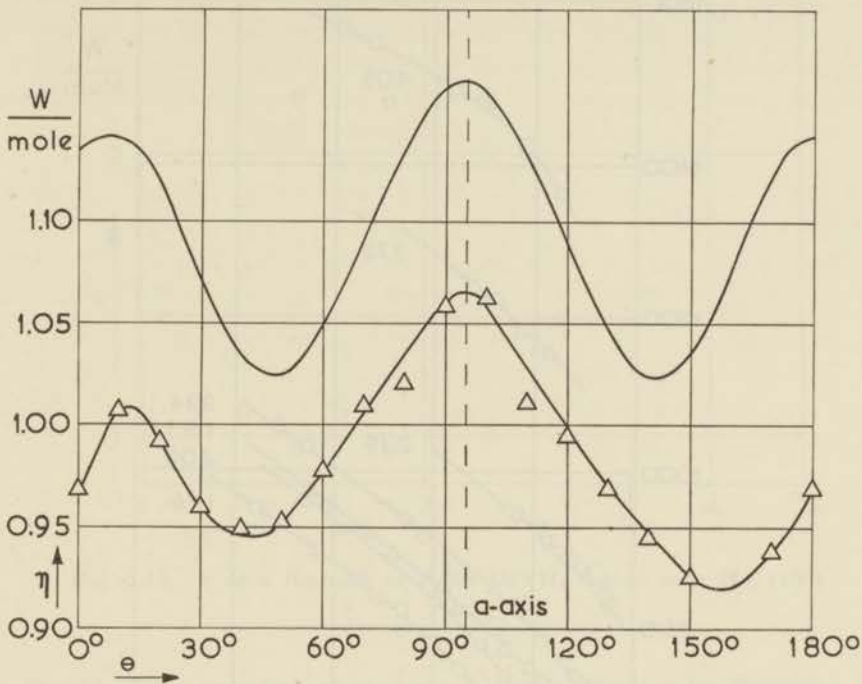


Fig. 3.8. CuK tutton salt, anisotropy of  $\eta_f$ ;  $\mathbf{H}$  in  $K_1K_3$  plane

$\Delta \eta$  ———  $g_{trr}$

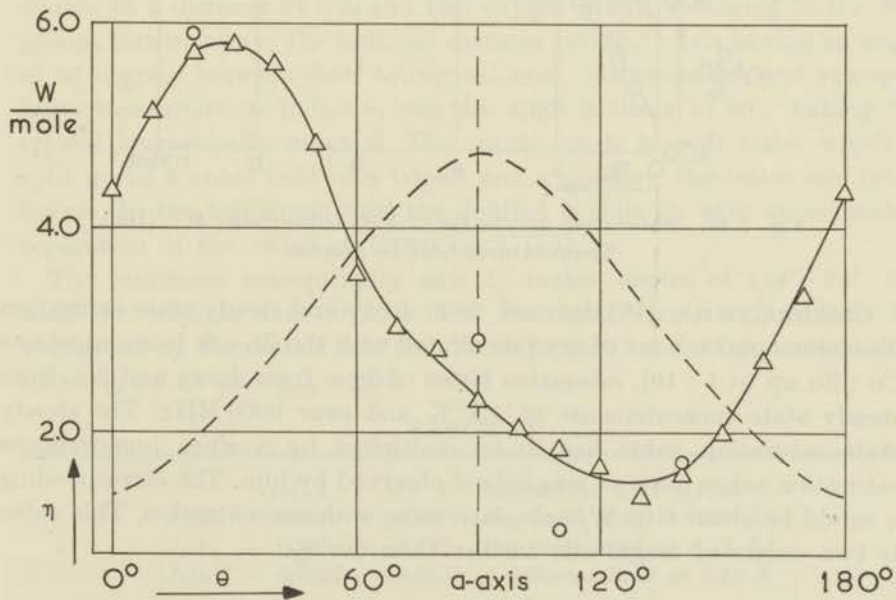


Fig. 3.9. CuK tutton salt, anisotropy of  $\eta_f$ ;  $\mathbf{H}$  in  $K_1K_2$  plane

$\Delta \eta_f$  from rotation measurement  
 $\circ \eta_f$  from complete saturation graph  
 ———  $g_{trr}$

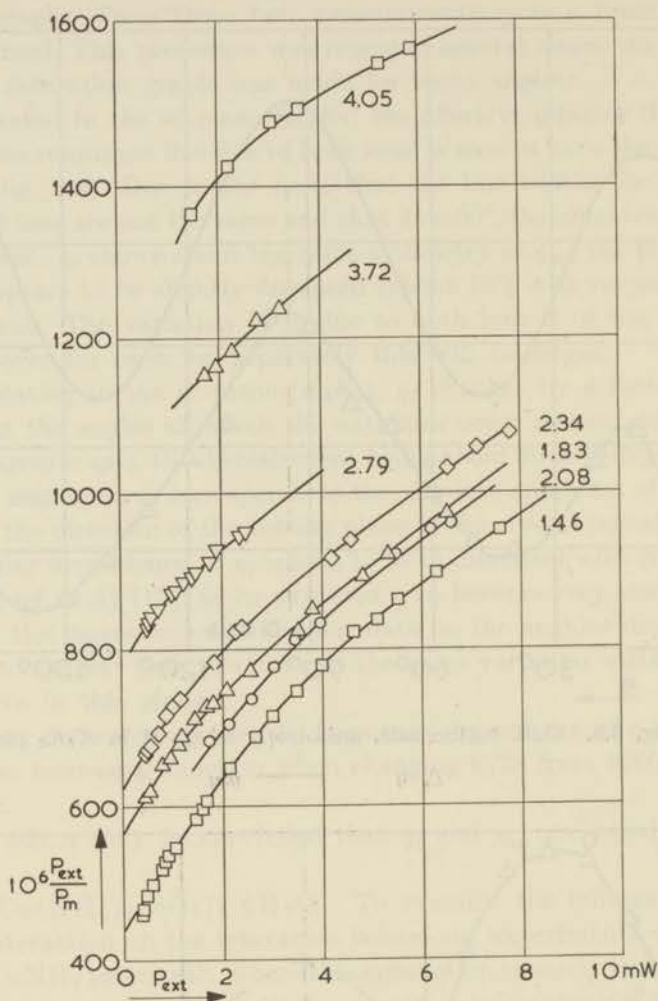


Fig. 3.10. Saturation graphs for  $\text{CuNH}_4$  tutton salt;  $\mathbf{H} \parallel (100)$ .  
Temperatures next to graphs.

GIORDMAINE e.a. [18] deduced, from decay and steady state saturation measurements on a set of crystals diluted with the Zn salt (concentrations Cu : Zn up to 1 : 10), relaxation times of 20 s. from decay and 2 s. from steady state measurements at  $1.3^\circ \text{K}$  and near 9000 MHz. The steady state saturation value has to be multiplied by 8 when homogeneous saturation takes place as was indeed observed by him. The corresponding  $\eta$  would be about 0.02 W/mole, increasing with concentration. This value is two orders of magnitude smaller than our  $\eta_f$ .

#### [3.4] Results on $\text{CuSO}_4 \cdot 5\text{H}_2\text{O}$

The exchange interaction in this salt is larger than the Zeeman energy used, and one therefore expects the relaxation times to be very short and of the order of  $\tau_2$  (see [1.4.3]).

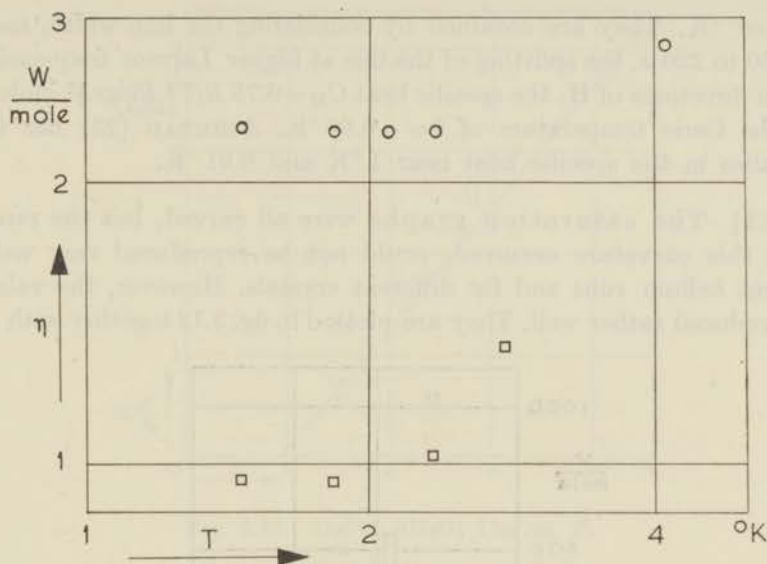


Fig. 3.11.  $\eta$  as a function of  $T$  for  $\text{CuNH}_4$  tutton salt;  $\mathbf{H} \parallel (100)$

○  $\eta_f$       □  $\eta_s$

[3.4.1] The crystal structure has been studied by BEEVERS and LIPSON [19] and is found to be triclinic. The cupric ion is in an electric field of nearly tetragonal symmetry, caused by four  $\text{H}_2\text{O}$  molecules in a square at a distance of  $2 \text{ \AA}$  and two oxygen atoms belonging to the  $\text{SO}_4$  groups further away. The unit cell contains two  $\text{Cu}^{++}$  ions having an angle of  $82$  degrees between their tetragonal axes, but resonance and susceptibility measurements indicate, that this angle is closer to  $90^\circ$ , making the crystal magnetically uniaxial. The cupric ion is in a  $D$  state, which is split up in a cubic field in a triplet and a doublet, the latter one lying lowest. In the tetragonal field the doublet is split up with an estimated separation of the order of  $12000 \text{ cm}^{-1}$  [15].

The minimum susceptibility axis  $L_1$  makes angles of  $154^\circ$ ,  $64^\circ$ ,  $51^\circ$  with the triclinic axes ( $a, b, c$ ). The resonance spectrum has been investigated by BAGGULEY and GRIFFITHS [20] at various frequencies, they found  $g_z = 2.46$  and  $g_{x,y} = 2.08$ .

TABLE VI

	sol. 1	sol. 2	interaction with 2 ions of
$J_1/k$	$0.93^\circ$	$0.97^\circ$	the same kind at $5.97 \text{ \AA}$ .
$J_2/k$	$-0.36^\circ$	$-0.23^\circ$	the same kind at $6.12 \text{ \AA}$ .
$J_3/k$	$0.085^\circ$	$-0.085^\circ$	a different kind at $5.19 \text{ \AA}$ .

In an analysis PRYCE [21] suggests that one has to distinguish the neighbours into three pairs, each pair having a different value for the exchange constant  $J$ . The possible solutions for  $J$  are given in table VI in

units of  $^{\circ}\text{K}$ . They are obtained by considering the line width, ranging from 50 to 220  $\sigma$ , the splitting of the line at higher Larmor frequencies in certain directions of  $\mathbf{H}$ , the specific heat  $C_M = 0.75 R/T^2$  (degr.)<sup>2</sup> mole [22] and the Curie temperature of  $\theta = -0.65^{\circ}\text{K}$ . ASHMEAD [23] has found anomalies in the specific heat near  $1^{\circ}\text{K}$  and  $0.01^{\circ}\text{K}$ .

[3.4.2] The saturation graphs were all curved, but the range in which this curvature occurred, could not be reproduced very well for different helium runs and for different crystals. However, the values of  $\eta_s$  reproduced rather well. They are plotted in fig. 3.12 together with some

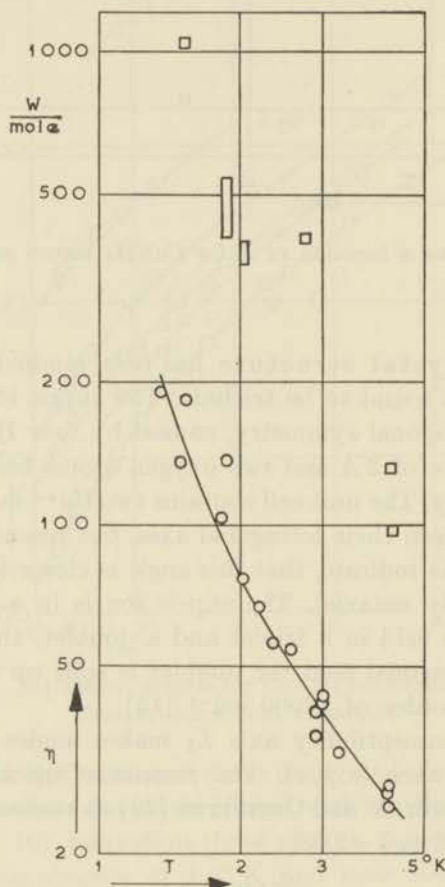


Fig. 3.12.  $\eta$  as a function of  $T$  for  $\text{CuSO}_4 \cdot 5\text{H}_2\text{O}$

□  $\eta_f$       ○  $\eta_s$

values of  $\eta_f$  and are seen to decrease faster than  $1/T$ . The direction of  $\mathbf{H}$  was close to the projection of  $L_1$  on the (110)-plane ( $5^{\circ}$  off). We have also plotted  $1/\eta_s$  vs  $T$  on a linear scale in fig. 3.13. The points lie very close to

$$1/\eta_s = 1.4 \times 10^{-2}(T - 0.94) (\text{W/mole})^{-1}.$$

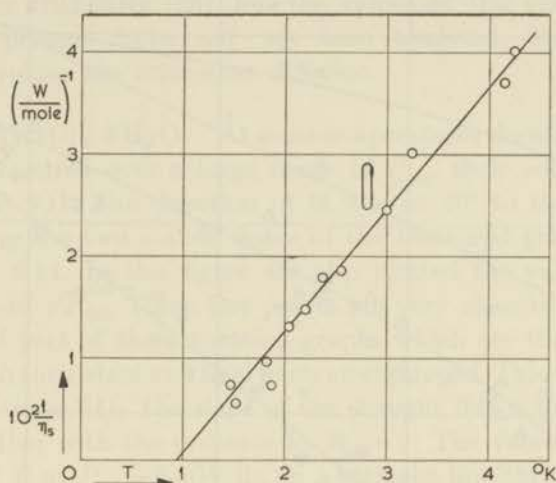


Fig. 3.13.  $\text{CuSO}_4 \cdot 5\text{H}_2\text{O}$ ;  $1/\eta_s$  vs.  $T$ .

This resembles a kind of Curie-Weiss law with a value of  $\theta = +0.94^\circ \text{K}$ , which is close to the maximum of the specific heat anomaly at  $1^\circ \text{K}$  and the temperature at which one might expect  $J_1$  to freeze out. Just above such a transition large fluctuations due to short range ordering occur in the local fields which might cause the increase of  $\eta$  near this transition. To check whether the relation  $\chi'' \propto \chi_0$  really holds at low values of  $P_{\text{ext}}$  (cf. [1.7.6]), a plot was made of  $P_{\text{ext}}/P_m$  versus  $T$  at  $P_{\text{ext}} = 5 \text{ mW}$  the lowest  $P_{\text{ext}}$  common to all curves considered. The points lie close to the straight line  $A(T+0.5)$ . The agreement is satisfactory.

For the best series we plotted  $P_{\text{ext}}/P_m$  against  $\sqrt{P_{\text{ext}}}$  as a trial. The points are very close to a straight line and resemble the curves of  $\text{CuK}_2\text{Cl}_4 \cdot 2\text{H}_2\text{O}$  to be presented later in fig. 3.14.

### [3.5] Results on $\text{CuK}_2\text{Cl}_4 \cdot 2\text{H}_2\text{O}$ and $\text{Cu}(\text{NH}_4)_2\text{Cl}_4 \cdot 2\text{H}_2\text{O}$

Measurements on these salts have been carried out partly because the exchange interaction is intermediate between that of copper sulfate and of  $\text{CuK}$  tutton salt, partly as preliminary measurements for a double resonance experiment to be discussed later.

[3.5.1] The crystal structure has been studied by CHROBAK [24] and WYCKOFF [25]. The crystal symmetry of these two salts is tetragonal. A unit cell contains two cupric ions each in a tetragonal field due to four  $\text{Cl}^-$  ions in a rhomb lying in the crystal  $ab$ -plane and two  $\text{H}_2\text{O}$  molecules along the normal ( $c$ -axis). For the two  $\text{Cu}^{++}$  ions the rhomb is rotated (around  $c$ -axis), so as to make the  $ac$ -plane a plane of reflection. For  $\text{CuK}_2\text{Cl}_4 \cdot 2\text{H}_2\text{O}$  the  $g$  values are  $g_{y,c} = 2.06$ ,  $g_x = 2.105$  and  $g_z = 2.30$ . The anisotropic line width  $\Delta H$  ranges from 110 to 250  $\phi$ . In the (001) direction  $\Delta H = 115 \phi$ . The average exchange constant  $J$  is estimated to be

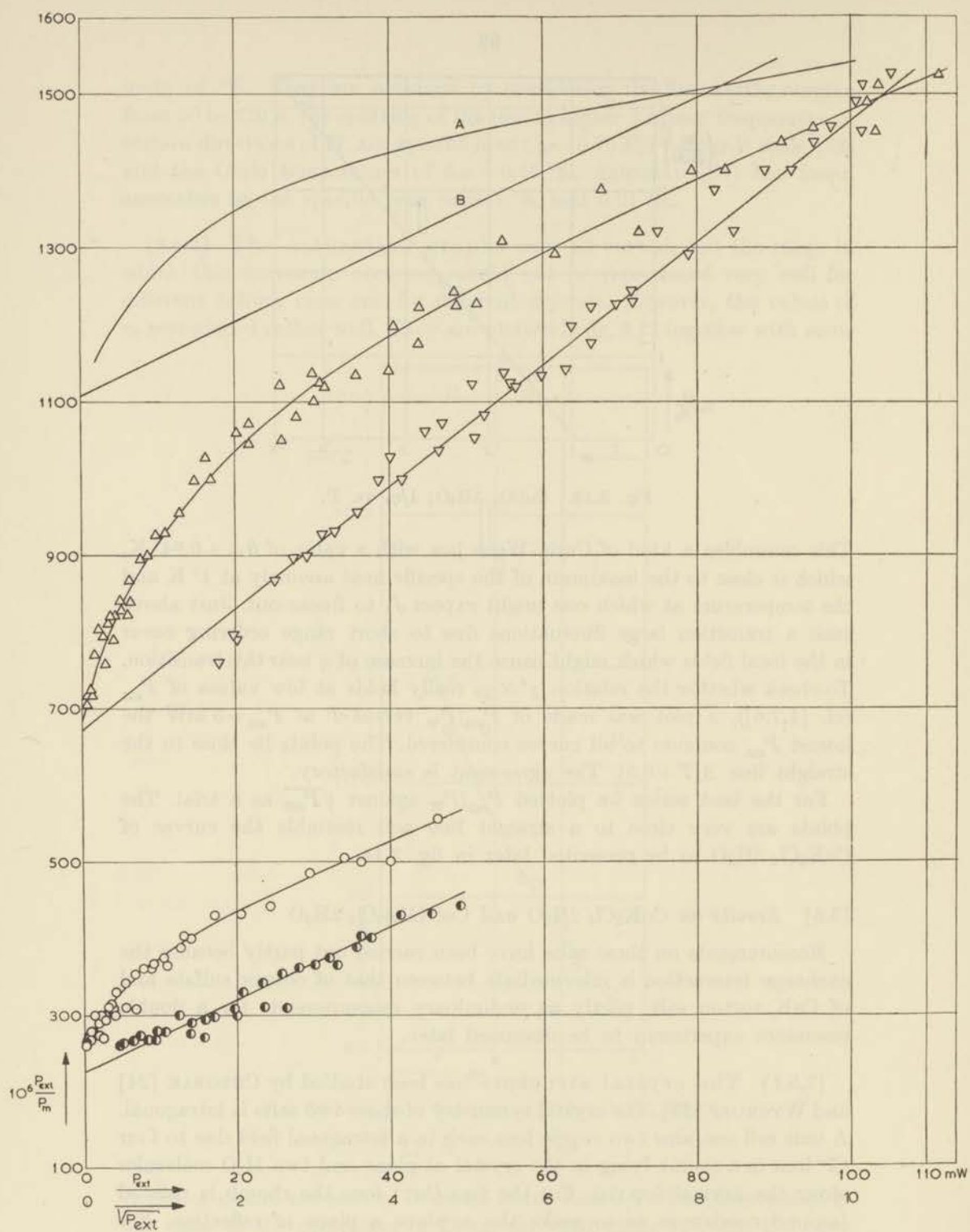


Fig. 3.14. Saturation graphs of  $\text{CuK}_2\text{Cl}_4 \cdot 2\text{H}_2\text{O}$ .

$10^6 P_{\text{ext}}/P_m$ vs $P_{\text{ext}}$ ;	vs $\sqrt{P_{\text{ext}}}$ ;	$T$
○	●	2.29° K
△	▽	3.22° K
A	B	4.25° K

$0.0931 \text{ cm}^{-1} \equiv 2792 \text{ MHz}$  [26], but the values of the various exchange interactions present have not yet been analysed. For  $\text{Cu}(\text{NH}_4)_2\text{Cl}_4 \cdot 2\text{H}_2\text{O}$  these values are somewhat different.

[3.5.2]  $\text{CuK}_2\text{Cl}_4 \cdot 2\text{H}_2\text{O}$ . At some temperatures the saturation graphs have been measured over a large range of  $P_{\text{ext}}$ , their coordinates being given in table VII. The direction of  $\mathbf{H}$  was at  $50^\circ$  to the  $c$ -axis in the plane bisecting the two  $a$ -axes. Some of the measured graphs have been drawn in fig. 3.14. In this figure are also plotted the values of  $P_{\text{ext}}/P_m$  as a function of  $\sqrt{P_{\text{ext}}}$ . These last points are very close to a straight line in the central part of the saturation graphs which are therefore close to parabolas with their start and final parts straightened. This was the case for all graphs of table VII. The slope of the straight line is given in the last column, together with the ordinate at  $P_{\text{ext}}=0$ . The values of  $P_{\text{ext}}/P_m$  as a function of  $T$  at  $P_{\text{ext}}=3 \text{ mW}$  lie on a straight line through the origin.

TABLE VII  
 $\text{CuK}_2\text{Cl}_4 \cdot 2\text{H}_2\text{O}$

$\frac{P_{\text{ext}}}{\text{mW}}$ $T^\circ\text{K}$	$10^6 \cdot P_{\text{ext}}/P_m$									$P_m$ min	$\eta_s$	$P_m$ max	$\eta_f$
	0	1	2	4	8	16	32	64	max				
1.87	511	552	586	640	716	830	982	—	1078	3.4	50.5	42	244
3.22	667	737	773	818	888	989	1137	1310	1474	2.6	33	73	220
4.25	—	—	1160	1191	1245	1323	1399	1476	1584	1.7	23.2	71	660

To determine more fully  $\eta_s$  and  $\eta_f$  more experiments were performed at only low or high values of  $P_{\text{ext}}$ . For different crystals the curved part was not completely in the same range of  $P_{\text{ext}}$  like for  $\text{CuSO}_4 \cdot 5\text{H}_2\text{O}$ , but  $\eta_s$  and  $\eta_f$  were reproducible. They are plotted in fig. 3.15 and fig. 3.16.

In the helium range we find when plotted on a double logarithmic scale  $\eta_s \approx 95/T \text{ W/mole}$ . But, when making a linear plot of  $\eta_s$  vs  $T$ , a slightly better fit is obtained by the formula:

$$\eta_s = \frac{117}{T+0.4} \text{ W/mole.}$$

The values of  $\eta_f$  suggest a discontinuity at the  $\lambda$  point of helium, (although we do not know if this is a reality) with a  $T^3$  or  $T^4$  dependence above this point.

For  $\mathbf{H} // c$ -axis the value of  $\eta$  was determined at a few temperatures, and found to be four times smaller than for the foregoing direction indicating a strong anisotropy of  $\eta$ . VAN DEN BROEK e.a. [27] measured

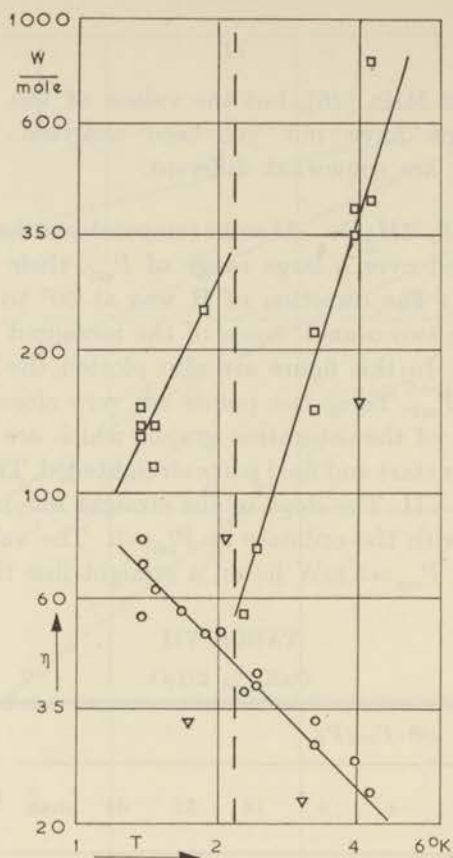


Fig. 3.15.  $\eta$  as a function of  $T$  for  $\text{CuK}_2\text{Cl}_4 \cdot 2\text{H}_2\text{O}$

□  $\eta_I$     ○  $\eta_s$     △  $\eta_{rel}$

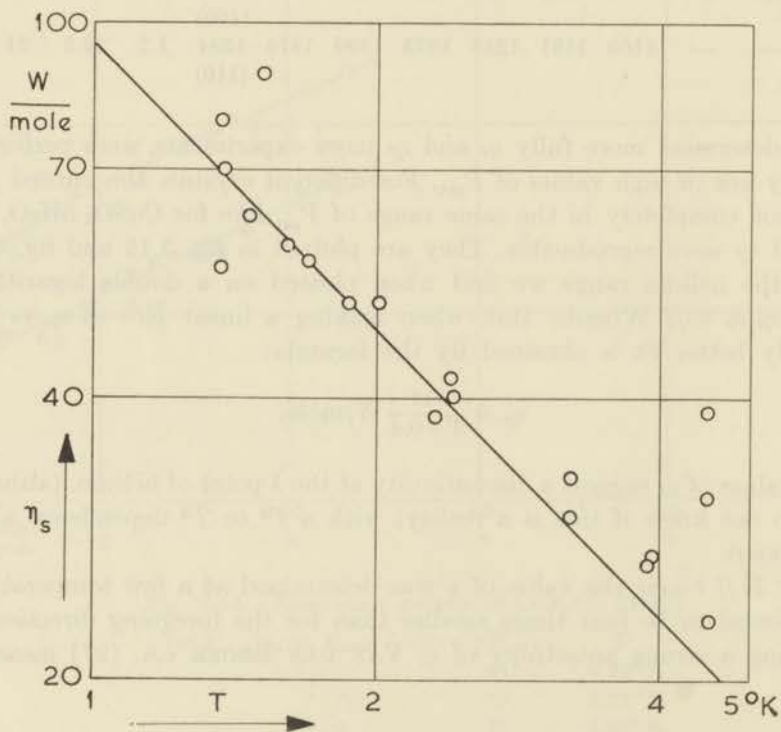


Fig. 3.16.  $\eta_s$  as a function of  $T$  for  $\text{CuK}_2\text{Cl}_4 \cdot 2\text{H}_2\text{O}$

$\eta_{rel}$  on a large single crystal. Their values for  $H = 3300$  o and parallel to the  $c$ -axis have been inserted in fig. 3.15 showing a dependence and the discontinuity at the  $\lambda$  point. So for this salt we find the relation  $\eta_{rel} \approx \eta_f$  to be fulfilled when taking the anisotropy into account.

[3.5.3] Preliminary results on  $\text{Cu}(\text{NH}_4)_2\text{Cl}_4 \cdot 2\text{H}_2\text{O}$  indicate  $\eta_f$  to be about the same as for the potassium salt. Also the temperature dependence has the same character. At  $17^\circ \text{K}$  it was found that  $\eta \approx 400$  W/mole which seems rather low when extrapolating  $\eta_f$ .

[3.6] *Results on  $\text{Mn}(\text{NH}_4)_2(\text{SO}_4)_2 \cdot 6\text{H}_2\text{O}$*

The manganese ion has a spin of  $5/2$  and is an  $S$  state ion. One has to go to a high order in perturbation theory to find the interaction between spins and lattice, and therefore expects to find small values of  $\eta$ .

One of the reasons for investigating this salt was the near independence of the temperature behaviour of  $\eta$  on magnetic dilution as found by VAN DER MAREL e.a. [10]. Only the concentrated salt has yet been investigated, but diluted crystals will be measured. The crystal structure of the tutton salts has been discussed in [3.3.1]. The angles mentioned there are  $\alpha = 32^\circ$  and  $\psi = 58^\circ$ . Due to the fact that  $S = 5/2$  one has to add terms of the fourth power in the spin operators to the spin Hamiltonian. The  $g$ -value is 2.00.

The saturation graphs are curved and the coordinates are given in table VIII. The resulting values of  $\eta$  are plotted in fig. 3.17 together with the values found by VAN DER MAREL. His sample contained impurities, probably of a physical nature, which increased the value of  $\eta_{rel}$ .

TABLE VIII  
 $\text{Mn}(\text{NH}_4)_2(\text{SO}_4)_2 \cdot 6\text{H}_2\text{O}$

$\frac{P_{ext}}{mW}$ $T^\circ \text{K}$	$10^6 \cdot P_{ext}/P_m$								$P_m$ min	$\eta_s$	$P_m$ max	$\eta_f$	coord. $\eta = 2\eta_s$
	0	0.4	0.8	1.5	3.0	6	12	max					
1.33	99.8	149	182	229	306	427	617	914	0.38	8.7	25.2	—	1.0/196
								(23)				37.6	
										14.7		34.4	
1.59	126	162	184	214	268	360	528	786	0.23	—	24.5	36	0.5/167
								(21)		11.6			
2.06	181	196	208	216	260	321	441	461	0.11	21.7	27.9	50.3	—
								(13)					
2.65	228	253	260	269	286	318	—	368	0.42	8.1	29.4	91	0.2/243
								(10.5)					
3.31	283	300	311	324	342	371	—	417	0.39	11.9	29.4	99	0.75/309
								(10.5)					
4.25	333	361	370	379	392	415	458	495	0.09	10.6	38.6	136.3	0.3/357
								(17)					

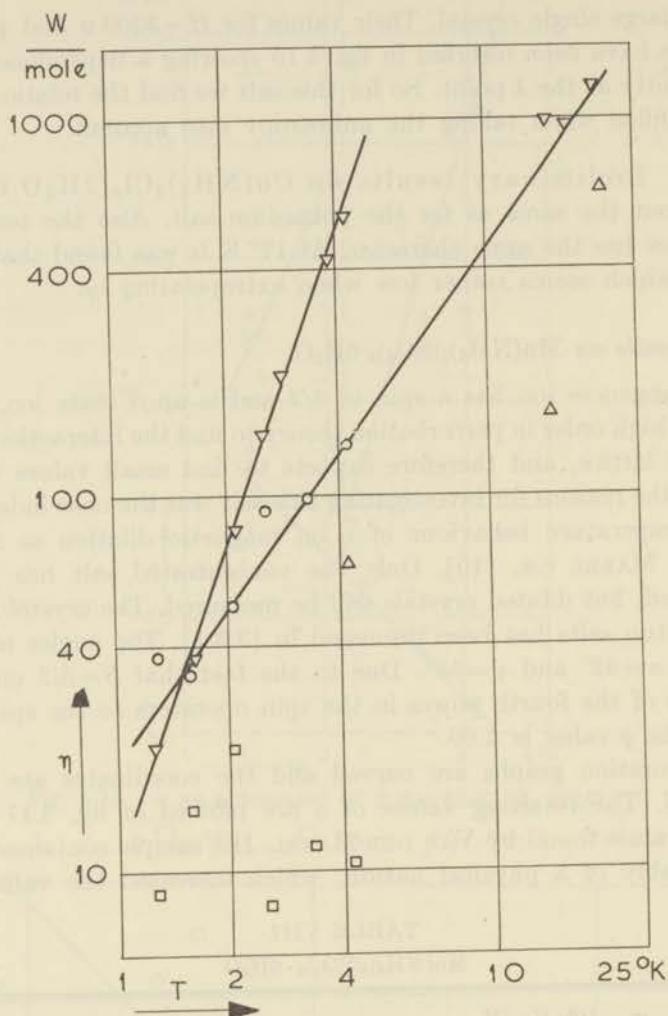


Fig. 3.17.  $\eta$  as a function of  $T$  for  $\text{MnNH}_4$  tutton salt

$\square$   $\eta_s$        $\nabla$   $\eta_{rel}$  VAN DER MAREL  
 $\circ$   $\eta_f$        $\triangle$   $\eta_{rel}$  BIJL

The value he finds for  $b/C$  is also 16% smaller than the ones of BROER [6] and of BIJL [28]. The results of the relaxation measurements for  $H = 3375 \text{ \AA}$  are also inserted in fig. 3.17. VAN DER MAREL e.a.'s values at hydrogen temperatures are seen not to correspond with the extrapolation of their helium measurements. Also the physical purity has been found to affect strongly the shape of the  $\chi(\omega)$  vs  $\omega$  curves, which do not always correspond with true Casimir-Du Pré curves. The measurements of BIJL corresponded satisfactorily with Casimir-Du Pré curves and  $\tau_1$  follows the Brons-Van Vleck formula (1.90) at low values of  $H$  with  $p = 0.43$ . We find:

$$\eta_f = 19.5 T^{1.4} \text{ W/mole}$$

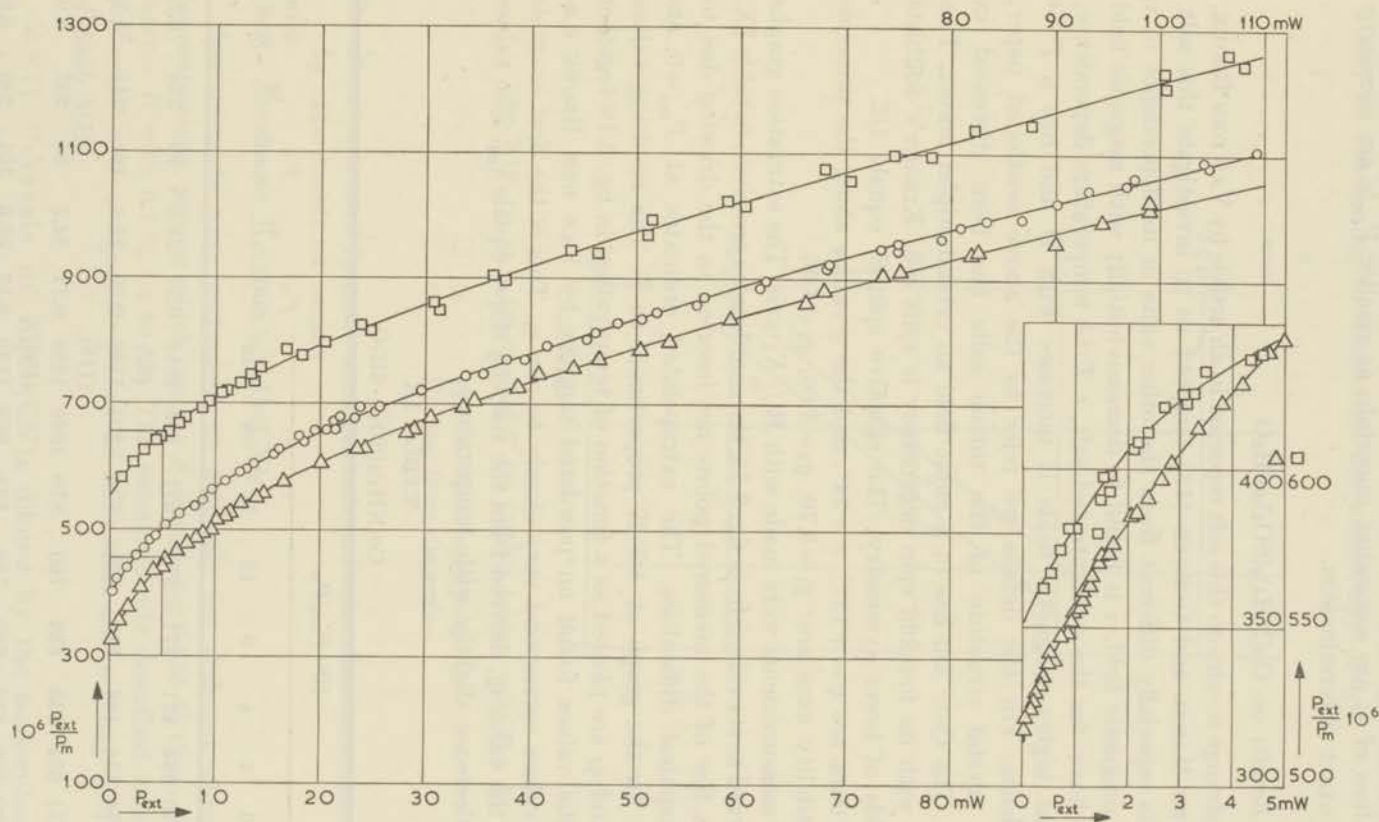


Fig. 3.18. Saturation graphs of  $\text{CoNH}_4$  tutton salt;  $\mathbf{H} // K_1$ . (Scales differ in the inlay)

$\triangle$   $T = 1.33^\circ \text{K}$        $\circ$   $T = 1.61^\circ \text{K}$        $\square$   $T = 2.06^\circ \text{K}$

which also coincides with van der Marel's values at hydrogen temperatures. The values of  $\eta_s$  are somewhat uncertain as smaller  $P_{\text{ext}}$ 's are necessary for its exact determination.

[3.7] *Results on*  $\text{Co}(\text{NH}_4)_2(\text{SO}_4)_2 \cdot 6\text{H}_2\text{O}$

The strange results on this salt reported in an article by VAN DEN BROEK, VAN DER MAREL and GORTER [12] tempted us to investigate this salt, which is especially different from the other salts in its dependence of  $\tau$  on the magnetic field.  $\tau$  is found to decrease initially with magnetic field and to have, for the concentrated salt, a  $T^{-1.0}$  temperature dependence, while at higher magnetic fields it increases with  $H$  and has a  $T^{-2.4}$  dependence. For the details we refer to the above-mentioned paper.

The crystal structure of the tutton salts has been discussed in [3.3.1]. The  $\text{Co}^{++}$  ion has in a cubic field an orbital triplet lowest. This triplet with its fourfold spin degeneracy is split into Kramer's doublets by fields of lower symmetry. The effective spin  $S'$  equals 1/2.

The data are  $\psi = +137^\circ$ ,  $\alpha = 34^\circ$ , and the  $g$ -values along the principle susceptibility axes are:  $g_1 = 5.70$ ,  $g_2 = 3.06$ ,  $g_3 = 4.36$ .

The measurements were made with  $\mathbf{H} \parallel K_1$  axis. The saturation graphs are curved as is evident from fig. 3.18, the coordinates are given in table IX. Only a few of the measured points are inserted in the drawing due to typographical difficulties. The extrapolated ordinates at  $P_{\text{ext}} = 0$  are except for the graph at 4.2° K proportional to  $T$ . The resulting values of  $\eta_s$  and  $\eta_f$  are plotted as a function of temperature in fig. 3.19 together with the values found on powdered samples by VAN DEN BROEK e.a. Their values correspond very closely to our  $\eta_s$ . This is the first example where the value  $\eta_s$ , derived from the starting slope, equals  $\eta_{\text{rel}}$ . The values of  $\eta_f$  decrease slightly with temperature.

TABLE IX  
 $\text{Co}(\text{NH}_4)_2(\text{SO}_4)_2 \cdot 6\text{H}_2\text{O}$

$\frac{P_{\text{ext}}}{\text{mW}}$	$10^6 \cdot P_{\text{ext}}/P_m$								$P_m$ min	$\eta_s$	$P_m$ max	$\eta_f$	coord. $\eta = 2\eta_s$
	0	2	4	8	16	32	64	max					
1.33	316	384	427	477	571	671	858	1010	0.57	21.8	99	228	3.6/423 (99)
1.61	394	454	488	542	620	734	907	1106	0.50	22.8	101	241	1.7/446 (110)
2.06	551	604	639	688	760	870	1040	1256	0.71	34.5	86	202	5.0/654 (108)
2.60	590	628	655	695	749	832	968	1139	0.17	53.6	101	299	5.9/678 (115)
3.30	724	755	780	827	904	1022	1232	1331	1.36	54	60	161	13.5/883 (80)
4.25	757	810	846	891	960	1074	1256	1314	0.39	85	57	182	4.3/850 (75)

As the coupling of the ion with the lattice is strongly anisotropic it would be interesting to determine the anisotropy of  $\eta$ .

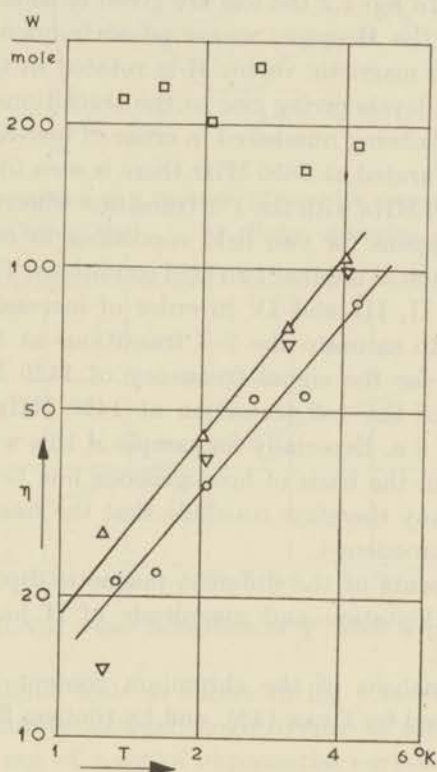


Fig. 3.19.  $\eta$  as a function of  $T$  for  $\text{CoNH}_4$  tutton salt;  $\mathbf{H} // K_1$

□  $\eta_r$       △  $\eta_{rel}$  from absorption  
○  $\eta_s$       ▽  $\eta_{rel}$  from dispersion

B. *Results obtained by pulse measurements and relaxation rates determined by experiments on masers*

[3.8] *Results on  $\text{K}_3\text{Cr}(\text{CN})_6/\text{K}_3\text{Co}(\text{CN})_6$*

Measurements were performed on this salt for different chromium concentrations, among which sample *A* containing 0.035 % Cr to Co and sample *B* with 0.1 % Cr to Co. The measurements described here were performed with a signal frequency of 1420 MHz and a pump frequency of 3850 MHz.

[3.8.1] Crystals of  $\text{K}_3\text{Cr}(\text{CN})_6$  diluted by the isomorphous Co salt have been studied by BAKER, BLEANEY and BOWERS [30] and recently by many others because of their application in masers. The zero field splitting of the  $\text{Cr}^{++}$  ion with  $S = 3/2$  corresponds with a frequency of 5700 MHz. There are two chromium ions in a unit cell, with their

magnetic axes rotated about the  $c$ -axis by  $\pm 6^\circ$  with respect to the crystal axes. In fig. 1.1 the energy levels were shown as a function of the magnetic field. In fig. 1.2 the loci are given of some of the absorption lines in a plane of the  $\mathbf{H}$  space, measured at frequencies of 1420, 3850 and 8600 MHz; the magnetic vector  $\mathbf{H}$  is rotated in the  $ac$ -plane of the crystal. The energy levels giving rise to the transitions are shown beside each locus, the levels being numbered in order of increasing energy. If the 1-3 transition is saturated at 3850 MHz there is seen to be a possibility of maser action at 1420 MHz with the 1-2 transition when the two resonances coincide, which happens for two field conditions in each quadrant, and with the 2-3 transition at another two field conditions. The operating points will be denoted I, II, III and IV in order of increasing magnetic field. It is also possible to saturate the 2-4 transitions at 8600 MHz and use the 2-3 transition for the signal frequency of 1420 MHz.

The line width of the 1-2 transition at 1420 MHz for both samples was of the order of  $8\sigma$ . Especially for sample  $A$  this width is much larger than one expects on the basis of homogeneous line broadening ( $\approx 0.8\sigma$ ) (cf. [1.4.4]). One may therefore conclude that the lines for sample  $A$  are inhomogeneously broadened.

The matrix elements of the different magnetic dipole transitions as a function of the orientation and magnitude of  $\mathbf{H}$  have been computed by HOWARTH [31].

The chemical analysis of the chromium content was performed by the method described by DEAN [32], and by röntgen fluorescence spectrography\*.

[3.8.2] The influence of a modulated pump power on the signal. One has to work with pump and signal frequencies, which are fixed by the cavity resonances. Finding the exact magnitude and direction of  $\mathbf{H}$  for which the pump influences the signal most, e.g. the operating points, may therefore present some difficulties. We found a quick method to trace the operating points by pulse modulating the pump power at a repetition rate lower than the relaxation rates. Near an operating point the signal power will also become modulated and the largest modulation will occur at its centre.

With the arrangement of fig. 2.6, using an unmodulated 1420 MHz signal, the time behaviour of the signal absorption is displayed on the oscillograph. This one, a tektronix type 532, had its time base synchronized to the pump modulation, and pictures like those in fig. 3.20 may be observed. Photographs were taken from the oscillograph pictures and afterwards projected on a screen. Two methods can then be followed to determine the time constants  $\tau$ . The first is to measure the deviation of the signal from its equilibrium value as a function of time and plot this

\*) I am very much indebted to Drs J. de Vries of the N.V. Philips' Gloeilampenfabrieken for performing this analysis.

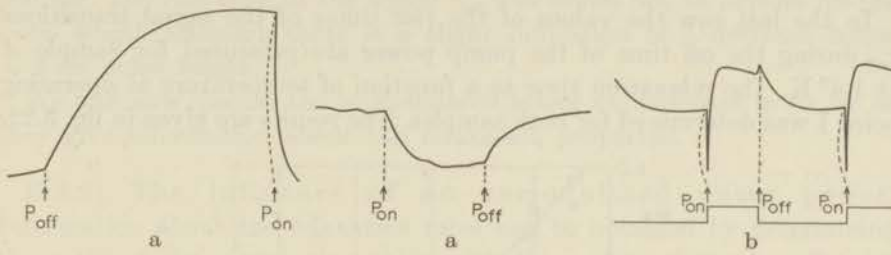


Fig. 3.20. Signal absorption as a function of time for a modulated pump power  $P$ .  
a)  $K_3Cr/Co(CN)_6$  b) Ruby operating point  $R_I$

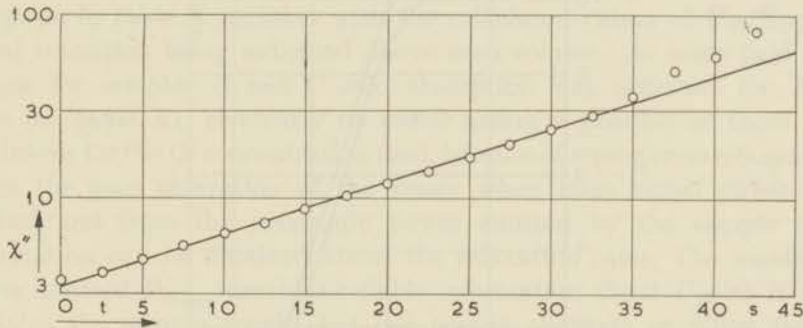


Fig. 3.21.  $K_3Cr/Co(CN)_6$ ; Time behaviour of  $\chi''$  after a pulse of pump power

on a single logarithmic scale as shown in fig. 3.21. The second, a much faster but less accurate method, is by trying to identify the projected pictures with one out of a set of exponential curves with different time constants, drawn on a glass plate. One should only know the time scale of the projection which is obtained from the projected oscillograph screen and its calibrated scale. Both methods to determine  $\tau$  have been used. The values of the magnetic field and its direction for the four operating points are given in table X.

TABLE X

Data of operating points in  $K_3Cr(CN)_6/K_3Co(CN)_6$   
Pump 3850 MHz (1-3 tr.); Signal 1420 MHz

Operating point	I	II	III	IV
Signal transition . . . . .	1-2	2-3	2-3	1-2
Magnetic field ( $\theta$ ) . . . . .	480	680	1170	1280
$\angle H$ to a-axis (in ac-plane) . . . . .	$11^\circ$	$25^\circ$	$14^\circ$	$3^\circ$
$\lim_{P_{\text{pump}} \rightarrow \infty} \frac{u_m}{(u_m)_{P_{\text{pump}}=0}}$				
A Cr/Co = 0.035 % . . . . .	-1.23	-1.05	-0.90	-1.3
B Cr/Co = 0.1 % . . . . .	0	0	0	0
C Cr/Co = 0.05 % . . . . .	$\approx -1$	0	0	$\approx -1$
For sample A				
$U_{23}/U_{13}$ . . . . .	4.6	1/3.1	1/2.3	5.7
$\tau_{\text{off}}$ (ms.) at 1.4 °K . . . . .	44.7	26.1	33.4	29.0

In the last row the values of the rise times of the signal transitions  $\tau_{\text{off}}$  during the off time of the pump power are presented for sample *A* at 1.4° K. The relaxation time as a function of temperature at operating point I was determined for both samples. The results are given in fig. 3.22.

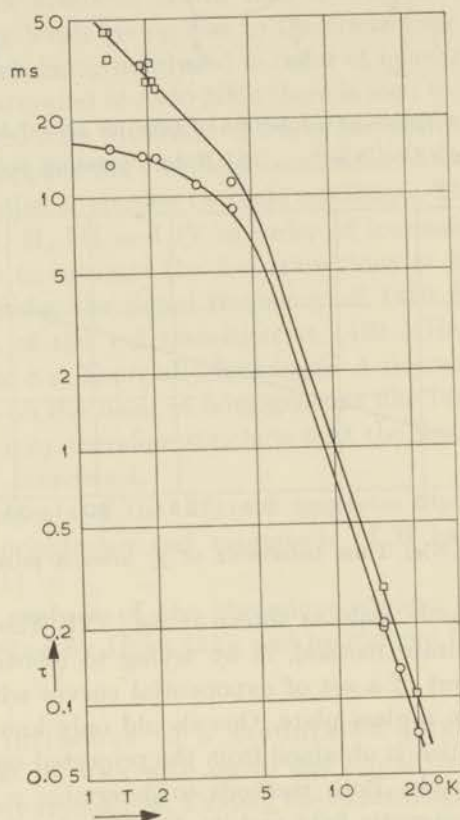


Fig. 3.22.  $\tau_{\text{off}}$  as a function of  $T$  for  $\text{K}_3\text{Cr/Co(CN)}_6$

□  $\tau_{\text{off}}$  sample *A*      ○  $\tau_{\text{off}}$  sample *B*

For both samples we may take  $\tau \propto T^{-3.3}$  between 6° K and 20° K but below this range the temperature dependences differ. For sample *A* we found at liquid helium temperatures

$$(3.03) \quad \tau_A = 62/T \text{ ms.}$$

For sample *B* the values of  $\tau_B$  in this temperature range can very well be represented by

$$(3.04) \quad \frac{1}{\tau_B} = \frac{1}{\tau_A} + \frac{1}{31} (\text{ms})^{-1}.$$

This curve has been drawn in fig. 3.22.

It was checked whether the pulse length of the pump modulation was of any influence on the characteristic times. For sample *B* at nearly all temperatures investigated the pump pulse was varied between 1 ms and

100 ms. The rise time of the signal  $\tau_{\text{off}}$  was found not to depend on the pulse length although there is a slight indication of a decrease below  $\approx 4$  ms pulse length.

We will now discuss the unmodulated maser experiments in so far as they give information about the relaxation properties.

[3.8.3] The influence of an unmodulated pump power. Information about the relaxation rates can be obtained by determining the ratio of the signal absorption with  $P_{\text{pump}}=0$  to that when  $P_{\text{pump}}$  is very large and by using formula (2.31). For the four operating points possible when  $\omega_p/2\pi \approx 3850$  MHz and  $\omega_s/2\pi=1420$  MHz these ratios are given in table X together with the calculated values of  $\bar{U}_{23}/\bar{U}_{12}$ , the signal transition being indicated above each column. At some field conditions for samples *B* and *C* zero absorption was obtained for  $P_{\text{pump}}$  large (cf. table X). Evidently no maser action is possible at those field conditions for the Cr concentration used, because of strong cross relaxations. From the gain saturation of the maser when large signal powers are applied and from the maximum power emitted by the sample more information can be obtained about the relaxation rates. The maximum power emitted  $P_{12_{\text{max}}}$  provides reliable information about  $U_{23}$  as it only contains the sample weight but not matrix elements or filling factors (see (2.32)). For the operating point no. I of sample *A*, the only point for which amplification was obtained, the measured value was

$$P_{12_{\text{max}}} = 2 \times 10^{-7} \text{ W.}$$

$$(Q_0 = 4000, Q_e = 1000, Q_m = -900).$$

The calculated value (with (2.32)) for a crystal of 6.45 g, and a Cr/Co percentage of 0,035 % as used by us, becomes

$$P_{12_{\text{max}}} = 7.6 \times 10^{-8} \times U_{23} \text{ W}$$

using the ratio of  $U_{23}/U_{12}$  given in table X. Comparing the measured and calculated values of  $P_{23_{\text{max}}}$  results in:

$$U_{23} = 2.6 \text{ s}^{-1} \text{ and } U_{12} = 0.6 \text{ s}^{-1}.$$

For the other operating points  $-u_m$  was for sample *A* not large enough to obtain amplification. For sample *B* the absorption approached asymptotically  $u_m=0$  when increasing the pump power.

A value of  $U_{12}+U_{23}$  can be derived from the saturation of the maser gain. As large samples are used in masers, one has to take into account the variation of the magnetic h.f. field over the sample size. The resulting value will not be too reliable.

[3.8.4] In-homogeneous saturation at the pump frequency. A crucial experiment was performed to test whether a homogeneous saturation by the pump is effected even when there are nodes of the

magnetic field at  $\omega_p$  inside the sample. By using the hot phonon theory, to be discussed later, MORRIS, KYHL and STRANDBERG [33] suggested that, because of the large mean free paths at low temperatures, phonons in a narrow band around  $\omega_p$  will transport energy from saturated towards unsaturated regions, thus providing a homogeneous spin temperature at the pump frequency throughout the crystal. They used this picture to explain the large values of  $-u_m$  obtained by them in a maser using a ruby and  $\omega_p/2\pi = 24$  KMHz.

Because of the importance of this question in the design of a maser and the understanding of the relaxation mechanisms we have carried out a simpler experiment than that performed by MORRIS e.a., where it was not possible to measure the emission for a saturating field uniform throughout the crystal.

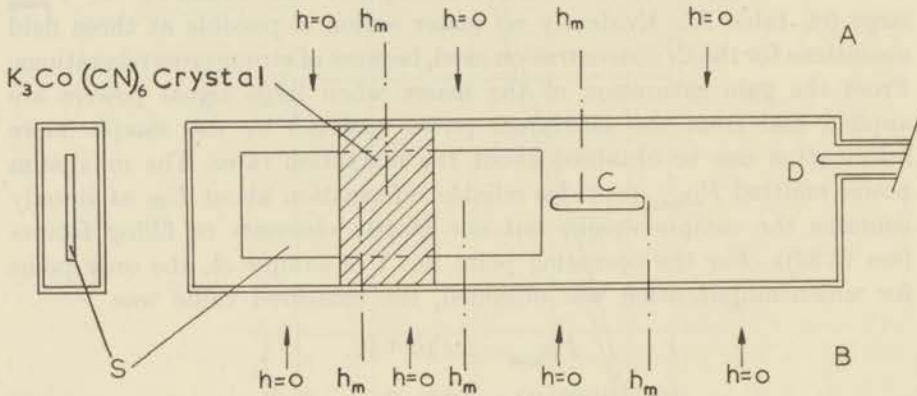


Fig. 3.23. Cavity for inhomogeneous pumping experiment

A	$TE_{103}$ mode	3850 MHz
B	$TE_{104}$ mode	4100 MHz
C	coupling slot	1420 MHz
D	coupling loop	3850 MHz
S	strip $\lambda/2$ at	1420 MHz
	h = 0 nodes of pumping field	

In figure 3.23 shows a section through a rectangular cavity (cavity no. 3) resonant in the  $TE_{103}$  mode at 3850 MHz. In the cavity a resonant strip is placed approximately  $\lambda/2$  long at 1420 MHz, and a large crystal of  $K_3Cr/(CN)_6/K_3Co(CN)_6$  with its centre at a point where the magnetic field at the  $TE_{103}$  mode is a maximum. As indicated on the figure the crystal extends about  $2/3$  of the way towards the magnetic field nodes. Under these conditions most of the crystal could be saturated with a power of 100 mW in the cavity at 3850 MHz, and the corresponding emission was measured (see fig. 3.24). For this cavity the  $TE_{104}$  resonance is at 4100 MHz, with the magnetic field distribution indicated at the bottom of figure 3.23. The magnetic field maximum is now near the edge of the crystal, and a field node lies within the crystal. Under these con-

ditions there was no net emission with a pump power of 100 mW in the cavity, at which level the  $u_m$  was close to an asymptotic value, but still decreasing with increasing  $P_{\text{pump}}$  as can be seen in fig. 3.24.

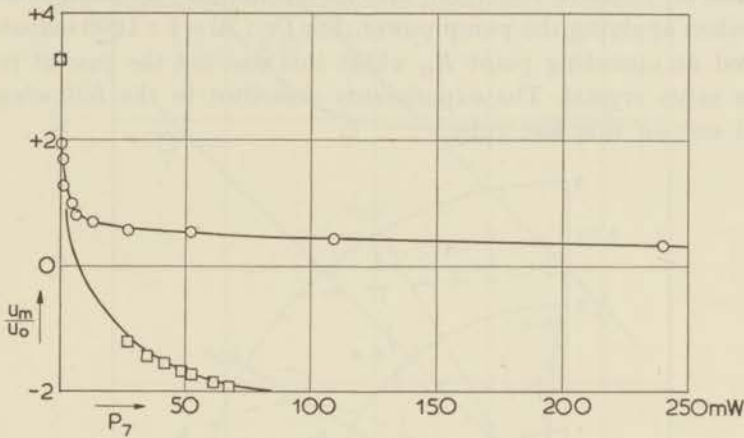


Fig. 3.24. Signal absorption as a function of pump power,  $P_7$

- pumped by  $TE_{103}$  mode (no pump node in crystal)
- pumped by  $TE_{104}$  mode (pump node in crystal)

An auxiliary experiment with another cavity confirmed that the emission from a small, uniformly saturated crystal was comparable for saturating frequencies of 3850 and 4100 MHz. These experiments suggest that, at least for  $K_3Cr(CN)_6/K_3Co(CN)_6$  and with these pump frequencies, it is not possible to saturate a crystal throughout its volume with a non-uniform field distribution. The experiment by MORRIS *et al.* might be explained by realizing that for large pump powers the regions where the pumping is insufficient become relatively small, which is demonstrated by the behaviour of  $u_{m104}$  (cf. fig. 3.24).

### [3.9] Results on synthetic ruby

Synthetic ruby,  $Al_2O_3$  with a small amount  $Cr_2O_3$ , has proved to be a suitable maser material.

The paramagnetic resonance spectrum of the  $Cr^{+++}$  ion in this substance has been studied by various investigators [34] [35] [36]. The zero field splitting corresponds with a frequency of 11593 MHz with no rhombic component being present and with an isotropic  $g$ -value of 2.00. In fig. 3.25 some of the loci of the transitions in  $\mathbf{H}$  space are shown ( $\mathbf{H}$  in  $ac$ -plane).

For the 1-2 transition at 1430 MHz it is possible to use the 1-3 transition at 10.7 KMHz as a pump frequency. An operating point occurs for  $H=430 \text{ G}$  and at  $23^\circ$  to the  $c$ -axis of the crystal, which point will be denoted by  $R_I$ . Another operating point investigated,  $R_{II}$ , was obtained

with  $\omega_p/2\pi = 8500$  MHz for the 1-3 transition and  $\omega_s/2\pi = 1430$  MHz for the 2-3 transition with  $H = 2100$  O and at  $21^\circ$  to the  $c$ -axis.

With a ruby of a nominal ratio of Cr : Al = 1 : 200 it was not possible to obtain an emissive condition, and all resonances saturated homogeneously when applying the pump power. For Cr : Al = 1 : 1000 emission was obtained at operating point  $R_{II}$  whilst this was not the case at point  $R_I$  for the same crystal. The experiments described in the following, were carried out on this last ruby.

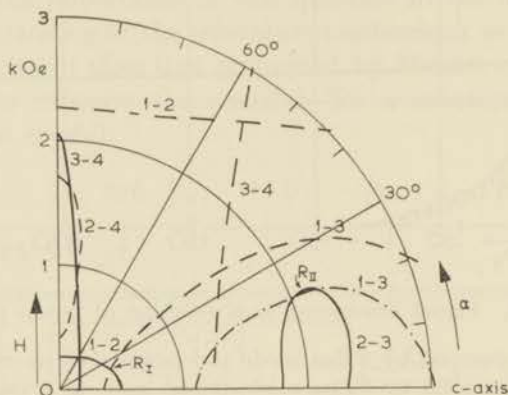


Fig. 3.25. Rotation diagram of ruby, symmetry axis is  $c$ -axis. Corresponding energy levels next to loci, lowest is 1.

—————	1430 MHz	
- - - - -	8500 MHz	$R_I$ and $R_{II}$ operating points
- · - · -	10.7 KMHz	

[3.9.1] Pump frequency 8500 MHz. Operating point  $R_{II}$ . In fig. 3.26 the rise times of the signal,  $\tau_{off}$ , are plotted as a function of temperature. It is seen that they are close to  $22/T$  ms. The temperature dependence appears to become less at the lower temperature range. For this operating point  $R_{II}$  emission was observed.

[3.9.2] Pump frequency 10.7 KMHz, operating point  $R_I$ . For the 1-2 transition at  $R_I$  the absorption observed was much stronger than for the 2-3 transition at  $R_{II}$ , in agreement with a calculation using the matrix elements.

However, on applying the saturating field, only a brief pulse of emission, lasting a few milliseconds was obtained. This can be seen in figure 3.20b where the 10700 MHz oscillator is pulsed on for 13 ms. every 40 ms., as indicated on the lower trace. The upper trace shows the signal reflected from the cavity at 1430 MHz, emission from the (unpolished) ruby causing a decrease in the reflection (downwards deflection) for the undercoupled cavity used. When the 10.7 KMHz oscillator is switched on, there is a short pulse of emission, followed by an increase in the absorption to above its equilibrium value. This was observed at both  $1.4^\circ$  K and  $20^\circ$  K. The

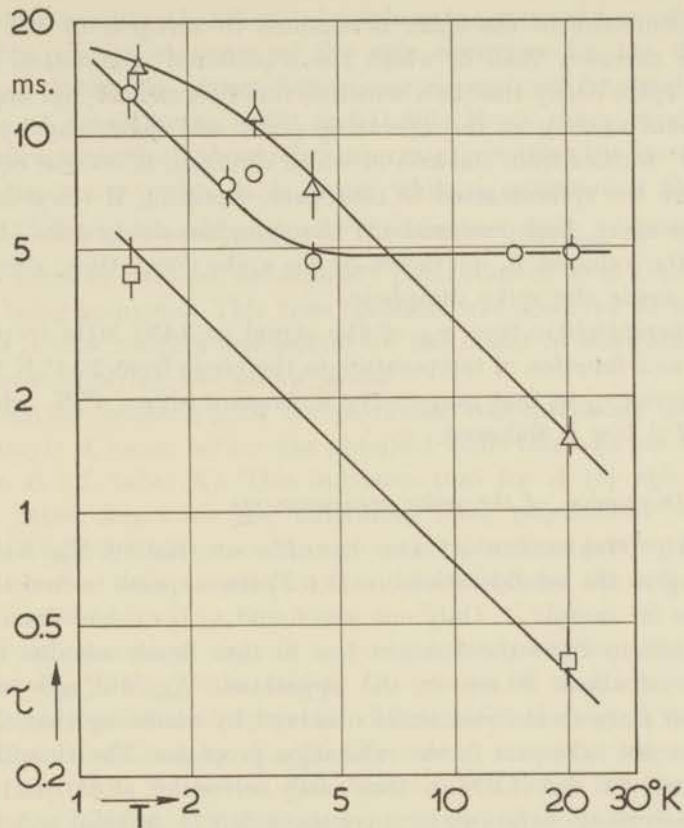


Fig. 3.26. Characteristic times of signal absorption for ruby

- △  $\tau_{\text{off}}$  pump 8.5 KMHz
- $\tau_{\text{off}}$  pump 10.7 KMHz
- decay time spike (pump 10.7 KMHz)

time constant has been plotted in fig. 3.26. Other measurements then showed that subsequently the absorption decreased slowly, and after about 1 s. (at 1.4° K) it had fallen to a steady value close to half the equilibrium absorption. Even with high saturating powers ( $\geq 200$  mW) the steady state absorption could not be further decreased.

As the population difference only decreased to half the equilibrium value at 1430 MHz one expects absorption at the 2-3 transition (9270 MHz), the idling frequency, to become negative when the pump is fully saturating. We therefore carried out a triple frequency experiment and observed the signals at 1430 MHz and 9270 MHz simultaneously. The 2-3 signal was seen to decrease to a very small value, but not to turn negative, indicating that the pump transition was not fully saturated which is surprising because of the large pump power used ( $\geq 200$  mW). This spike behaviour may be related to the intermittent oscillations observed for continuously pumped ruby maser at 9000 MHz by MAKHOV, e.a. [37].

The occurrence of the spike is confined to a region of the field and its angle narrower than in which the transferred modulation is visible. Also the spike decay time is a sensitive function of field and angle, being a minimum exactly at the operating point and increasing by a factor four,  $2.5^\circ$  further from the axis in which direction it became equal to  $\tau_{\text{off}}$  and where the spike started to disappear. Rotating  $\mathbf{H}$  towards the axis made the spike disappear without changing the decay time. Increasing  $\mathbf{H}$  from the value at  $R_I$  on, increased the spike decay time; decreasing  $\mathbf{H}$  from  $R_I$  made the spike disappear.

The characteristic time  $\tau_{\text{off}}$  of the signal at 1430 MHz is plotted in fig. 3.26 as a function of temperature in the range from  $20.4^\circ \text{K}$  to  $1.4^\circ \text{K}$ . One observes  $\tau_{\text{off}}$  in that range to be a constant above  $4^\circ \text{K}$ , while below  $4^\circ \text{K}$  a  $T^{-1}$  law is followed.

### [3.10] Discussion of the pulse measurements

[3.10.1] Discussion of the results on  $\text{K}_3\text{Cr}(\text{CN})_6/\text{K}_3\text{Co}(\text{CN})_6$ . According to the considerations in [1.6.2] one expects to find three time constants for sample *A*. Only one was found as is evident from fig. 3.21. The deviations from the straight line in that figure are due to a time constant of about 80 ms. in the apparatus. We will now relate the relaxation rates to the rise times observed by assuming that the fourth level does not take part in the relaxation processes. The time dependent equations (1.64) and (1.62) are then easily solved (cf. (1.65)) and one finds for the reciprocal of the two time constants left (1-2 signal and 1-3 pump transition)

$$(3.05) \quad \lambda_{1,2} = \bar{V}_{12} + \bar{V}_{13} + \bar{V}_{23} \pm \sqrt{\bar{V}_{12}^2 + \bar{V}_{13}^2 + \bar{V}_{23}^2 + \bar{V}_{12}\bar{V}_{13} + \bar{V}_{12}\bar{V}_{23} + \bar{V}_{13}\bar{V}_{23}}$$

This expression can be simplified when it is allowed to expand the root and one then finds with  $r = \bar{V}_{12}/\bar{V}_{23}$  and  $R = \bar{V}_{13}/\bar{V}_{23}$

$$(3.06) \quad \begin{cases} \lambda_1 = \bar{V}_{23} \frac{Rr + r + R}{2(1+R+r)} \\ \lambda_2 = 2\bar{V}_{23}(1+R+r) - \lambda_1. \end{cases}$$

For the time behaviour after shutting off the pump power we can try to identify the reciprocal rise time observed with  $\lambda_1$  or with  $\lambda_2$ . Inserting the values found by steady state measurements at  $1.4^\circ \text{K}$  for  $U_{12}$ ,  $U_{23}$  in [3.8.3] and  $\lambda = 10^3/44 \text{ s}^{-1}$  for operating point I of sample *A*, results in a negative value of  $R$  when  $\lambda_1$ , and  $R = 3.1$  when  $\lambda_2$  is the reciprocal rise time observed.

Only the last solution is acceptable, so we find:

$$\bar{U}_{12} = 0.6 \text{ s}^{-1}; \quad \bar{U}_{23} = 2.6 \text{ s}^{-1}; \quad \bar{U}_{13} = 8.1 \text{ s}^{-1}$$

and  $\lambda_1 = 1.2 \text{ s}^{-1}$  for  $T = 1.4^\circ \text{K}$ . The values of  $U$  when plotted as a function of  $\omega$  on a double logarithmic scale are on a straight line so that  $U \propto \omega^{2.6}$ .

This proportionality should not be taken too seriously as according to (1.51) the matrix elements of the spin operators for the different transitions do enter. The expected frequency dependence for equal matrix elements is  $\omega^2$  according to (1.53) and (1.60). From these experiments no information is obtained about relaxation rates involving the fourth level.

During the pump pulse,  $\lambda_2$  is large, while  $\lambda_1$  approaches the limit  $\lambda_{1\text{pulse}} = \frac{\bar{U}_{12} + \bar{U}_{23}}{2}$  which equals  $1.6 \text{ s}^{-1}$ . The constant  $1/\lambda_{1\text{pulse}}$  characterizes the time it takes to establish a stationary population of level 2, the pump transition being saturated. This time constant was observed to be really so long, as it took roughly one second for the maser to start amplifying after stepwise applying the pump power.

The reason for working with the particular concentrations used was, that for sample *A* maser action was obtained while this was not the case for sample *B* (cf. table X). This indicates that for *A* the spin lattice relaxation rates determine the individual level populations while in sample *B* the spin system comes through cross relaxations into equilibrium in a time shorter than a critical value determined by the spin lattice relaxation times.

When cross relaxations become important two situations may arise. In the first  $U_{\text{cr}} \gg U_{ij\text{max}}$  (the largest  $U_{ij}$  present at that temperature), the time behaviour of the population difference of the signal transition is essentially determined by  $U_{ij\text{max}}$ . The second situation may be met with when the cross relaxation rate forms a bottleneck for the energy transfer, but is still fast enough to prevent maser action. So when we have (see [38])

$$(3.07) \quad \bar{U}_{\text{cr}} \omega_{kl} > \bar{U}_{lm} \omega_{lm} - \bar{U}_{kl} \omega_{kl}$$

where  $\omega_{kl} = \omega_s$ , and

$$(3.08) \quad \bar{U}_{\text{cr}} < U_{ij\text{max}}$$

As the  $U_{ij}$ 's are temperature dependent, while this is not the case for  $U_{\text{cr}}$ , these conditions may be fulfilled at one temperature, but at a lower temperature the first situation, or at a higher one maser action may be expected. We suggest that in the measured temperature range below  $4^\circ \text{ K}$  the second situation exists for sample *B* with  $U_{\text{cr}} \approx 10^3/31 \text{ s}^{-1}$ .

Above this temperature an inverted difference in populations of transition 1-2 or at least a non-equilibrium situation in the spin system seems also possible for sample *B*. At temperatures much lower than the ones measured at  $\tau_{\text{off}}$  is expected to increase again (situation I). Condition (3.08) can be fulfilled by assuming that at least one of the relaxation rates from the fourth level towards the three levels just considered is fast. Theoretically this is expected to be  $U_{14}$ .

[3.10.2] Discussion of the results on the ruby. The characteristic times  $\tau_{\text{off}}$  observed at the operating point  $R_1$  (pump 10.7 KMHz)

can be explained in the following way. Relation (3.07) holds for the whole temperature range measured, but below  $4^\circ$  K we have  $U_{cr} > U_{ij_{max}}$ . As  $U_{ij_{max}} \propto T$  condition (3.08) may be fulfilled at a higher temperature and this appears to be the case above  $4^\circ$  K, with  $U_{cr} \approx 10^3/5 \text{ s}^{-1}$ .

As for operating point  $R_{II}$  emission was observed, the inequality (3.07) does not hold. Cross relaxations appear to become important in the lower temperature range. The spike behaviour is not quite understood. If only three levels are concerned, relaxation processes will not increase the absorption above its equilibrium value. However, this could be explained if there were cross relaxations involving the fourth level. Since  $\tau_{spike} \propto T^{-1}$  a relaxation rate towards this fourth level would then have to be the determining factor.

## REFERENCES

1. LIPSON, H. and C. A. BEEVERS, Proc. Roy. Soc. A 148, 664 (1935).
2. LIPSON, H., Proc. Roy. Soc. A 151, 347 (1935).
3. VAN VLECK, J. H., Phys. Rev. 7, 61 (1939).
4. BLEANEY, B., Proc. Roy. Soc. A 204, 203 (1950).
5. KRAMERS, H. C., D. BIJL and C. J. GORTER, Physica 16, 65 (1950) Comm. Kamerlingh Onnes Lab. no. 280a.
6. BROER, L. J. F., Thesis, Amsterdam (1945).
7. DIJKSTRA, L. J., C. J. GORTER and O. VAN PAEMEL, Physica 69, 673 (1942).
8. DE VRIJER, Thesis Leiden (1951).
9. ESCHENFELDER, A. H. and R. T. WEIDNER, Phys. Rev. 92, 869 (1953).
10. VAN DER MAREL, L. C., Thesis, Leiden (1958).  
VAN DER MAREL, L. C., J. VAN DEN BROEK and C. J. GORTER, Physica 24, 101 (1958) Commun. no. 310a.
11. TUTTON, Phil. Trans. Roy. Soc. A 216, (1916).
12. VAN DEN BROEK, J., L. C. VAN DER MAREL and C. J. GORTER, Physica 25, 371 (1959) Commun. no. 314c.
13. BLEANEY, B., R. P. PENROSE and B. I. PLUMPTON, Proc. Roy. Soc. A 198, 406 (1949).
14. BAGGULEY, D. M. S. and J. H. E. GRIFFITHS, Proc. Phys. Soc. A 65, 594 (1952).
15. POLDER, D., Physica 9, 709 (1942) Commun. 92b.
16. BENZIE, R. J. and A. H. COOKE, Nature, Lond. 164, 837 (1949).
17. NAGAOKA, Y. K., Phys. Soc. of Japan 13, 1328 (1958).
18. GIORDMAINE, J. A., L. E. ALSOP, F. R. NASH and C. H. TOWNES, Phys. Rev. 109, 302 (1958).
19. BEEVERS, C. A. and H. LIPSON, Proc. Roy. Soc. A 146, 570 (1934).
20. BAGGULEY, D. M. S. and J. H. E. GRIFFITHS, Proc. Roy. Soc. A 201, 366 (1950).
21. PRYCE, M. H. L., Conf. les phénomènes cryomagnétique Collège de France 80 (1948).
22. DUYNCKAERTS, Mem. Soc. Roy. Sci. Liège VI, 195 (1942).
23. ASHMEAD, Nature Lond. 143, 853 (1939).
24. CHROBAK, L., Z. krist. A 88, 35 (1934).
25. WYCKOFF, R. W. G., Crystal Structures (New York, 1951) Vol. II table X B, 1(2).
26. TOMITA, K., Int. Conf. on Theor. Phys. Kyoto (1953).
27. VAN DEN BROEK, J., L. C. VAN DER MAREL and C. J. GORTER, to be published in Physica and Commun.

28. BYL, D., *Physica* **16**, 269 (1950) Commun. no. 280b.
29. LINGANE, J. J. and R. L. PECSOK, *J. Amer. Chem. Soc.* **72**, 425 (1949).
30. BAKER, J. M., B. BLEANEY and K. D. BOWERS, *Proc. Phys. Soc. B* **69**, 1205 (1956).
31. HOWARTH, D. J., R.R.E. Memorandum no. 1501 (1958).
32. DEAN, J., *Anal. Chem.* **30**, 977 (1958).
33. MORRIS, R. J., R. L. KYHL and M. W. P. STRANDBERG, *Proc. I. R.E.* **47**, 80 (1959).
34. ZAPIRO, M. M. and Y. Y. SHAMONIN, *Sov. Phys. J.E.T.P.* **3**, 171 (1956).
35. MANENKOV, A. A. and A. M. PROKHOROV, *Sov. Phys. J.E.T.P.* **1**, 611 (1955).
36. GEUSIC, J. E., *Phys. Rev.* **102**, 1252 (1956).
37. MAKHOV, G., C. KIKUCHI, J. LAMBE and R. W. TERHUNE, *Phys. Rev.* **109**, 1399 (1958).
38. BLOEMBERGEN, N., S. SHAPIRO, P. S. PERSHAN and J. O. ARTMAN, *Phys. Rev.* **114**, 445 (1959).

## DISCUSSION OF THE RESULTS

[4.1] *The connection between  $\tau_1$  and  $\eta$* 

On the basis of the interpretation of their results ESCHENFELDER and WEIDNER stated the occurrence of large discrepancies between the values of  $\tau_1$  determined by the relaxation and saturation method. To obtain  $\tau_1$  from the measured values of  $\eta$ , they made use of (1.86). We have compared the measured values of  $\eta$  with  $\eta_{\text{rel}}$  derived from the relaxation measurements using (1.101), which relation is very probably fulfilled under the experimental conditions.

From the double resonance measurements it followed, that we have to distinguish between three situations as to the degree in which internal spin equilibrium is established during a time  $\tau_1$ .

1) The cross relaxation rates are negligible compared with the spin lattice rates. So  $U_{cr} \ll U_{ij_{\text{min}}}$ .

In general the saturation and relaxation measurements will not give the same results. When present, different resonance lines will generally have different values of  $U_{ij}$ .

Examples are  $\text{K}_3\text{Cr}(\text{CN})_6/\text{K}_3\text{Co}(\text{CN})_6$ , sample A of which the  $U_{ij}$ 's are computed in [3.8.3] and [3.10.1] and further the ruby at operating point  $R_{\text{II}}$  (cf. [3.9.1]). The variation of the magnetic moment as a function of time will depend on the initial conditions and will in general not be according to a simple exponential. The relaxation method will yield an average relaxation time, which together with the behaviour of  $\mathbf{M}$  under saturation conditions, can be calculated with the method of [1.6.2]. Generally there will not be a simple relation between  $\tau_{1_{\text{rel}}}^{\text{av}}$  and  $\eta_{\text{sat}}$ . In the case of  $S=1/2$  we may also have  $\eta_{\text{rel}}^{\text{av}} \neq \eta_{\text{sat}}$ , if there are ions with differing  $g$ -values in a unit cell, and if the resonance line is broadened inhomogeneously, that is for a spatially distributed inhomogeneity.

2) The cross relaxation rates are of the same order of magnitude as those between spins and lattice, so when (3.07) and (3.08) are valid.

At some resonance lines it is possible to measure by saturation directly  $U_{cr}$  as this may be the rate determining  $\tau_{\text{off}}$  for that transition. An example is the ruby at operating point  $R_{\text{I}}$  above 4° K [3.9.2].

3) Complete spin equilibrium:  $U_{cr} \gg U_{ij_{\text{max}}}$ . The transition to this situation is demonstrated by the behaviour of  $\tau_{\text{off}}$  for the ruby, operating point  $R_{\text{I}}$ , near 4° K [3.9.2].

In general this situation is expected to be realised in concentrated salts, at not too high temperatures and magnetic fields. The energy transfer between spins and lattice can be described by the scheme used in [1.7]. Saturation and relaxation experiments are expected to yield the same value of  $\eta$  as in both experiments the spin system is presumably in internal equilibrium, so that

$$(4.01) \quad \eta_{\text{sat}} = \eta_{\text{rel}} = \frac{b + CH^2}{T_L \tau_{1\text{rel}}}.$$

In Chapter III, section A, this relation has been shown to hold under certain conditions set to the size of the magnetic r.f. field  $\mathbf{h}$ , such as  $\mathbf{h}$  large for most of the salts investigated and  $\mathbf{h}$  small for  $\text{CoNH}_4$  tutton salt.

Which of the three situations is realised will depend on the magnetic concentration (influences  $U_{cr}$  and more or less  $U_{ij}$ ), the vector  $\mathbf{H}$  ( $U_{cr}$  and  $U_{ij}$ ) and temperature ( $U_{ij}$ ). Transitions between the three situations are demonstrated in Chapter III, section B.

As for the relation between  $\eta_{\text{sat}}$  and  $\tau_1$  it is seen that for none of the three situations (1.86) is satisfied. This relation was derived by making use of (1.26), in analogy with the case of nuclear resonance where  $b \approx 0$  and where there is no spin equilibrium (situation 1).

#### [4.2] Phenomenological description

[4.2.1] The values of  $\eta_s$  of CrK alum  $\mathbf{H} // (111)$  were found to depend only slightly on concentration and not on the temperature. This is in accordance with the expectations for  $\eta$  at magnetic fields much larger than the internal fields. Only for  $\text{CoNH}_4$  tutton salt it was found that  $\eta_s = \eta_{\text{rel}}$ .

When comparing  $\eta_s$  for the different salts the empirical rule is found that the exponent  $\beta$  in  $\eta_s \propto T^\beta$  decreases with increasing exchange interactions, and is about  $-1$  ( $\tau_1$  independent of  $T$ ) for  $\text{CuK}_2\text{Cl}_4 \cdot 2\text{H}_2\text{O}$  and  $\text{CuSO}_4 \cdot 5\text{H}_2\text{O}$ . This is expected when relaxation processes within the spin system are the bottleneck for the power transfer towards the lattice. An example of such a situation is the case of  $\omega_{\text{ex}} \gg \omega_L$  considered by BLOEMBERGEN e.a. (cf. [1.5.3]).

For CuK tutton salt the anisotropy of  $\eta_s$  was measured for a few directions of  $\mathbf{H}$  in the  $K_1K_2$  plane, indicating  $\eta_s$  to have the same symmetry as the  $g$ -value.

In some salts investigated the slopes of the saturation graphs might increase further upon use of still lower  $P_{\text{ext}}$ .

[4.2.2] The values of  $\eta_f$  are found to correspond to  $\eta_{\text{rel}}$  for most salts investigated.  $\text{CoNH}_4$  tutton salt appears to be an exception. The relaxation measurements showed this salt to be also anomalous in other respects.  $\text{MnNH}_4$  tutton salt was found by the relaxation methods to be exceptional compared to the other salts as the temperature dependence of  $\eta_{\text{rel}}$  is independent of the concentration and as the values at helium and hydrogen temperatures cannot be fitted to a simple function of  $T$ .

When writing for  $\eta_{\text{rel}}$  at low magnetic fields:

$$(4.02) \quad \eta_{\text{rel}} \propto c^\varepsilon (b/C + pH^2)^{\delta/2} T^\beta$$

then for some salts the exponent  $\varepsilon$  in the limit of  $H \rightarrow 0$  and  $\delta$  and  $\beta$  for  $c=1$  and  $H$  not being too large become approximately:

	$\varepsilon$	$\delta$	$\beta$	$\delta + \beta$
Fe NH <sub>4</sub> alum	1.3-1.5	0	4-4.5	≈ 4-4.5
CrK alum	1.2	2	1.9	≈ 4
MnNH <sub>4</sub> tutton	1.1	2	4.1	≈ 6
CuK <sub>2</sub> Cl <sub>4</sub> 2H <sub>2</sub> O	-	0	4	≈ 4
CuK tutton	neg.	2	2	≈ 4

$\varepsilon$  decreases for  $c$  smaller than about 0.1 and  $\beta$  becomes smaller for higher magnetic fields (2-3 K $\theta$ ), for lower temperatures and for lower concentrations.

Our experiments have shown  $\eta_f$  to be anisotropic in temperature dependence and magnitude, for instance for CrK Alum  $\mathbf{H} // (111)$  and  $\mathbf{H} // 100$ , and for CuK tutton salt. The anisotropy of the size of  $\eta_f$  is for this last salt difficult to relate to crystalline or magnetic anisotropies.

[4.2.3] The curvature of the saturation graphs. The curvature of the saturation graphs has been found to depend on the magnetic concentration and it is felt that once the mechanism determining  $\eta_f$  is found, the explanation for the curvature will follow in a simple way.

The main difficulty to obtain a consistent description is that one finds in most cases  $\eta_{\text{rel}} = \eta_f$  while one would expect the relation  $\eta_s = \eta_{\text{rel}}$  to hold, as in the relaxation measurements the fractional change in  $T_s$  is at most 1 %.

From the experimental data it can be seen that no instrumental error is involved. An inhomogeneous distribution of the magnetic r.f. fields over the sample dimensions will result in a concave curvature (convex is observed). Moreover, small samples were always taken so as to make this inhomogeneity of no importance.

The following causes for a curvature may be mentioned:

1) the lattice temperature  $T_L$  may depend on  $P_m$  due to limited heat conductivities inside the crystal or transfer to the environments. This effect together with the so-called hot phonon theory will be discussed later in [4.3]. A curvature has been predicted [1] due to these effects.

2) For inhomogeneous broadened resonance lines the ordinates of the saturation graphs are expected to be proportional to  $\sqrt{1 + 1/4\gamma^2 h^2 \tau_1 \tau_2}$  (cf. (1.39)), when the cross relaxations are slower than  $U_{ij}$ . This function cannot be fitted to the observed graphs, however. Moreover it is difficult to visualize how it is possible to have inhomogeneous broadening for the concentrated salts, and homogeneous broadening for the diluted ones. This mechanism can therefore be rejected.

3) If in (1.76)  $\hbar\omega_{ij}$  becomes of the order of  $kT_L$ ,  $\eta_d$  is strongly dependent on the spin temperature. This mechanism will be discussed in [4.5].

4) A spatial distribution of  $\eta$  over the crystal due for instance to impurities with a large  $\eta$  may result in  $\eta_f = \eta_{rel}$ . An explanation on this basis will be presented in [4.6].

5) The phonon wavelength corresponding to the Larmor frequency is about 200 lattice spacings. For neighbouring ions in undiluted salts the phase of the lattice vibration  $\mathbf{q}$  should not be changed much and it is conceivable that the coherence of the magnetic moments induced by  $\mathbf{h}$  entails a change in  $\eta$  because of phase relations between  $\mathbf{h}$  and  $\mathbf{q}$ . However, the experiments were all made with  $|\mathbf{h}| \ll \omega_d/\gamma$  so that these coherence effects and those discussed by REDFIELD [2] are unlikely.

Some considerations pertaining to these mechanisms and to the influence of spin-spin interactions on  $\eta$  will now be presented.

#### [4.3] *General considerations on the phonon household*

In this section we shall consider whether it is allowed to regard the lattice to be in equilibrium at a temperature  $T_L$  and whether this temperature is equal to that of the surroundings.

It will be shown that neither the assumption of the selective heating of certain lattice vibrations, the so-called hot phonon theory, nor the heating of the whole crystal, provides an explanation for the observed relaxation behaviour.

A fact important when determining  $T_L$  by non-stationary methods is that in CrK alum for instance the lattice and spin specific heats are equal at 2° K ( $C_M = C_L$ ).

[4.3.1] The thermal conductivity  $K$  due to all lattice vibrations is too large to allow appreciable temperature gradients in our experiments. BIJL [3] has measured the value of  $K$  in CrK alum at liquid helium temperatures and found that this quantity depended on the way the salt was cooled. At 2° K,  $K$  was found to have a value between 0.03 and 0.12 Wcm<sup>-1</sup>deg.<sup>-1</sup>.

A representative crystal of CrK alum used by us, of dimensions 1 × 0.5 × 0.2 cm<sup>3</sup>, weighing about 200 mg, required about 70 mW to be heated from a spin temperature of 2.5° K to one of 10° K. This results in a temperature difference of roughly 1° K over the dimensions of the crystal for the most unfavourable value of  $K$ . In the region of the largest curvature this temperature difference will only be about 0.2° K.

In the numerator of (1.85) the first term is  $T_L$  while the second term contains a temperature dependence through  $\eta$ , but both vary not enough with  $T_L$  to explain the observed curvatures.

Another reason for rejecting heating of the whole crystal as a possible mechanism is, that while the thermal conductivity increases with temperature ( $K \propto T^{2.3}$ ) the curvature is observed to be more pronounced at higher

temperatures. For instance the ratio of  $\eta_f$  to  $\eta_s$  for CrK alum has a  $T^{1.9}$  dependence, while  $P_{\text{ext}}$  for  $\eta = 2\eta_s$  hardly changes.

[4.3.2] The phonon mean free path. At low temperatures the mean free path of the elastic waves may become comparable to the dimensions of the crystal. For this case CASIMIR [4] assumed that the lattice waves are scattered at the walls and he arrives, for very low temperatures, at a value of  $K \propto C_V \propto T^3$ . The scattering of the lattice waves may take place also at mosaic structures or other lattice imperfections and  $K$  will have the same temperature dependence. This theory is confirmed by the experimental results.

From Bijl's results for CrK alum one can derive the order of magnitude of the mean free path  $\lambda$  of the phonons which determine the thermal conductivity, by using the formula (cf. [5]);

$$(4.03) \quad K = \frac{1}{3} AC_V v \lambda$$

where  $C_V = \frac{4,11}{273} 10^{-3} T^3$  [6] is the lattice specific heat per unit volume,  $v = 2 \times 10^5$  cm/s the average sound velocity and  $A$  a factor of the order unity. One obtains for the liquid helium region  $\lambda \approx 4$  to  $15 \times 10^{-3}$  cm and consequently for the time between two subsequent scattering processes of a phonon about 2 to  $8 \times 10^{-8}$  s., depending on the temperature treatment of the sample. In other crystals such as quartz or ruby,  $\lambda$  may be much larger than found for CrK alum.

These results show that it is important to consider whether the transfer of energy between lattice oscillators, when differently excited, occurs at a sufficient rate to establish a uniform temperature among the oscillators of different frequencies.

We shall first consider the influences of the paramagnetic ions on the mean free path.

[4.3.3] The oscillators on speaking terms. If the direct processes govern the power transfer between spins and lattice, only those lattice oscillators play a rôle which have a frequency close to that of a spin transition. As the frequencies contained in the spectrum of the magnetization (of order of  $2\pi \times 10^{10}$  s $^{-1}$  at a field of  $H = 3000$  o) are generally much smaller than  $kT/\hbar$  for helium temperatures, the number of oscillators "on speaking terms" with the spin system  $N_{\text{o.s.t.}}$  will be comparatively small. These will therefore be frequently interrupted by the spin system as has been stressed by VAN VLECK [7].

If  $\delta\omega$  is the width of the band of oscillators around frequency  $\omega$  and  $v$  the sound velocity, assumed to be equal for the transverse and the longitudinal polarization, then  $N_{\text{o.s.t.}}$  per mole will be

$$(4.04) \quad N_{\text{o.s.t.}} = \frac{3\omega^2 V \delta\omega}{2\pi^2 v^3}$$

where  $V$  is the ionic volume.

The width of the band of phonons o.s.t. will be partly due to the width  $\Delta\omega$  of the spectrum of the interaction ions-phonons, and partly to a lifetime broadening ( $1/\tau_{\text{int}}$ ) caused by the many inelastic collisions with the magnetic ions. So approximately we may write

$$\delta\omega = \Delta\omega + 1/\tau_{\text{int}}$$

where for the time between interruptions

$$(4.05) \quad \tau_{\text{int}} = \frac{N_{\text{o.s.t.}}}{\text{number of spin flips/sec.}} = \frac{3\omega^2 V \delta\omega}{2\pi^2 v^3 N/\tau_1}$$

where  $\tau_1$  is the spin lattice relaxation time and  $N$  the number of paramagnetic ions. We have for undiluted CrK alum;  $V \approx 270 \text{ cm}^3$ ,  $\tau_1 \approx 10^{-2} \text{ s}$  and  $v \approx 2 \times 10^5 \text{ cm/s}$  [6]. Taking  $\omega = 2\pi \times 10^{10} \text{ s}^{-1}$  and  $\Delta\omega/\omega = 1/10$  for the case  $\Delta\omega$  equals the full resonance line width, one obtains  $\tau_{\text{int}} \approx 2 \times 10^{-9} \text{ s}$  and  $N_{\text{o.s.t.}} \approx 2 \times 10^{17}$  per mole.

Apparently the width of the phonon band "on speaking terms" is mainly determined by the resonance line shape ( $\tau_{\text{int}} \times \Delta\omega \approx 12$ ).

A lifetime broadening of  $1/2 \times 10^9 \text{ s}^{-1}$  will be an overestimate as the interruptions due to the paramagnetic ions are treated at random. At a frequency of  $2\pi \times 10^{10} \text{ s}^{-1}$  the wave length of the lattice vibrations is  $2 \times 10^{-5} \text{ cm}$ , and as it overlaps about 200 unitcells, its phase is not changed much for neighbouring ions. Coherence effects between phonons and spins would decrease  $\tau_{\text{int}}$  substantially, and has to be taken into account. If the magnetically absorbed power is  $P_m \text{ W/mole}$  then for complete coherence:

$$(4.06) \quad \tau_{\text{int}} = N_{\text{o.s.t.}} \hbar\omega / P_m \approx 10^{-6} / P_m \text{ s.}$$

If there is no exchange present, one has, when diluting a crystal magnetically,  $\Delta\omega \propto \sqrt{c}$  for  $c > 0.1$  and  $\Delta\omega \propto c$  at lower concentrations, till inhomogeneous broadening of hyperfine splittings becomes important. One finds with (4.05) for the above taken example that the life time broadening becomes comparable to the resonance line width for  $c$  about 0.04.

The spectrum of the phonon-spin interaction is more complicated, partly due to spin-spin interactions, than the simple resonance line shape considered before. We will discuss this later in more detail.

The mean lifetime of the phonons derived in [4.3.2], is seen to be longer than  $\tau_{\text{int}}$ , calculated with  $\Delta\omega$  equal to the resonance linewidth. We shall therefore discuss whether the bottleneck for the energy transfer is between the phonons on speaking terms and the surrounding liquid helium bath.

[4.3.4] Heat can be conducted by the oscillators o.s.t., which are supposed to have a mean temperature of  $T_L$ , towards the liquid helium bath at temperature  $T_b$ , either via the h.f. phonons or by direct contact at the walls of the sample.

VAN VLECK [8] made an estimate of the rate at which three phonon scattering processes take place. He finds for the power transfer

$$(4.07) \quad P_{\text{tr}} = \beta(T_L - T_b)$$

where

$$\beta_{\text{anh}} = DT_b^4 \omega N_{\text{o.s.t.}}$$

For the example given above the value of  $\beta_{\text{anh}}$  would be about  $10^{-2}$  W mole $^{-1}$  deg. $^{-1}$ , corresponding to a mean free path  $\lambda_{\text{o.s.t.}}$  of about 2 cm for these phonons. This path is much longer than that of the phonons giving rise to the thermal conductivity. Destruction at the walls of the sample makes the mean free path of the phonons of the order of the sample dimensions, in our case about 0.2 cm, so that this mechanism seems more important than the three phonon collisions.

Processes in which two phonons  $\hbar\omega$  combine to one of  $2\hbar\omega$  will be more effective to carry away energy, at high excitations of the phonons o.s.t.

The calculations of VAN VLECK were made for an isotropic crystal and for such a case the wave vectors  $\mathbf{k}$  of the three phonons, have to be collinear, apart from having a zero sum. For anisotropic crystals, however, the condition for collinearity is changed, increasing the collision probability and causing the temperature function to depend on the crystal symmetry. Calculations of HERRING [9] showed that independently of the crystal symmetry the following scaling law for three phonon processes holds:

$$(4.08) \quad \beta_{\text{anh}}(\zeta\mathbf{k}, \zeta T) \propto \zeta^7 \beta_{\text{anh}}(\mathbf{k}, T).$$

where  $\zeta$  is the scaling factor. The effect of these processes, when they limit the power transfer, on the spin-bath relaxation, will be dealt with in [4.4].

The rate at which these three phonon collisions occur is still comparatively small. Also other processes, such as phonon combination or direct coupling of the phonons "on speaking terms" and the liquid helium bath, seem to have too slow a rate to give reasonable values of the mean free paths. Presumably the inelastic scattering of the phonons therefore takes place at the surfaces of the crystal or at lattice imperfections.

This scattering at the lattice imperfections does not necessarily bring about an equilibrium between the lattice oscillators. VAN VLECK [8] remarked that the redistribution of temperature between oscillators of different frequencies is not governed by the processes determining the thermal resistivity as he takes for these processes phonon reflections at the walls of the crystal. In the theory of CASIMIR, however, it is immaterial whether the phonons are reflected diffusely or destructed completely, and for the last case re-distribution is insured, making  $\lambda$  about equal for all phonons.

#### [4.4] *Application to the saturation of paramagnetic resonance*

[4.4.1] A simple model for the heat contact. The effect of a small lattice conductivity on the experiments can be treated by a simple

model as proposed by GORTER, VAN DER MAREL and BÖLGER [1]. Suppose we are concerned with three systems each of which is in internal thermodynamic equilibrium; the magnetic spinsystem  $S$  the system of low frequency oscillators  $L$  on speaking terms with  $S$ , and the constant temperature bath  $b$ , which may consist of the high frequency oscillators or the helium bath. For the energy transfer between  $L$  and  $b$  we write  $\beta(T_L - T_b)$  and for that between spins and lattice  $\eta T_L (1/T_L - 1/T_S)$  as usual. The hot phonon theory supposes this last transfer to be much greater than the former (phonon o.s.t. bottleneck), so that  $T_S \approx T_L$ .

It would be better to work with the quantum numbers  $p_i$  of the lattice modes  $q_i$ , but as we do not specify the size of the quanta by which the energy is exchanged, we characterize  $\langle p_i \rangle_{av}$  by  $T_L$  (cf. (1.52)). A distribution of  $T_L$  over the dimensions of the crystal could exist, depending on the processes governing  $\beta$ . This would lead to a nonlinear diffusion equation in  $T_S$ . In the following we will take  $T_L$  homogeneous over the crystal dimensions.

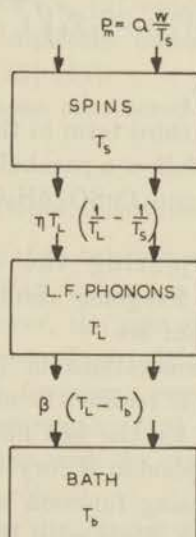


Fig. 4.1. Model for the power transfer.

The energy balances for the systems when the spin-system is heated by a microwave power  $P_m = QW/T_S$  are (fig. 4.1)

$$(4.09) \quad P_m = \frac{QW}{T_S} = \frac{dU_S}{dt} + \eta T_L \left( \frac{1}{T_L} - \frac{1}{T_S} \right)$$

and

$$(4.10) \quad \eta T_L \left( \frac{1}{T_L} - \frac{1}{T_S} \right) = \frac{dU_L}{dt} + \beta (T_L - T_b)$$

where  $U_S$  and  $U_L$  represent the internal energies of spins and l.f. phonons respectively. When the number of low frequency oscillators o.s.t. is small, their heat capacity may be neglected. A disturbance of  $T_S$  will die out

exponentially with a characteristic time  $\tau_1$  which is for  $P_m=0$ :

$$(4.11) \quad \tau_1 = (b + CH^2) \left( \frac{1}{\eta} + \frac{1}{\beta T} \right).$$

From the steady state solutions of (4.09) and (4.10) one finds for the saturation graphs, eliminating  $T_L$

$$(4.12) \quad \frac{P_{\text{ext}}}{P_m} = \frac{P_{\text{ext}} T_b}{QW} + P_{\text{ext}} \left( \frac{1}{\eta} + \frac{1}{\beta T_s} \right).$$

We are mainly interested in the case that at low powers  $\eta \gg \beta T_b$ . The starting slope is then  $1/\eta + 1/\beta T$  which corresponds to the value (4.11) obtained by the transient method. When increasing the spin temperature to the extent that  $\beta T_s \gg \eta$ , the slope is given by  $1/\eta$ .

If  $\beta$  is independent of  $T_L$ , which is not necessarily the case, we can solve (4.09) and (4.10) for  $T_s$  and find

$$(4.13) \quad T_s = 1/2(T_b + QW/\eta) + 1/2 T_b \sqrt{1 + \frac{4QW}{\beta T_b^2} + \left( \frac{QW}{\eta T_b} \right)^2}$$

where we suppose  $\eta \gg 1/2 \beta T_b$ .

For small values of  $W$ , the third term in the root can be neglected and the saturation graphs should follow a parabola. This is in agreement with the data on  $\text{CuK}_2\text{Cl}_4 \cdot 2\text{H}_2\text{O}$ , and  $\text{CuSO}_4 \cdot 5\text{H}_2\text{O}$ .

[4.4.2] Reasons for rejecting the hot phonon theory are found when comparing the foregoing results with those obtained by experiment, and some of them are:

1) According to the considerations in [4.4.1] one expects  $\eta_s = \eta_{\text{rel}}$ , while experimentally  $\eta_f = \eta_{\text{rel}}$  is realised in most cases. This reason is of course not exclusively valid for the hot phonon theory.

2) According to the hot phonon theory one expects  $\eta$  calculated for one gramion, to be a decreasing function of the concentration  $c$  when diluting magnetically. For CrK alum with  $\mathbf{H} // (111)$  the value of  $\eta_s$  was found to be practically independent of  $c$  and  $\eta_f$  to be increasing with  $c$ . The scheme proposed in [1] to explain the concentration dependence of  $\tau_1$  does not hold here because of the relatively large fields used.

3) If three phonon processes determine the heat contact of phonons o.s.t. and bath, then by the relaxation method one would determine  $\beta_{\text{anh}} T$  (cf. (4.11)).

According to (4.08)  $\beta_{\text{anh}} T$  contains the scaling factor  $\zeta$  to the eighth power. From the experiments it was found that the exponent of  $\zeta$  is in most cases four and not larger than six for the salts investigated (cf. [4.2.2]).

4) The experiments on inhomogeneous pumping of a maser, described in [3.8.4] showed that the phonons o.s.t. are not able to establish a uniform spin temperature differing from the bath temperature.

5) A strong argument for the case negative temperatures can be obtained in the sample has been put forward by BLOEMBERGEN [10]. The statement is the following: when the contact between the phonons o.s.t. and the spin system is much better than with the bath, so that  $T_S = T_L$ , then the attainment of negative spin temperatures is impossible. As negative temperatures can only be obtained in systems in which the energy levels have an upper bound [11],  $T_L$  can never become negative. Justification for this statement can be found in formula (4.09) and (4.10). To reach negative spin temperatures one has to go through  $T_S = \infty$  making  $T_L$  also  $\infty$ . For that case the power transfer increases beyond all limits,  $T_S$  remaining positive. So for salts in which it has been possible to make the population of a higher energy level larger than that of a lower one, the hot phonon theory is also not tenable.

The last two arguments are valid for diluted samples such as the maser material.

The results of GIORDMAINE e.a. [2], explained by them with the hot phonon theory, can be completely understood when assuming cross relaxations to be present [13] [14].

For other crystals as those considered by us, such as quartz, the situation may be different.

#### [4.5] *The influence of spin-spin interactions on $\eta$*

[4.5.1] The heat transfer between spin and lattice systems is in the theory of KRONIG and VAN VLECK, as discussed in [1.5], essentially a single spin process. However, the spin-spin interactions mix the spin operators of an ion with those of its neighbours causing the Heisenberg operator  $\mathbf{S}(t)$  to have higher frequency components than expected from the single spin spectrum. TEMPERLEY [15] suggested therefore the possibility that multiple spin jumps, with the emission of a phonon at the sum energy, play an important rôle.

If for the direct process the largest quanta which still contribute appreciably to the power transfer become of the order of  $kT_L$  it is not allowed to expand the exponentials in (1.76), and for  $T_S \approx T_L$ ,  $\eta_d$  will be strongly temperature dependent.

When increasing  $T_S$  the probability for an ion to have neighbours in a higher energy state increases. Therefore  $\eta_d$  will be enhanced and the saturation graphs curved. The ratio of  $\eta_f$  to  $\eta_s$  is not expected to be very large, however (about a factor 2 to 4).

In the limit of  $T_S \rightarrow \infty$ ,  $\eta_d$  becomes independent of  $T_L$  as the transfer is governed by spontaneous emission of phonons (cf. (1.76)).

This mechanism to obtain a curvature for the saturation graphs results in:  $\eta_s = \eta_{rel}$ , and can therefore not explain our observations, except perhaps those on  $\text{CoNH}_4$  tutton salt.

TEMPERLEY made a rough calculation of the influence of spin-spin

interactions, but by using a diagonal sum method this can be carried out exactly.

The calculations to be presented here must be considered as an extension of the theory dealt with in [1.5] and [1.7]. The results will be compared to the values of  $\tau_1$  obtained by the relaxation method.

[4.5.2] Considering the formulae (1.79) and (1.82) for  $\eta$ , we see that, as  $\mathcal{H}_{sp}$  contains also the spin-spin interactions, the adiabatic terms in  $\eta_a$  can at most contain four spin processes, and the non-adiabatic terms six spin processes. Both terms are affected by exchange interactions. The indirect process (1.82) is affected by interactions between two spins only and may be influenced by the exchange if  $S > 1/2$  (cf. [1.7]) or by exchange between inequivalent ions if  $S = 1/2$ , for instance.

In (1.51) and (1.56) the relaxation rates were calculated by averaging over the resonance line shape of the transition involved. For the calculation of the  $\eta$ 's this would mean that we have to compute the truncated moments and to assume that the dipole-dipole interactions are not strong enough to produce transitions in the Zeeman energy. The Temperley effect can be calculated by taking the full untruncated moments.

These calculations are lengthy, but for the case that  $S = 1/2$  and that only the component  $S_x$  is important in the relaxation process, we can use the results of [1.7] eq. (1.35-37), supposing  $\mathbf{H} // z$ -axis.

When calculating the values of  $\eta$  for one gram ion one finds for the truncated case in a simple cubic crystal lattice with  $\mathbf{H} // (001)$  axis,

$$(4.14) \quad \eta_{\text{ad}} \propto \langle \omega^4 \rangle_{\text{av}} = \omega_L^4 + 6\omega_L^2 \omega_a^2 + 3\omega_a^4 \left( 0.742 + \frac{0.07}{c} \right) + c' (\pi/2) \omega_{\text{ex}}^2 \omega_a^2$$

with

$$(4.15) \quad \omega_a^2 = 7.5 c \gamma^4 \hbar^2 d^{-6}$$

where  $d$  is the lattice constant,  $c$  the concentration, and  $c' = c$  for  $c > 1/z$  and  $c' \approx 0$  for  $c < 1/z$ ,  $z$  being the number of neighbours an ion has an exchange interaction with. It is seen that at lower concentrations ( $c < 0.1$ ) the term with  $1/c$  in (4.14) is important. Further we have

$$(4.16) \quad \eta_{\text{ind}} \propto \omega_a^2 + \omega_L^2.$$

For the Temperley effect we take the untruncated moments as calculated by Miss WRIGHT [17]

$$(4.17) \quad \eta_{\text{ad}} \propto \omega_L^4 + 20\omega_L^2 \omega_a^2 + \frac{100}{3} \omega_a^4 (3\omega_{\text{ex}}^2 / \omega_a^2 + 2.5).$$

It is seen that the term with  $\omega_a^4$  has become more important by a factor of about 34, while this factor is about 64 for the term with  $\omega_{\text{ex}}^2 \omega_a^2$ .

For the non-adiabatic processes one finds:

$$(4.18) \quad \eta_{\text{nad}} \propto \omega_L^6 + 50\omega_L^4 \omega_a^2 + 15\omega_L^2 \langle \Delta \omega^4 \rangle_{\text{av}} + \langle \Delta \omega^6 \rangle_{\text{av}}$$

where  $\langle \Delta\omega^4 \rangle_{av}$  is the last term of (4.17) and

$$(4.19) \quad \langle \Delta\omega^6 \rangle_{av} = \left(\frac{10}{3}\right)^3 \omega_d^6 \left[ 2 \times 10^{-3} \cdot \left(\frac{\omega_{ex}}{\omega_d}\right)^4 + 0.424 \left(\frac{\omega_{ex}}{\omega_d}\right)^2 + 15 \right].$$

Concentration dependent terms such as in (4.14) ought to be added to (4.17) and (4.18). For the indirect process the untruncated  $\eta$  becomes:

$$(4.20) \quad \eta_{ind} \propto \omega_L^2 + \frac{10}{3} \omega_d^2.$$

To calculate the relaxation times we need the specific heat:

$$(4.21) \quad C_H = \frac{b + CH^2}{T^2} = \frac{C}{\gamma^2 T^2} \left[ \frac{5}{3} \omega_d^2 \left( 1 + 2.55 \frac{\omega_{ex}^2}{\omega_d^2} \right) + \omega_L^2 \right].$$

It is better to use the measured values, however.

Miss WRIGHT used for the exchange interaction the following expression instead of (1.03)

$$\mathcal{H}_{ex} = A \sum_{i>j} \frac{\gamma^2 \hbar^2}{r_{ij}^3} \mathbf{S}_i \mathbf{S}_j.$$

To convert  $A$  to the values used by us the following relations are given for a simple cubic crystal and  $S=1/2$

$$(4.22) \quad J = 2A^2 \hbar^2 \omega_d^2 / 30 = \frac{\hbar^2 \omega_{ex}^2}{2.12}.$$

As  $T\tau_{...} = (b + CH^2)/\eta_{...}$ , where  $\tau$  has the same index as  $\eta$ , we see that for  $\omega_L=0$ ,  $\omega_{ex}=0$  and for concentrations higher than about 0.1:

$$(4.23) \quad \begin{cases} \tau_{dad} \propto c^{-1} \\ \tau_{dad} \propto c^{-2} \\ \tau_{ind} \propto c^0 \end{cases}$$

while for  $c$  smaller than about 0.1 we expect

$$\tau_{dad} \propto c^0.$$

The values of  $T\tau$  (scale arbitrary) due to the various processes for different concentrations and exchange interactions have been plotted in fig. 4.2 and fig. 4.3. As the measurements of VAN DER MAREL [18] [19] give  $\tau$  as a function of  $H$  we also plotted  $\tau$  and not  $\eta$  vs  $H$  on a double logarithmic scale, for easier comparison.

Of the graphs for  $T\tau_{ind}$  (fig. 4.2), only curve  $E$  has a resemblance to those observed experimentally, with  $p=0.5$  for  $\omega_{ex}=0$ . For larger exchange interactions  $p$  becomes larger, which does not tally with the experimental data. However, one has to keep in mind that exchange between inequivalent ions influences  $\eta$  and that in second order the  $S_z$  component may be important. The second and fourth moment of  $S_z$  depends strongly on the exchange.

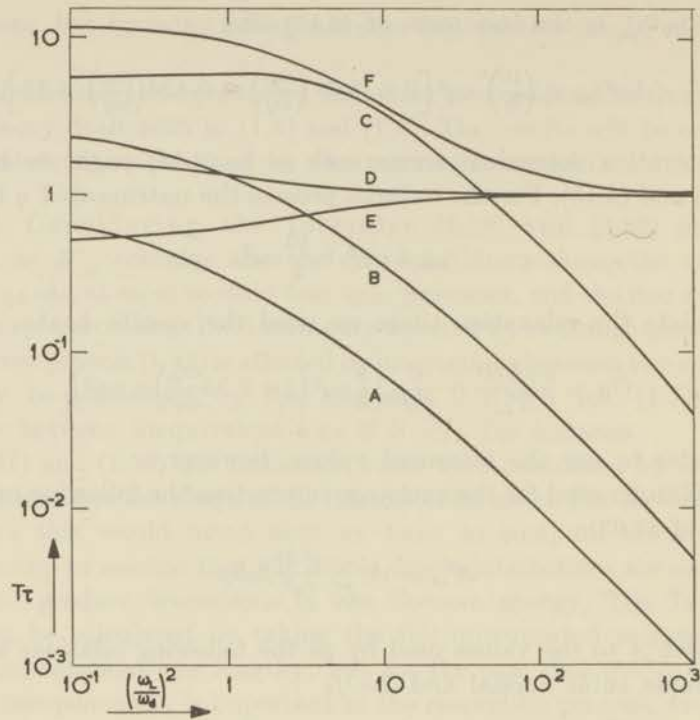


Fig. 4.2. The influence of spin-spin interactions on  $T\tau$ .

$A$	$T\tau_{ad}$	$c = 1$	}	trunc. $\omega_{ex} = 0$	$D$	$T\tau_{ind}$	trunc.	
$B$	$T\tau_{ad}$	$c = 1/5$			$E$	$T\tau_{ind}$	untr.	$\omega_{ex} = 0$
$C$	$T\tau_{ad}$	$c = 1/50$			$F$	$T\tau_{ind}$	untr.	$\omega_{ex}/\omega_d = 3$

The concentration dependence of  $\tau_{ad}$  is displayed in fig. 4.2; curves  $A$ ,  $B$  and  $C$  for  $c=1, 1/5$  and  $1/50$  respectively. Through  $\omega_d^2 \propto c$  the abscis in this figure is concentration dependent.

The observed concentration dependence of  $\eta_{rel}$ , discussed in [4.2.2], are intermediate between those calculated for the indirect and adiabatic direct processes as are also the temperature dependences. The values of  $\eta$  as a function of  $T$  obtained by us (chapter III) cannot be represented as a sum of  $\eta_a$  and  $\eta_{ind}$  in view of the temperature dependence.

The curves  $E$  and  $F$  for  $T\tau_{ad}$  (fig. 4.3) are seen to be nearly horizontal up to  $(\omega_L/\omega_d)^2 \approx 10$  and not to increase like curve  $D$  ( $\omega_{ex}=0$ ). This is due to the exchange interactions, the influence of which on the spin specific heat predominates over that on the fourth moment. The increase of curve  $D$  with  $\omega_L$  is much less than observed experimentally (cf. [4.2.2]) and there has to be a mechanism, which makes  $\eta$  less dependent on  $\omega_L$ . Neither larger exchange nor larger dipole interactions will make the factor by which  $T\tau_{ad}$  initially increases, larger.

It is found in this section that the Temperley effect does exist but, as has been stressed by VAN VLECK [16] previously, it is by far not as large as TEMPERLEY suggested.

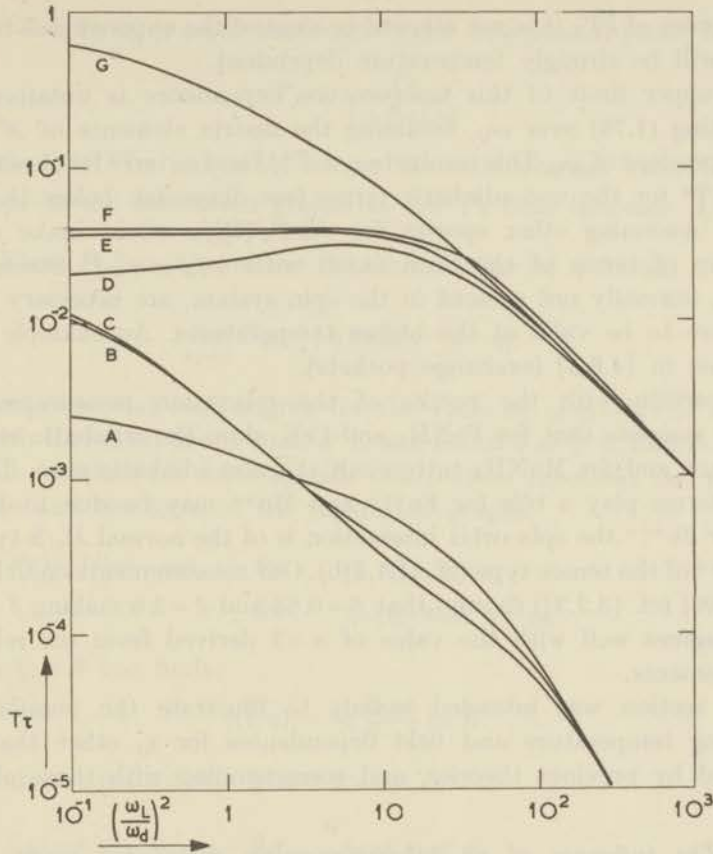


Fig. 4.3. The influence of spin-spin interactions on  $T\tau_a$ ;  $c = 1$ .

$$\left. \begin{array}{l}
 A \ (\omega_{\text{ex}}/\omega_d)^2 = 0 \\
 B \ (\omega_{\text{ex}}/\omega_d)^2 = 3 \\
 C \ (\omega_{\text{ex}}/\omega_d)^2 = 9
 \end{array} \right\} T\tau_{\text{ad}} \text{ untrunc.} \quad \left. \begin{array}{l}
 D \ (\omega_{\text{ex}}/\omega_d)^2 = 0 \text{ untr.} \\
 E \ (\omega_{\text{ex}}/\omega_d)^2 = 3 \text{ untr.} \\
 F \ (\omega_{\text{ex}}/\omega_d)^2 = 9 \text{ untr.} \\
 G \ (\omega_{\text{ex}}/\omega_d)^2 = 0 \text{ trunc.}
 \end{array} \right\} T\tau_{\text{ad}}$$

[4.5.3] The spectrum of the phonons, which the spin system is able to excite is according to the foregoing not simply that of the resonance line at  $\omega_L$  with a half width  $\omega_d$ , but, when  $S = 1/2$ , a spectrum like that drawn in fig. (1.5). Apart from the peak at  $\omega_L$  all other peaks at multiples of the Larmor frequency will be broadened by exchange interactions. When  $S > 1/2$  the situation becomes even more involved as the perturbation  $\mathcal{H}'_1(S)$  has non-zero matrix elements for nearly all single ion transitions.

For these reasons the number of phonons on speaking terms with the spin system will be substantially increased and this is one of the reasons for the failure of the hot phonon theory.

[4.5.4] The temperature dependence of  $\eta$ . If the largest quanta which still contribute appreciably to the power transfer become

of the order of  $kT_L$  it is not allowed to expand the exponentials in (1.76), and  $\eta$  will be strongly temperature dependent.

The upper limit of this temperature dependence is obtained when integrating (1.76) over  $\omega_{ij}$ , assuming the matrix elements of  $\mathcal{H}_1'(\mathbf{S})$  to be independent of  $\omega_{ij}$ . This results in  $\eta \propto T^{\alpha+1}$  and so in  $T^4$  for the adiabatic and in  $T^6$  for the non-adiabatic terms (see discussion below (1.60) and (1.61)). Assuming other spectra for  $\langle i | \mathcal{H}_1'(\mathbf{S}) | j \rangle$  would make  $\eta$  to be made up of terms of the form (4.02) with  $\delta + \beta = \alpha + 1$ . Strong interactions, normally not present in the spin system, are necessary for this procedure to be valid at the higher temperatures. An example will be presented in [4.6.3] (exchange pockets).

Comparison with the results of the relaxation measurements (cf. [4.2.2]) suggests that for  $\text{FeNH}_4$  and  $\text{CrK alum}$  the adiabatic terms are important and for  $\text{MnNH}_4$  tutton salt the non-adiabatic ones. That different terms play a rôle for  $\text{Fe}^{+++}$  and  $\text{Mn}^{++}$  may be due to the fact that for  $\text{Fe}^{+++}$  the spin-orbit interaction is of the normal  $\lambda \mathbf{L} \cdot \mathbf{S}$  type, and for  $\text{Mn}^{++}$  of the tensor type (cf. [1.1.1]b). Our measurements on  $\text{CrK alum}$ ;  $\mathbf{H} // (100)$  (cf. [3.2.3]) showed that  $\beta = 0.88$  and  $\delta = 2.8$  making  $\beta + \delta = 3.7$  which agrees well with the value of  $\alpha + 1$  derived from the relaxation measurements.

This section was intended mainly to illustrate the possibility for obtaining temperature and field dependences for  $\eta$ , other than those expected by previous theories, and corresponding with those observed.

#### [4.6] *The influence of an inhomogeneously distributed power transfer constant*

The values of  $\eta$  may differ from ion to ion, and when saturating this would result in a spatially inhomogeneous distribution of the spin temperature over the sample.

[4.6.1] The power absorbed by the sample from a radio frequency field is obtained by averaging  $P_m$  over the whole crystal. Suppose the fraction  $f(\eta)d\eta$  of the  $N$  ions have a value of the power transfer constant between  $\eta$  and  $\eta + d\eta$ . Normalising  $f(\eta)$  makes  $\int_0^\infty f(\eta)d\eta = 1$ . We then have (cf. (1.85))

$$(4.24) \quad P_m = \int_0^\infty \frac{QWf(\eta)d\eta}{T_L + QW/\eta} = \int_0^\infty \frac{P_0f(\eta)d\eta}{1 + P_0/\eta}$$

where  $P_0 = QW/T_L$  is the power that would have been absorbed when  $\eta = \infty$ .

Without knowing the distribution function, of course it is not possible to calculate the shape of the saturation graphs, but we can say some generalities about the slope at very high and very low powers  $P_0$ .

a) When  $P_0 \ll \eta_1$  ( $\eta_1$  is the lowest value of  $\eta$  found) (4.24) becomes:

$$(4.25) \quad P_m = \frac{P_0}{1 + P_0 \overline{(1/\eta)}}$$

where the bar over a symbol means that the average value is taken. The slope of the saturation graphs at low  $P_0$  thus becomes:  $\overline{1/\eta} = 1/\eta_s$ .

b) When  $P_0 \gg \eta_2$  ( $\eta_2$  is the maximum value of  $\eta$  found)

$$(4.26) \quad \lim_{P_0 \rightarrow \infty} P_m = \int_0^{\infty} \eta f(\eta) d\eta = \bar{\eta} = \eta_f.$$

The experimental results give for the ratio of  $\eta_f/\eta_s = \bar{\eta} \overline{(1/\eta)}$  for CrK alum with  $\mathbf{H} // (111)$  about 10 at 4° K and about 5 at 2° K for  $H = 3300 \text{ \AA}$ . We shall calculate for some specific distribution functions the value of this ratio and the form of the saturation graphs.

$$\text{I) } \begin{aligned} f(\eta) &= 1/(\eta_2 - \eta_1) & \text{for } \eta_1 \ll \eta \ll \eta_2 \\ &= 0 & \text{for } \eta < \eta_1 \text{ and } \eta > \eta_2. \end{aligned}$$

With  $\eta_2/\eta_1 = R$  one finds:

$$\bar{\eta} \overline{(1/\eta)} = 1/2 \frac{R+1}{R-1} \ln R.$$

This product equals 5 for  $R \approx 2.2 \times 10^4$ .

$$\text{II) } \begin{aligned} f(\eta) &= a/\eta^2 & \text{for } \eta_1 \ll \eta \ll \eta_2 \\ &= 0 & \text{for } \eta < \eta_1 \text{ and } \eta > \eta_2. \end{aligned}$$

The expression for  $\bar{\eta} \overline{(1/\eta)}$  is the same as for case I.

$$\text{III) } \begin{aligned} f(\eta) &= a/\eta & \text{for } \eta_1 \ll \eta \ll \eta_2 \\ f(\eta) &= 0 & \text{for } \eta < \eta_1 \text{ and } \eta > \eta_2 \\ \bar{\eta} \cdot \overline{1/\eta} &= \frac{R+1/R-2}{\ln^2 R} & \text{which equals 5 for } R = 115. \end{aligned}$$

$$\text{IV) } f(\eta) = a \delta(\eta - \eta_1) + (1-a) \delta(\eta - \eta_2) \quad a \ll 1$$

where  $\delta$  is the wellknown delta function.

One finds  $\bar{\eta} \overline{(1/\eta)} = 1 + a(1-a)(R+1/R-2)$ .

This product equals 5 for values of  $a = 1/2, 10^2, 10^3$  when  $R = 18, 400, 4000$  respectively.

For the distribution functions discussed, drawings have been made of the saturation graphs (fig. 4.4 and fig. 4.5) as would have been found for  $\bar{\eta} = 1$  and  $\overline{1/\eta} = 5$ .

The distributions III and IV with  $a = 1/2$  and 0.990 are seen to have the required curvature for reasonable values of  $R = \eta_2/\eta_1$ .

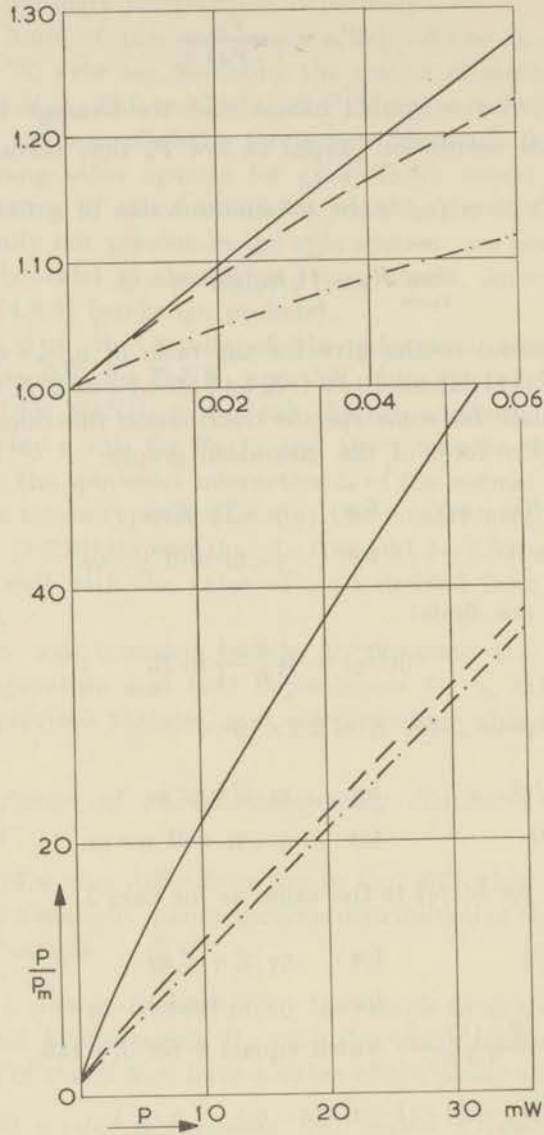


Fig. 4.4.  $P_0/P_m$  vs.  $P_0$  assuming a distribution for  $\eta$ .

· · · · · I      ————— II      - - - - - III

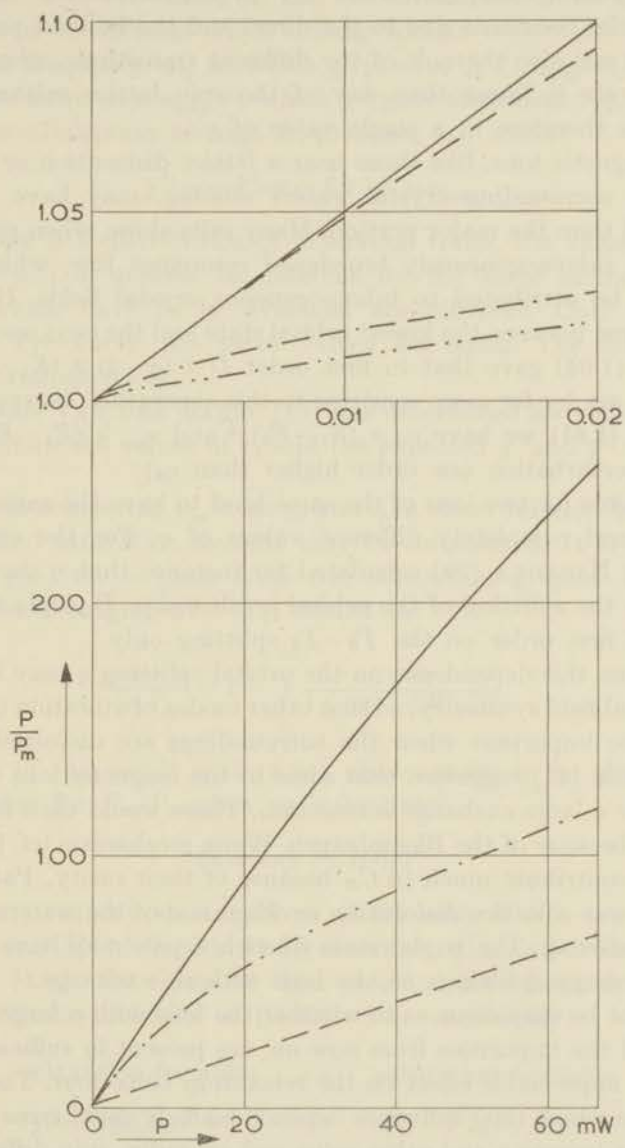


Fig. 4.5.  $P_0/P_m$  vs.  $P_0$  assuming distribution IV for  $\eta(\eta_2 > \eta_1)$ .

- $a = 1/2$
- · - · -  $a = 10^{-2}$
- · · · ·  $a = 10^{-3}$
- · · · ·  $a = 0.990$
- $a = 0.999$

[4.6.3] The possible cause of a distribution in  $\eta$ . The power transfer constants due to the direct and the indirect processes are additive, as are also the  $\eta_{ij}$ 's of the different transitions, when the cross relaxation rate is faster than any of the spin lattice relaxation rates. This results therefore in a single value of  $\eta$ .

Some magnetic ions, like those near a lattice dislocation or those with one of the surrounding crystal waters missing, may have a different crystal field than the major portion. Many salts show, when magnetically diluted, an inhomogeneously broadened resonance line, which in most cases may be attributed to inhomogeneous crystal fields. If  $E_1 - E_0$  is the separation between the lowest orbital state and the next one, equations (1.05) and (1.04) gave that in first order  $D \propto (\bar{g} - 2) \propto (E_1 - E_0)^{-1}$ . The values of  $\eta$  are by far more sensitive to this separation, however, as with (1.59) and (1.61) we have  $\eta_a \propto (E_1 - E_0)^{-4}$  and  $\eta_{\text{ind}} \propto (E_1 - E_0)^{-6}$  ( $\eta_{\text{ind}}$  is due to a perturbation one order higher than  $\eta_a$ ).

It is possible for two ions of the same kind to have the same resonance spectrum, and completely different values of  $\eta$ . For the case of CuK tutton salt, NAGAOKA [20] calculated for instance that  $\eta$  should depend strongly on the splitting of the orbital levels inside  $I_3$  while the  $g$ -factor depends in first order on the  $I_3 - I_5$  splitting only.

Apart from this dependence on the orbital splitting  $\eta$  may be sensitive to the crystal field symmetry, so that other modes of vibration  $Q_i$  (cf. [1.5]) may become important when the surroundings are distorted.

VAN VLECK [21] suggested that some of the magnetic ions might have accidentally a large exchange interaction. These would then have a large value of  $\eta$  because of the Bloembergen-Wang mechanism (cf. [1.5.3]), but would not contribute much to  $C_H$  because of their rarity. Pairs like this may exist near a lattice dislocation or when one of the waters of crystallization is missing. The triplet state of such a pair may have practically the same energy splittings as the ions without exchange.

One might be suspicious as to whether the ions with a large value of  $\eta$ , to be called the impurities from now on, are present in sufficient number to have an appreciable effect on the relaxation behaviour. There are two processes on which their influence depends, namely rapid cross relaxations between the impurity and other spins and secondly, spin diffusion to the vicinity of the impurity which in both cases acts as an energy sink.

[4.6.3] By the relaxation method the dependence of  $\chi$  on frequency is measured. According to (1.102) one has

$$(4.27) \quad \chi(\omega)/\chi_0 = (1 - F) + F/(1 + i\omega\tau_1).$$

For many salts the  $\chi(\omega)$  vs.  $\omega$  plots deviate strongly from the simple CASIMIR-DU PRÉ curves. To explain the observed curves a distribution of relaxation times had to be assumed [18] [19].

The value of  $\tau_1 = (b + CH^2)/\eta T$  can be determined from the plots of  $\chi'$  or  $\chi''$  vs.  $\omega$  in different ways, among which:

- 1) from the frequency  $\omega_{1/2}$  at which  $\chi'/\chi_0 = 1 - 1/2 F$ ;  $\tau_{\text{disp}} = 1/\omega_{1/2}$ ,
- 2) from the frequency  $\omega_{\text{max}}$  at which  $\chi''/\chi_0$  is maximum;  $\tau_{\text{abs}} = 1/\omega_{\text{max}}$
- 3) from the absorption at high frequencies,  $\tau_{hf}$ , where

$$(4.28) \quad \chi''/\chi_0 = F/\omega\tau_{hf} \text{ for } \omega \gg \omega_{\text{max}}.$$

When there is a distribution of relaxation times, the values of  $\tau_1$  thus determined will in general be different for the three methods, as the functions which have to be averaged are different. Only for a true Casimir-du Pré curve the three values are equal. The third method clearly determines  $\bar{\eta} = \eta_f$ .

In his thesis VAN DER MAREL [18] has determined for different distribution functions the values of  $\tau_1$  and the expected  $\chi'$  and  $\chi''$  vs.  $\omega$  plots.

Apart from comparing  $\eta_{\text{rel}}$  with  $\eta_s$  and  $\eta_f$  a closer relation between the relaxation and saturation method may be formulated. It is possible to obtain the  $\chi(\omega)$  vs.  $\omega$  plots from our saturation graphs. Inserting  $\eta$  in (4.27) and averaging over  $f(\eta)$  results in:

$$(4.29) \quad \frac{\chi(\omega) - \chi_0}{\chi_0 F} + 1 = \int_0^{\infty} \frac{f(\eta) d\eta}{1 + i\omega(b + CH^2)/\eta T}.$$

Comparison of this result with (4.24), shows (4.29) to be identical with the expression for  $P_m/P_0$  when we substitute

$$(4.30) \quad P_0 = i\omega(b + CH^2)/T.$$

To solve (1.102) by starting from (1.83) with  $W=0$ , one may also contain  $\Delta T$  and  $\Delta H$  (defined in [1.8]) as variables instead of the procedure followed in [1.8]. The formulas then obtained are identical with those for the stationary solution of (1.83) when we identify:

relaxation-formulas	$\leftrightarrow$	saturation-formulas
$(\chi(\omega) - \chi_0)/\chi_0 F + 1$	$\leftrightarrow$	$P_m/P_0$
$i\omega(b + CH^2)/T_L$	$\leftrightarrow$	$P_0$

$$(4.31) \quad \frac{H_c}{Fh} \left( \frac{1}{T_L} - \frac{1}{T_s} \right) \quad \leftrightarrow \quad \left( \frac{1}{T_L} - \frac{1}{T_s} \right).$$

This procedure becomes more interesting when terms have to be added to (1.83), due for instance to cross relaxations towards impurities with temperature  $T_i$  or terms due to spin diffusion. Also certain boundary conditions may have to be fulfilled, an example of which will be presented later (cf. (4.35)). It is straightforward to show that this transformation can be performed when the added terms and the additional boundary conditions are homogeneous linear functions of or linear operators on

$(1/T_L - 1/T_S)$  and  $(1/T_L - 1/T_i)$ . These variables namely all contain a factor  $H_c/hF$  in the relaxation formulas, but not in the saturation formulas (see substitution (4.31)).

By representing the saturation graphs by an analytical expression, the corresponding plots for  $\chi'(\omega)$  and  $\chi''(\omega)$  can thus be derived. This has been carried out (cf. fig. 4.6) for two of the saturation graphs of CrK alum presented in fig. 3.1. The maximum of  $\chi''(\omega)$  corresponds to  $\eta_s$  at both temperatures, and its height is about 80 % of the value for a true Casimir-du Pré curve.  $\chi'(\omega)$  at high frequencies is larger than for C.D. curves.

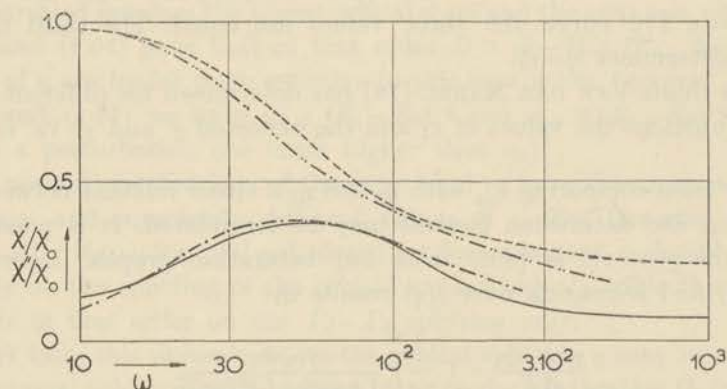


Fig. 4.6. Transformed saturation graphs of CrK alum fig. 3.1.

$$\begin{array}{ll} \text{---} & \chi'/\chi_0 \left. \vphantom{\chi'/\chi_0} \right\} T = 3.36^\circ \text{ K} \\ \text{---} & \chi''/\chi_0 \left. \vphantom{\chi''/\chi_0} \right\} T = 3.36^\circ \text{ K} \\ \text{- - -} & \chi'/\chi_0 \left. \vphantom{\chi'/\chi_0} \right\} T = 2.55^\circ \text{ K} \\ \text{- - -} & \chi''/\chi_0 \left. \vphantom{\chi''/\chi_0} \right\} T = 2.55^\circ \text{ K} \end{array}$$

According to the measurements of KRAMERS e.a. on a powdered sample the maximum of  $\chi''(\omega)$  is at  $\omega = 260 \text{ s}^{-1}$  for  $T = 2.55^\circ \text{ K}$  and at  $\omega = 590 \text{ s}^{-1}$  for  $T = 3.36^\circ \text{ K}$ , practically corresponding to  $\eta_f$ .

The agreement is miserable and we will consider whether cross relaxations or spin diffusion may improve the matters.

[4.6.4] The effect of cross relaxations and spin diffusion. Depending on the energy level separations, cross relaxations may occur between the impurities and the neighbouring spins. The energy transfer due to this, for the case of dipolar interactions, may be written as

$$(4.32) \quad Br^{-6} \left( \frac{1}{T_i} - \frac{1}{T_s} \right) = \frac{(\hbar\omega)^2}{k} U_{cr} \left( \frac{1}{T_i} - \frac{1}{T_s} \right).$$

As we do not know the magnitude of the quanta which the impurity exchanges with the lattice, it is better to characterize the differences in level populations by the effective temperatures.

Spin diffusion, which is the transport of Zeeman energy over a distance through flip-flop processes between ions with the same energy spacing, may transport energy to the vicinity of the impurity, where cross relaxations take over.

The rate  $U_{\text{dif}}$  at which this energy exchange between two equivalent nearest neighbours takes place can be calculated by considering the term  $B$  of  $\mathcal{H}_d$  as a perturbing r.f. field. According to BLOEMBERGEN [22] one finds for a gaussian resonance line shape in a cubic crystal with  $\mathbf{H}$  parallel to a crystal axis and  $S=1/2$  that:

$$(4.33) \quad \begin{cases} U_{\text{dif}} \approx \omega_d/50 \text{ for } \mathbf{H} // \mathbf{r}_{ij} \text{ and} \\ U_{\text{dif}} \approx 4\omega_d/50 \text{ for } \mathbf{H} \perp \mathbf{r}_{ij} \end{cases}$$

where  $\mathbf{r}_{ij}$  is the radius vector between the two ions  $i$  and  $j$ , and  $\omega_d$ , defined in (1.35a), represents the dipolar interaction.

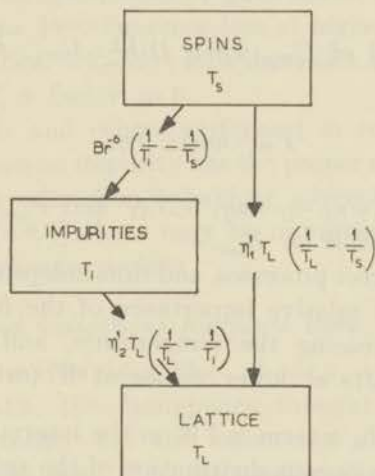


Fig. 4.7. Model for the power transfer with cross relaxations for spins at a distance  $r$ .

Equation (1.83) has to be modified in analogy to the procedure followed by BLOEMBERGEN (cf. fig. 4.7)

$$(4.34) \quad Q'W/T_s = \frac{dU_s'}{dt} + \eta_1' \left(1 - \frac{T_L}{T_s}\right) + Br^{-6} \left(\frac{1}{T_i} - \frac{1}{T_s}\right) + \frac{(\hbar\omega)^2}{k} D\Delta \left(\frac{1}{T_s}\right)$$

and for the impurities:

$$(4.35) \quad \int_a^R Br^{-6} \left(\frac{1}{T_i} - \frac{1}{T_s}\right) 4\pi r^2 n dr = \eta_2' \left(1 - \frac{T_L}{T_s}\right)$$

where  $D \approx a^2 U_{\text{dif}}$  ( $a$  is the lattice spacing),  $n$  is the number of spins per unit volume and the prime above a variable or coefficient means that the average value per ion is taken. In these formulae  $r$  is the distance spin-impurity and  $R$  an average radius, so chosen, that all spins within a distance  $R$  from an impurity have the largest interaction with that one. We have approximately  $4\pi R^3/3 = N$ , with  $N$  the number of impurities per unit volume.

The general solution for  $T_S(r)$ , which is a function of  $r$ , is difficult to obtain. As  $U_{cr} \propto r^{-6}$ , the corresponding term in (4.34) will only be appreciable near the impurity. It is therefore reasonable to assume that in certain regions one of the two last terms in (4.34) may be neglected.

The solutions of (4.34) and (4.35) in those regions have been calculated. If  $U_{crR}$  is the cross relaxation rate, and  $D/R^2$  the diffusion rate, from the boundary  $R$  to the impurity, then the expression for  $P_m$  integrated over the volume of the sample becomes, at intermediate values of  $W(P_0 \gg \eta_1)$  and  $\eta_2' \gg \eta_1'$ :

$$(4.36) \quad P_m \approx \frac{Q}{T_L} \sqrt{U_{crR} W} + \eta_1$$

or with  $D/R^2$  instead of  $U_{crR}$  when  $D/R^2 > U_{crR}$ . At high values of  $W$  we have

$$(4.37) \quad P_m = n\eta_1' + N\eta_2'$$

We therefore find  $\eta_s = \eta_1$ ,  $\eta_f = n\eta_1' + N\eta_2'$  and  $P_{\text{ext}}/P_m \propto \sqrt{W} \propto \sqrt{P_{\text{ext}}}$  at intermediate values of  $W$  or  $P_{\text{ext}}$ .

If  $\eta_1$  is due to the direct processes, and thus independent of concentration and temperature, the relative importance of the first term in (4.36) is increasing when decreasing the temperature, and the curving of the saturation graphs starts at lower values of  $W$  (or  $P_{\text{ext}}$ ).

That one finds in  $P_m$  a term  $\propto \sqrt{W}$  in the intermediate region of  $W$  is caused by the inhomogeneous distribution of the spin temperature which is somewhat analogous to the case met when saturating an inhomogeneously broadened resonance line (cf. (1.39)).

A rough estimate of the distance over which energy can be transported during a time  $\tau_1$  ( $\approx 10^{-2}$  s), with (4.33) and  $\omega_d \approx 2\pi \times 10^9$  s $^{-1}$ , shows this to be about a hundred lattice spacings. When diffusion over such a large distance really takes place, there would be practically no gradient of  $T_S$ .

In [4.6.3] we have found some conditions for the validity of the transformation of  $\chi(\omega)$  plots into saturation graphs. These conditions are fulfilled for formulas (4.34) and (4.35) so that for the mechanisms discussed here the transformation can be carried out. As the discussion of fig. 4.5 showed, there exists then a serious discrepancy between our results and those obtained by the relaxation method.

[4.6.5] Experiments have been performed on the spin lattice relaxation times of substances with impurities added.

a) FEHER and SCOVIL [23] measured the spin lattice relaxation times of Gd and Ce doped lanthanum ethyl sulphate (Gd : Ce : La = 5 : 2 : 1000).

A large influence of the Ce $^{+++}$  ion ( $\tau_1$  short) was only noticeable when the Ce resonance practically coincided with a Gd transition.

b) The experiments of BROER [24] on  $\text{MnNH}_4$  tutton salt with impurities of the isomorphous Co salt showed that at  $90^\circ\text{K}$  and  $3200\text{ o}$  the values of  $\tau_1$  were  $1.7\ \mu\text{s}$  and  $0.048\ \mu\text{s}$  with a 0 % and 9 % Co salt content respectively. A  $1\frac{1}{2}\%$  Co content gave a value of  $\tau$  of about 5 % smaller than for the pure Mn salt. At higher temperatures the relative decrease is less. The Co ion has in these salt and at these temperatures a much shorter relaxation time than the Mn ion.

c) HASEDA [25] measured at  $4.2^\circ\text{K}$  the Co relaxation time in  $\text{CoNH}_4$  tutton salt doped with  $\text{Fe}^{++}$  or  $\text{Ni}^{++}$  ions. A ratio of  $\text{Fe} : \text{Co} = 1 : 30$  gave at low fields a decrease of about a factor 9 in  $\tau_1$ , while for  $\text{Fe} : \text{Co} = 1 : 5.5$  the factor is  $\approx 50$  and the value of  $\tau_1$  becomes an increasing instead of the decreasing function of  $H$  as found in pure  $\text{CoNH}_4$  tutton salt. The effect of the  $\text{Fe}^{++}$  becomes less at higher fields. The reverse is true for  $\text{Ni}^{++}$  impurities. 7 %  $\text{Ni}^{++}$  ions decreases  $\tau_1$  by a factor of about 9 at  $855\text{ o}$  and 1 % a factor  $\approx 6$ .

These experiments and others performed in connection with masers suggest that only when an impurity has the proper energy level separations it will influence the relaxation behaviour appreciably.

As discussed in [4.6.2] there may be impurities having this feature, for instance the exchange pockets.

#### [4.7] *Conclusion and indications for future work*

[4.7.1] By reconsidering the theory and comparing the experimental data, the discrepancy thought to exist between the results of the relaxation and the saturation measurements has been lifted for the diluted salts. For the undiluted salts agreement exists between both methods at either high or low radio frequency powers.

There remain some questions such as the origin of the curvature of the saturation graphs and the dependence on field and temperature of  $\eta_{\text{rel}}$  and  $\eta_f$ . A tentative explanation might be given on the basis of an inhomogeneous distribution of the power transfer constant, due to fast relaxing impurities. VAN VLECK [21] proposed the existence of exchange pockets, with a random distribution in the size of the exchange interaction, as a possible source of those impurities. The relaxation method determines mainly the power transfer constant of the impurities, because of fast spin diffusion and cross relaxation. The temperature and field dependence of  $\eta$  of a group of ions having a large interaction has been discussed in [4.5.4] and theory and experiment agree remarkably well in this respect. The number of exchange pockets, and the number of ions they contain, decreases when diluting magnetically. Also less ions will feel them as the most important energy sink. This causes a dependence on concentration of  $\eta$  and of its temperature dependence.

The correspondance of saturation and relaxation measurements on the basis of the simple spin diffusion picture of [4.6.4] is not satisfactory, however, as has been shown by the transformation of some saturation

graphs. This transformation has been shown to be applicable for the case spin diffusion or cross relaxation to an impurity is important.

In the relaxation method the magnetic field is varied in magnitude and thus the populations of all levels are varied. A spatial diffusion in which the entire spectrum of the transitions takes part, carries energy to and from the impurity at a relatively fast rate.

In the saturation method the spin system is excited at one frequency only, and we have to consider diffusion in the frequency domain (cross relaxation) as well as spatially (spin diffusion). The rate for this last process is presumably faster than for the first as it does not require a change in the Zeeman energy. Therefore the resonance line, averaged over a time  $1/U_{\text{diff}}$ , will appear as a not completely homogeneously broadened resonance line, saturated at one frequency. Only the few ions in the narrow saturated band take part in the diffusion process. The total energy transport is therefore much smaller than for the experiments by the relaxation method.

Averaged over the much longer time  $1/\bar{U}_{ij}$ , the resonance line will appear to be homogeneously saturated as we have  $\bar{U}_{ij} \ll U_{cr}$ .

It is therefore suggested that the difference between the relaxation and saturation experiments can be attributed to the power which diffusion processes are able to transport.

Cross relaxations towards the impurity might lead to a similar effect, as the frequency spectrum of the impurity transitions has a larger overlap with the spin transitions when these are all excited than when excited at the frequency  $\omega$  only.

The assumption of impurities gives a simple explanation for the discontinuity at the  $\lambda$  point of liquid helium in the value of  $\eta_I$  and in the pronounced broadening of the  $\chi'(\omega)$  and  $\chi''(\omega)$  relaxation curves which occur in several non-diluted salts. Neither on the basis of homogeneous heating of the crystal, in view of the magnitude of the thermal conductivity, nor on the basis of an inadequate energy transfer to the liquid helium bath at the surfaces of the crystal these effects can be understood. The impurities act as point sources of energy for the lattice, and they will radiate and absorb relatively large amounts of heat in a confined space. For such a case heating effects may become important.

The impurities are probably situated near lattice dislocations such as cracks in the crystal, in which superfluid helium can penetrate. The better heat contact of the impurities below the  $\lambda$  point then accounts for the observed discontinuities.

[4.7.2] For undiluted CrK alum, CuK, CuNH<sub>4</sub> and MnNH<sub>4</sub> tutton salt, the spin diffusion is important at the higher microwave powers, while at low powers  $\eta$  is not influenced by the impurities and behaves approximately according to VAN VLECK'S early theory. The region over which the saturation graphs are straight is determined by

the ratios of  $U_{crR}$  (or  $D/R^2$ ),  $\bar{U}_{ij}$  and  $W$ . For these salts we have to assume  $2\bar{U}_{ij} > U_{crR}$  (or  $D/R^2$ ). At high r.f. powers the transfer due to the impurities (or exchange pockets) is measured according to (4.37).

An exchange coupling between the ions will increase the spin diffusion rate. For  $\text{CuK}_2\text{Cl}_4 \cdot 2\text{H}_2\text{O}$  and  $\text{CuSO}_4 \cdot 5\text{H}_2\text{O}$  at low r.f. powers, the diffusion processes seem to determine the power transfer between spins and lattice, so that  $\bar{U}_{ij} \ll \bar{U}_{crR}$  (or  $D/R^2$ ). The largest exchange coupling in  $\text{CuSO}_4 \cdot 5\text{H}_2\text{O}$  is of an antiferromagnetic nature and the diffusion rate therefore increases when  $\hbar\omega_{\text{ex}} \approx kT_L$ . So we have  $\eta_s \propto 1/(T - 0.94)$  ( $J_1/k \approx 0.94^\circ \text{K}$  cf. [3.4.2]). For  $\text{CuK}_2\text{Cl}_4 \cdot 2\text{H}_2\text{O}$  the exchange has a ferromagnetic character ( $\theta \approx +1^\circ \text{K}$ ) and the diffusion rate decreases somewhat at lower temperatures;  $\eta_s \propto 1/(T + 0.4)$  (cf. [3.5.2]).

[4.7.3] Proposed experiment on spin temperature distribution. One would like to determine experimentally whether the relation  $P_m \propto \chi_0 \propto 1/T_S$  holds and whether  $T_S$  has a homogeneous or an inhomogeneous distribution over the sample. The relation  $P_m \propto \chi_0$  can be tested by measuring the static susceptibility while saturating. To solve the second problem a measurement of  $T_S$  on a microscopic basis is required. An elegant solution for both problems could be obtained by carrying out an electron-nuclear double resonance experiment.

The nuclear moments of the non-paramagnetic atoms in the crystal, for instance the protons in the water of hydration, precess at frequencies which are shifted from their free particle value by the local dipole field  $H_{\text{loc}}$  which is due to the neighbouring magnetic ions. Measurements and calculations on the shift of the proton resonance in  $\text{CuSO}_4 \cdot 5\text{H}_2\text{O}$  have been carried out by BLOEMBERGEN [26] and POULIS [27]. They showed that  $H_{\text{loc}} \propto \chi_{0\text{Cu}}$  and is mainly due to near neighbours. The proton resonance lines are relatively sharp, due to the exchange interaction between the copper ions.

Suppose we perform a simultaneous nuclear-electron resonance experiment. When saturation of the electronic resonance results in a homogeneously distributed spin temperature, then we have  $H_{\text{loc}} \propto 1/T_S$  and the spin temperature of the electron moments can be measured. When an inhomogeneously distributed  $T_S$  arises, the nuclear resonance will be spread out and from its shape the distribution of  $T_S$  can be determined. On the basis of the foregoing arguments a difference in shape is expected, when the measurements are made with a rapidly modulated or an unmodulated magnetic field.

When pulse modulating the microwave power and observing the proton resonance at a certain value of  $H_{\text{loc}}$ , then pictures analogous to fig. 3.20a are expected. The characteristic times may yield information about the diffusion (or cross relaxation) time.  $\text{CuK}_2\text{Cl}_4 \cdot 2\text{H}_2\text{O}$  as well as  $\text{CuSO}_4 \cdot 5\text{H}_2\text{O}$  may be useful materials to study this effect.

[4.7.3] To gain deeper insight in the relaxation mechanisms more detailed investigations of the following properties may provide basic information:

- 1) the temperature dependence of the  $p$  appearing in the BRONS-VAN VLECK formula,
- 2) the anisotropy of  $p$  and the influence of an exchange interaction on it (cf. [1.7.5] and [4.5.2]),
- 3) the anisotropies of  $\eta_s$  and  $\eta_f$  (relating these to the magnetic and crystal symmetries may disclose the mechanisms governing them),
- 4) steady state saturation experiments at lower magnetic fields, as there the curvatures are expected to become larger,
- 5) comparison between pulsed and stationary microwave saturation experiments on the same crystal, preferably performed during the same low temperature run.

## REFERENCES

1. GORTER, C. J., L. C. VAN DER MAREL and B. BÖLGER, *Physica* 21, 103 (1955); and Comm. Kamerlingh Onnes Lab. no. 109 c.
2. REDFIELD, A. G., *Phys. Rev.* 98, 1787 (1955).
3. BIJL, D., *Physica* 14, 684 (1948); Comm. no. 276 b.
4. CASIMIR, H. B. G., *Physica* 5, 495 (1938); Comm. Suppl. no. 85 b.
5. KITTEL, CH., *Introduction to solid state physics*, Wiley and Sons N.Y. p. 143 (1956).
6. KAPADNIS, D. G., Thesis, Leiden (1956).
7. VAN VLECK, J. H., *Phys. Rev.* 59, 724 (1941).
8. ———, *Phys. Rev.* 59, 730 (1941).
9. HERRING, C., *Phys. Rev.* 95, 954 (1954).
10. BLOEMBERGEN, N., *Phys. Rev.* 109, 2209 (1958).
11. RAMSEY, N. F., *Phys. Rev.* 103, 20 (1956).
12. GIORDMIANE, J. A., L. E. ALSOP, F. R. NASH and C. H. TOWNES, *Phys. Rev.* 109, 302 (1958).
13. BLOEMBERGEN, N., S. SHAPIRO, P. S. PERSHAN and J. O. ARTMAN, *Phys. Rev.* 114, 445 (1959).
14. NASH, F. R., *Conf. on Quantum Electronics*, Bloomfield N.Y. (1959).
15. TEMPERLY, H. N. V., *Proc. Camb. Phil. Soc.* 35, Pt. II, 256 (1939).
16. VAN VLECK, J. H., *Phys. Rev.* 57, 426 (1940).
17. WRIGHT, A., *Phys. Rev.* 76, 1826 (1949).
18. VAN DER MAREL, L. C., Thesis, Leiden (1958).
19. ———, J. VAN DEN BROEK and C. J. GORTER, *Physica* 24, 101 (1958). Commun. no. 310 a.
20. NAGAOKA, Y. K., *Phys. Soc. of Japan* 13, 1328 (1958).
21. VAN VLECK, J. H., *Conf. on Quantum Electronics*, Bloomfield N.Y. (1959).
22. BLOEMBERGEN, N., *Physica* 15, 386 (1949); Commun. no. 277 a.
23. FEHER, G. and H. E. D. SCOVIL, *Phys. Rev.* 105, 760 (1957).
24. BROER, L. J. F., Thesis (1945) Amsterdam.
25. HASEDA, T., *Physica* 24, 93 (1958).
26. BLOEMBERGEN, N., *Physica* 16, 144 (1950); Commun. no. 280 c.
27. POULIS, N. J., *Physica* 17, 392 (1951); Commun. no. 283 a.

## SAMENVATTING

*l'araignée du matin* - *chagrin*

*l'araignée du midi* - *soucis*

*l'araignée du soir* - *espoir*

(oude franse volksspreuk).

In dit proefschrift worden twee reeksen van experimenten beschreven, die tot doel hadden nadere gegevens te verkrijgen omtrent de relaxatiemechanismen die een rol spelen bij het instellen van evenwicht tussen paramagnetische spins en het kristalrooster.

In hoofdstuk I wordt een overzicht gegeven van de theorie der paramagnetische resonantie- en relaxatieverschijnselen. De invloed van een radio frequent magnetisch veld wordt besproken voor het geval dat een gedeeltelijk of een volledig intern spin evenwicht zich heeft ingesteld gedurende de gemiddelde spin rooster relaxatie tijd  $\tau_1$ . De vermogensoverdrachtcoëfficiënt  $\eta$  wordt ingevoerd, daar dit de grootte is die men met stationnaire verzadigingsmetingen bepaald.

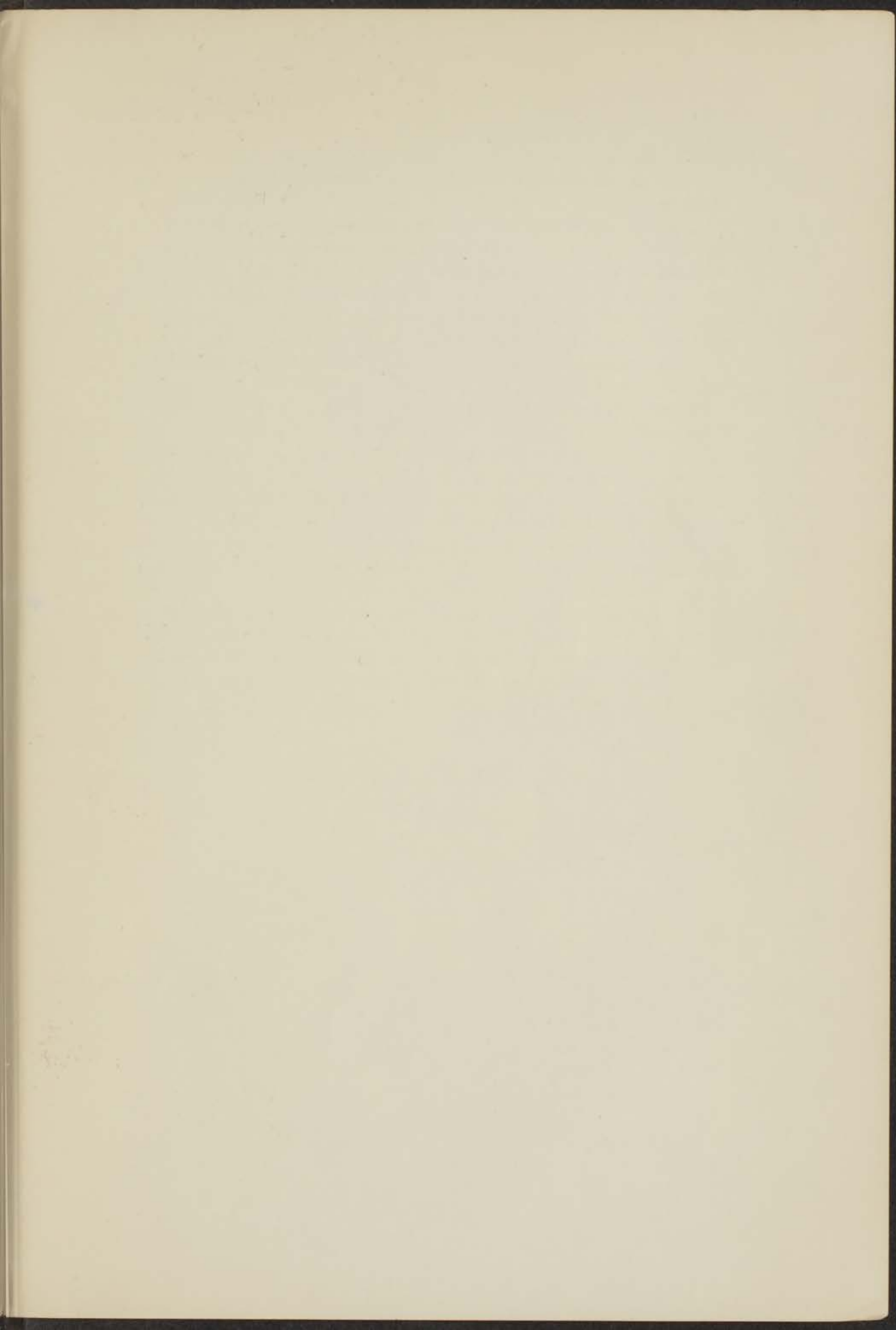
Hoofdstuk II bevat een overzicht van de gebruikte experimentele methoden en meetopstellingen. Enkele daarmee samenhangende problemen worden aan een nader onderzoek onderworpen. Het principe van de drie-niveau-maser is in het kort besproken.

Hoofdstuk III bevat de resultaten der metingen. In het eerste gedeelte worden de resultaten der stationnaire verzadigingsmethode behandeld en de gevonden waarden van  $\eta$  vergeleken met die bepaald met de relaxatiemethode. Voor de verdunde zouten stemmen verzadigings- en relaxatieexperimenten en theorie goed overeen. Voor geconcentreerde zouten is dit niet het geval en de verzadigingsgrafieken blijken gekromd te zijn, terwijl men rechte lijnen zou verwachten. Voor de meeste zouten stemt de theoretische waarde van  $\eta$  overeen met de experimentele waarde bij kleine microgolf vermogens, en  $\eta$  bij grote vermogens met de bij de relaxatiemetingen gevonden waarde.

In het tweede gedeelte worden de resultaten met een gepulste verzadigingsmethode besproken. Deze metingen werden gedaan aan zodanig verdunde zouten dat de tijd benodigd voor het instellen van een spin-spin evenwicht van dezelfde orde van grootte is als de spin-rooster-relaxatietijd. In sommige gevallen bleek het mogelijk beide relaxatietijden te bepalen. Uit de experimenten kan geconcludeerd worden dat het mogelijk is om voor de constructie van een drie-niveau-maser bij hogere temperaturen materialen met grotere magnetische concentraties te gebruiken dan bij lagere temperaturen mogelijk is.

In hoofdstuk IV wordt eerst de relatie tussen  $\tau_1$  en  $\eta$  besproken aan de hand van de metingen. Geconcludeerd wordt dat de vermeende discrepantie tussen de resultaten van de relaxatie- en van de verzadigingsmetingen op een verkeerde interpretatie berust, hetgeen in hoofdstuk I theoretisch en in hoofdstuk III experimenteel aangetoond werd. De kromming der verzadigingsgrafieken blijkt moeilijk te verklaren en beschouwde mechanismen blijken zonder verdere hypothese allen eigenschappen te hebben, die niet stroken met de experimenten. Dit wordt o.a. aangetoond met behulp van een transformatie, welke de grootheden uitgezet in de verzadigingsgrafieken doet overgaan in de complexe susceptibiliteit en de frequentie zoals gemeten met de relaxatiemethode.

De meest waarschijnlijke verklaring voor de kromming is te vinden in de invloed van magnetische verontreinigingen, die een goed warmtecontact met het rooster hebben. Zulke verontreinigingen zouden kunnen bestaan uit een groepje magnetische ionen met een grote exchange interactie. Door z.g. „cross”-relaxaties en spin-diffusie kunnen deze verontreinigingen een grote invloed hebben. Temperatuur, concentratie en veld afhankelijkheid kunnen dan verklaard worden, alsmede de waargenomen discontinuïteiten bij het  $\lambda$  punt van vloeibaar helium in de waarde van  $\eta$  en de vorm der  $\chi'(\omega)$  en  $\chi''(\omega)$  curven. Om echter volledige overeenstemming met de experimenten te verkrijgen moet men aannemen dat het diffusie- of „cross”-relaxatieproces bij de relaxatiemetingen sneller is dan bij de verzadigingsmetingen. Dit wordt aannemelijk gemaakt. Een experiment wordt voorgesteld dat kan beslissen of boven beschreven mechanismen werkelijk de relaxatieverschijnselen beïnvloeden.



The first part of the report deals with the general situation of the country and the progress of the war. It is followed by a detailed account of the military operations in the various theaters of war. The author then discusses the political and economic conditions of the country and the impact of the war on the population. The report concludes with a summary of the findings and a list of recommendations.

The second part of the report contains a detailed analysis of the military operations in the various theaters of war. It discusses the tactics used by the different sides and the results of the various battles. The author also discusses the impact of the war on the economy and the political situation of the country.

The third part of the report discusses the political and economic conditions of the country and the impact of the war on the population. It discusses the various political parties and their policies, as well as the economic situation of the country and the impact of the war on the different sectors of the economy.

The fourth part of the report contains a summary of the findings and a list of recommendations. The author concludes that the war has had a profound impact on the country and that the government should take certain steps to address the various challenges that have arisen as a result of the war.

